Aqueous Decomposition Behaviour of Oxygen Releasing Peroxy-Compounds and Assessment of their Therapeutic Potential

Arghavan Rastinfard
Department of Experimental Surgery
McGill University, Montréal
December 2021

A thesis submitted to McGill University in partial fulfillment of the requirements of the degree of Master of Science in Experimental Surgery

© Arghavan Rastinfard 2021

ABSTRACT

Impaired blood perfusion and ischemia/reperfusion injury may contribute to deleterious changes within tissue and vasculature and finally tissue necrosis. Oxygen has been shown to positively impact wound healing, and through the years, many ways have been developed to deliver oxygen to wounds. Solid peroxy- compounds can generate molecular oxygen instead of simply delivering it and can be used in oxygen delivery studies to provide prolonged oxygen delivery. However, peroxy- compounds can also decompose to form hydrogen peroxide upon contact with water. Therefore, most studies of solid peroxides are intended to augment oxygen release efficiency and whilst minimizing cell and tissue contact with peroxide compounds via loading solid peroxides in hydrophobic biomaterials and/or adding hydrogen peroxide catalysts. However, not one study considered pH as a factor in designing oxygen releasing materials, yet due to the impact of pH values and catalytic activity of certain cations/anions on peroxides' decomposition it is clearly a critical parameter. This study then compared for the first-time decomposition products of calcium peroxide (CaO_2), magnesium peroxide (MgO_2), zinc peroxide (ZnO_2), sodium percarbonate ($Na_2CO_3.1.5H_2O_2$), and hydrogen peroxide (H_2O_2) at pH 5, 7 and 9. We identified a strong effect of pH on peroxide decomposition and also confirmed the activity of carbonate ions on hydrogen peroxide decomposition. These key findings informed the formulation of implantable oxygen generating film to sustain oxygen directly to flap tissues subdermally. We reduced hydrogen peroxide generation by adding a peroxidase catalyst (iron oxide), a compound known to react with hydrogen peroxide (bicarbonate), and a hydrophobic polymer barrier (polycaprolactone). We also adjusted pH with an acidic calcium dihydrogen phosphate. This reduced cytotoxicity since iron oxide reduced hydrogen peroxide release and calcium dihydrogen phosphate controlled shifting pH values. Preclinical efficacy in reducing ischemic necrosis of random skin flaps was confirmed. Oxygen generating films delayed skin flap necrosis but could not prevent flap necrosis, especially in the distal zone. Necrosis appeared multifactorial; and combined strategies would seem required to sustain skin integrity in which there is no blood flow.

RÉSUMÉ

L'altération de la perfusion sanguine et les lésions d'ischémie/reperfusion peuvent contribuer à des changements délétères dans les tissus, le système vasculaire et finalement à la nécrose des tissus. Il a été démontré que l'oxygène a un impact positif sur la cicatrisation des plaies et au fil des ans, de nombreux moyens ont été mis au point pour fournir de l'oxygène aux plaies. Les composés peroxydés solides peuvent générer de l'oxygène moléculaire au lieu de simplement le délivrer et peuvent être utilisés dans les études sur l'apport d'oxygène pour fournir une libération prolongée d'oxygène. Cependant, au contact de l'eau, les composés peroxydés peuvent également se décomposer pour former du peroxyde d'hydrogène. Par conséquent, la plupart des études sur les peroxydes solides visent à augmenter l'efficacité de la libération d'oxygène tout en minimisant le contact des cellules et des tissus avec les composés peroxydés, en chargeant les peroxydes solides dans des biomatériaux hydrophobes et/ou en ajoutant des catalyseurs de peroxyde d'hydrogène. Cependant, aucune étude n'a considéré le pH comme un facteur dans la conception de matériaux libérant de l'oxygène, pourtant, en raison de l'impact des valeurs de pH et de l'activité catalytique de certains cations/anions sur la décomposition des peroxydes, il s'agit clairement d'un paramètre critique. Cette étude a donc comparé pour la première fois les produits de décomposition du peroxyde de calcium (CaO_2), du peroxyde de magnésium (MgO_2), du peroxyde de zinc (ZnO_2), du percarbonate de sodium ($Na_2CO_3.1.5H_2O_2$), et du peroxyde d'hydrogène (H_2O_2) à pH 5, 7 et 9. Nous avons identifié un fort effet du pH sur la décomposition du peroxyde et avons également confirmé l'activité des ions carbonate sur la décomposition du peroxyde d'hydrogène. Ces résultats clés ont permis de formuler des films générateurs d'oxygène implantables afin de fournir de l'oxygène directement aux lambeaux sous-cutanés. Nous avons réduit la production de peroxyde d'hydrogène en ajoutant un catalyseur de peroxydase (oxyde de fer), un composé connu pour réagir avec le peroxyde d'hydrogène (bicarbonate), et une barrière polymère hydrophobe (polycaprolactone). Nous avons également ajusté le pH avec un dihydrogénophosphate de calcium acide. Cela a réduit la cytotoxicité puisque l'oxyde de fer a réduit la libération de peroxyde d'hydrogène et le dihydrogénophosphate de calcium a contrôlé le déplacement des valeurs de pH. L'efficacité préclinique dans la réduction de la nécrose ischémique de lambeaux de peau aléatoires a été confirmée. Les films générateurs d'oxygène ont retardé la nécrose des lambeaux de peau mais n'ont pas pu l'empêcher, en particulier dans la zone distale. La nécrose semble multifactorielle et

des stratégies combinées semblent nécessaires pour maintenir l'intégrité de la peau dans laquelle il n'y a pas de flux sanguin.

ACKNOWLEDGEMENTS

Foremost, I would like to sincerely appreciate Dr. Jake Barralet, for his continuous support and incredible supervision during my studies. I deeply grateful for his scientific guidance and valuable inputs over my research path. Working under his supervision was a great opportunity for me to learn and grow as much as possible.

I would also like to heartily thank all the members of our lab team who contributed to this project, Mrs. Yu Ling Zhang, Dr. Benjamin Dalisson, and Dr. Yassine Ouhaddi for their help, support, and advice throughout these two years.

Finally, to my parents Simin and Khodabakhsh, my brother Saeed, my sister Sara, and my best friend Sahand, thank you for the endless love and support and for helping me to always move forward.

TABLE OF CONTENTS

LIST OF FIGURES AND TABLES

ABBREVIATIONS

Bcl-2: B-cell lymphoma 2

cAMP: Cyclic adenosine monophosphate (cAMP)

cFLIP: Cellular FLICE like inhibitory protein

cGMP: Cyclic guanosine monophosphate (cGMP)

CP: Calcium peroxide

CPM: Contralateral prophylactic mastectomy

DAMPs: Damage-associated molecular patterns

DED: Death effector domain

DISC: Death inducing signalling Complex

DOX: Doxorubicin

ECM: Extracellular matrix

EGF: Epidermal growth factor

EPCs: Endothelial progenitor cells

FGF: Fibroblast growth factor

FADD: Fas-associated protein with DD

GSH: Glutathione (GSH)

H&E: Hematoxylin and eosin

HBO: Hyperbaric oxygen

HIF-1: Hypoxia-inducible factor 1

MDCK: Madin-Darby canine kidney

MLKL: Mixed-lineage kinase domain–like

MOMP: Mitochondrial outer membrane permeabilization

MP: Magnesium peroxide

MPT: Mitochondrial permeability transition pore

MRP2: Multidrug resistance-associated protein 2

mTOR: Mammalian target of rapamycin

OGB: Oxygen generating biomaterials

OPB: Oxygen producing biomaterial

PCL: Polycaprolactone

PDE: Phosphodiesterase inhibitor

PDGF: Platelet-derived growth factor

PDMS: Polydimethylsiloxane

PDT: Photodynamic therapy

PGS: Poly (glycerol sebacate)

PLGA: Poly (D, L-lactide–co–glycolide)

PLLA: Poly (L-lactic acid)

PRRs: Pathogen recognition receptors

PS: Photosensitizer

PTMC: Poly (1,3-trimethylene carbonate)

PUAO: Antioxidant polyurethane polymer

PUAO: Encapsulated antioxidant polyurethane

PVA: Polyvinyl alcohol

PVDC: Polyvinylidene chloride

RCD: regulated cell death

RHIMs: RIP homotypic-interacting motifs

RIPK: Receptor-interacting protein kinases

ROS: Reactive oxygen species

SAP: Self-assembling peptide

SPC: Sodium percarbonate

TGF- β: Transforming growth factor-β

TNF: Tumor necrosis factor

TNFR1: Tumor necrosis factor receptor

VEGF: Vascular endothelial growth factor

XIAP: X-linked inhibitor of apoptosis protein

XRD: X-ray diffraction

ZP: Zinc peroxide

CONTRIBUTION OF AUTHORS

In accordance with the thesis guidelines outlined by McGill Graduate and Postdoctoral studies, I decided to present my thesis in a manuscript-based format fulfilling the criteria. Chapter 1 and 2 present an introduction and background review to my research.

Chapter 3 represents my original experimental work written in the form of a submitted paper. Being the first author, I established the research questions and methodology under the guidance of my supervisor. I performed the bulk of all experiments (more than 400 experiments), data collection, and analysis. I drafted the paper and performed all revisions under the guidance of my supervisor. Chapter 4 represents the other experimental work written in the form of a paper in the process of submission. This work was a partially completed manuscript performed by a previous student. First, I confirmed reproducibility by remaking and repeating *in vivo* experiments. I processed *in vitro* characterization, data collection, and performed analysis. I performed cytotoxicity experiments and determined that particle loading in the polymer matrix was a key parameter determining oxygen generating film performance. I rewrote the paper under the guidance of my supervisor. The specific contributions of the co-authors for each manuscript are outlined below.

Aqueous decomposition behavior of solid peroxides: effect of pH and buffer composition on oxygen and hydrogen peroxide release

Benjamin Dalisson helped in designing the experiments and provided technical assistance with characteristic methods. Dr. Jake Barralet provided supervision to all steps of the project and edited the manuscript for publication.

A pilot study of the efficacy of oxygen delivery biomaterial for ischemic skin preservation

Benjamin Dalisson designed the oxygen delivery sheet, executed the skin flap surgeries, analyzed *in vivo* results, and drafted the first version of the paper. Yassine Ouhaddi provided technical assistance with analyzing immunohistochemistry results. Dr. Jake Barralet supervised all steps of the project and edited the manuscript for publication.

CHAPTER 1. INTRODUCTION AND RESEARCH OBJECTIVES

Solid peroxy- compounds include substances derived from hydrogen peroxide by substitution of both hydrogen atoms by a metal cation like Ca, Mg, and Zn. They have potential use in wound healing [1], but historically were used as antimicrobials before the development of antibiotics [2], depending on conditions, either oxygen, hydrogen peroxide or oxygen radicals can be released during their decomposition. Developing formulations that are compatible with mammalian cells has not been attempted previously because the means to engineer tissues did not exist when peroxides were developed in the 1940s as antimicrobials. Nowadays, they have a lot of therapeutic applications like wound healing [3], skin flap viability [4], and tissue engineering [5]. For these applications, solid peroxides should be encapsulated within hydrophobic polymers to control the release rate of caustic byproduct (hydroxide), reduce the cytotoxic hydrogen peroxide generation, and provide sustained and prolonged oxygen release [6]. Recently oxygenation level of tumors has become an area of active research, and there have been several reports of formulations of nanoperoxides that can modify tumor microenvironment through killing tumor cells by releasing hydrogen peroxide/reactive oxygen species (ROS) [7] and also playing a role as an adjunct to other therapies [8]. Solid peroxides can generate molecular oxygen instead of simply delivering it. This enabled peroxides to produce prolonged and sustained oxygen release. The oxygen released by 1 cm^3 of calcium peroxide (CaO_2) is equivalent to oxygen in 57 liters of air. Such a high amount of oxygen can be released progressively via different pH values and/or different hydrophobic materials. The pH value, particle size, temperature, solid peroxides' solubility, buffer composition and catalysts affect solid peroxides' hydrolysis significantly [9]. Until now, the oxygen and hydrogen peroxide formation upon peroxides' decomposition in different buffers with various pH values was not compared, and yet is an important foundation for designing an intended biological effect.

Unmet Clinical Need:

A skin flap is a part of skin, subcutaneous tissue, and sometimes underlying fascia that is excised and transferred with its own blood supply to the defect site located adjacent to or near the flap [10, 11]. Skin flap surgery is common among women with breast cancer. About 1:8 women in the world suffer from invasive breast cancer in their lifetime [12]. Of these women, 33.4% underwent a unilateral mastectomy, and 7.0% underwent contralateral prophylactic mastectomy (CPM) [13].

The incision of mastectomy skin flap necrosis is reported between 5 and 30% in the literature [14]. Insufficient blood supply, oxidative stress and inflammatory response are three main factors that can lead to flap necrosis [15]. There are different techniques to reduce flap necrosis clinically or experimentally. Hyperbaric oxygen therapy (HBO), vasodilators and leeches were considered as clinical methods in reduction of flap necrosis. Although the studies showed the positive impact of HBO on improving flap survival by increasing oxygen tension and angiogenesis, early recognition of flap compromise is necessary to prevent tissue loss. The positive correlation between flap survival and early HBO therapy confirmed the impact of prompt HBO, while the study showed 100% graft loss following starting HBO therapy after 3 days [16]. Because HBO is not available and practical in every situation [17], oxygen delivery to the tissues following the surgical procedure and skin flap surgery can be an addressable method to prevent skin flap failure until perfusion reestablishment. Several studies used topically or subdermally applied biomaterials with oxygen release ability to reduce skin flap necrosis [1, 4, 18]. This release is intended to be sustained to prevent necrosis before the tissue has been sufficiently revascularized [19].

Potential Solutions:

This thesis presents a characterization study of solid peroxides at different pH values and buffer compositions. This was a pre-requisite study for the second publication. We conducted more than 400 experiments to compare different peroxides decomposition and prepare a reference study. These results are not only applicable for oxygen delivery systems allowing enough time for revascularization and reducing hypoxic tumor environment, but they can also be used in designing hydrogen peroxide/ROS release structures in antibacterial applications and tumor killing. The main objectives of the first study were comparing all low toxicity metal cation peroxide decomposition as a function of pH, time, and buffer compositions for the first time. We confirmed the correlation between solid peroxides' decomposition and pH and catalytic impacts of some buffers. All prior work on solid peroxides neglected this effect and just considered incorporation of peroxidase to convert hydrogen peroxide to water and oxygen. Then, we developed an oxygen generating film with sustained oxygen-release capabilities based on previous significant findings. The main objective of the second study was to design a prolonged oxygen delivery system that can support tissues in the absence of vascular blood supply, necrosis, and reperfusion injury. This system provided a sustained oxygen release profile for two weeks and a controlled generation of

hydrogen peroxide. Other objectives were investigating the impact of oxygen delivery on skin flap necrosis.

CHAPTER 2. LITERATURE REVIEW

2.1. Solid Peroxides

Compounds containing O^{2-} or oxygen of -2 oxidation number are called oxides, and prefixes like mono-, di-, etc., demonstrate the number of oxygen atoms within their structures. Substances containing O_2^- like KO_2 with -1/2 oxidation number are called superoxides. These compounds can be considered as derivatives of the acid HO_2. Peroxides or peroxy- compounds contain -O-O- group and present -1 oxidation number for oxygen. Elements with electronegativity less than 2.1 can form peroxy- substances. However, a few elements which have higher electronegativity appear as exceptions, such as Sulfur, Mercury, Nitrogen, and Carbon, that also seem to form peroxy-compounds [20]. Table 2.1 shows peroxides and superoxides of group I and II elements.

Table 2.1. Peroxides and superoxides of group I and II elements [20]. Compounds in parentheses are doubtful substances and those have not yet prepared in a pure state.

Group I		**Group II**	
a	**b**	**a**	**b**
H_2O_2; (HO_2) Li_2O_2; (LiO_2) Na_2O_2; NaO_2 K_2O_2; (K_2O_3) ; KO_2; (KO_3) Rb_2O_2; (Rb_2O_3); RbO_2 Cs_2O_2 ; (Cs_2O_3); (CsO_2) $(NH_4)_2O_2$	($CuO_2.H_2O$)	($MgO_2.xH_2O$) CaO_2; (CaO_4) SrO_2; (SrO_4) BaO_2; (BaO_4) $K_2Ba(O_2)_2O_2$	(ZnO_2) (CdO_2) (Hg_2O2); (HgO_2)

Solid peroxides can be unstable in contact with water and can release molecular oxygen (Eq.1, 2, 3) [21]. Oxygen release from peroxy- compounds contrary to liquid hydrogen peroxide solutions that directly decompose to molecular oxygen, do so in a two-step process [22]. As a matter of fact, inorganic peroxides often form hydrogen peroxide as a result of the hydrolysis process when exposed to water and then release oxygen gas by decomposition of hydrogen peroxide [23, 24].

However, Wang et al. [25] noted that oxygen could also be released directly from the hydrolysis reaction of calcium peroxide (CaO_2) because the endpoint of oxygen and hydrogen peroxide release and the start point of the plateau which express the depletion of CaO_2 was similar for oxygen and hydrogen peroxide release curve. Therefore, there is no oxygen release over depletion of CaO_2 from hydrogen peroxide decomposition and oxygen released directly from CaO_2 at the beginning of experiment.

$$MO_2 + 2H_2O = M(OH)_2 + H_2O_2 \quad (1)$$

$$2Na_2CO_3.1.5H_2O_2 = 2Na_2CO_3 + 1.5H_2O_2 \quad (2)$$

$$2H_2O_2 = 2H_2O + O_2 \quad (3)$$

Simultaneous production of oxygen and hydrogen peroxide by solid peroxides expands the medical application of solid peroxides. Calcium peroxide (CaO_2), Magnesium peroxide (MgO_2), Zinc peroxide (ZnO_2) and, Sodium percarbonate ($Na_2CO_3.1.5H_2O_2$) are the mostly evaluated compounds in biological applications. Their use is not just limited to oxygen delivery and reduction in apoptosis and necrosis; they have also been explored in antibacterial [26] and tumor therapy applications [27]. We will discuss these therapeutic applications in the next section.

2.1.1. Therapeutic applications of solid peroxides

Table 2.2 summarize several applications of solid peroxides as oxygen releasing biomaterials. For these applications, solid peroxides should be encapsulated within hydrophobic polymers to control the release rate of caustic hydroxide byproduct ($M(OH)_2$) over the reaction (Eq.1), reduce the cytotoxic hydrogen peroxide generation, and provide sustained and prolonged oxygen release [6]. For example, CaO_2 nanoparticles were loaded in poly (D, L-lactide–co–glycolide) (PLGA) to slow down oxygen generation [28]. Encapsulation of CaO_2 in polycaprolactone (PCL) by Tripathi et al. [3] prevented burst release of oxygen from the scaffold. In another work, a wound dressing was developed, which was composed of four different layers. $Na_2CO_3.1.5H_2O_2$ and CaO_2 as oxygen sources were loaded in layer 2 and incorporated into PCL and polyvinyl alcohol (PVA). Layer 1 was a gelatin-based layer, forming the contact surface with the wound. Layer 3 provided the mechanical stability and flexibility as a silicon-based layer and the last layer was a polyvinylidene chloride (PVDC)-based layer with low gas and vapor permeability. Therefore, oxygen delivery can be controlled by peroxides concentration, polymer matrix elements in layer 2, and/or

modifying layer 1 in the wound dressing. In this study, this formulation provided a sustainable oxygen release for 3-4 days [29].

Table 2.2. Recent biomedical applications of peroxides.

Application	Solid peroxides	Formulation	Catalysts	Ref
Wound Healing	$Na_2CO_3.1.5H_2O_2$	PCL	—	[30]
	$Na_2CO_3.1.5H_2O_2$, CaO_2	Gelatin/PVA/PCL	$MnCl_2$	[29]
	CaO_2	Alginate	Catalase	[31]
		PCL	Catalase	[3]
Ischemic Skin Flap Treatment	CaO_2	PTMC	—	[18]
		PUAO	—	[4]
	$Na_2CO_3.1.5H_2O_2$	PLGA	—	[1]
Tissue Engineering Scaffold	CaO_2	Keratin/Silk	—	[32]
		PLGA	MnO_2	[33]
		PGS/PCL	Catalase	[34]
		Gelatin Methacryloyl	—	[5]
		PLLA	Catalase	[35]
		Gelatin/SAP/PLGA	—	[36]
Cell Viability Enhancement	CaO_2	PDMS	—	[37]
		PTMC	Catalase	[38]
		PCL	—	[39]
		Alginate	—	[40]
Improvement of Chemotherapy Efficiency	CaO_2	Cross-linked alginate	Catalase	[41]
		Cross-linked gellan gum	Catalase	[42]
		Dioleoyl-sn-glycero-3-phosphate sodium salt (DOPA)	—	[43]
Enhancement of PDT Treatment Efficiency	CaO_2	—	MnO_2	[44]
		Hydrophobic halogenated aza-BODIPY dye (B1)/NH_4HCO_3 liposomes	—	[45]
		Methacrylate based co-polymer coating	—	[8]

Recently oxygenation level of tumors has become an area of active research, and there have been several reports of formulations of nanoperoxides that can modify the tumor microenvironment [27, 45, 46]. Chemotherapy is used to treat cancer by using anticancer drugs like doxorubicin (DOX). The effectiveness of DOX is dependent on oxygen availability, which is restricted in hypoxic tumor tissue. Therefore, local oxygen delivery to tumor cells by solid peroxides can improve DOX cytotoxicity [41]. In one study, lipid coated CaO_2/cisplatin nanocarriers were used to improve the anticancer effect of cisplatin by glutathione (GSH) oxidation and blockage of the drug efflux pathway. In fact, GSH binding interaction with cisplatin and its antioxidant activity reduce chemotherapy efficiency. Also, inadequate oxygen levels in hypoxic tumors activates hypoxia-inducible factor 1 (HIF-1) and then multidrug resistance-associated protein 2 (MRP2), leading to excretion of cisplatin from the tumor. They reported the diminished expression of HIF-1, downregulation of MRP2, and then inhibition of efflux pathway by using CaO_2 based nanocarriers (Fig. 2.1). Therefore, CaO_2 improved cisplatin anticancer therapy [43]. Newland et al. [42] developed a cross-linked gellan gum hydrogel loaded with CaO_2, catalase, and DOX. They investigated the impact of oxygen delivery on DOX anti-tumor efficiency. The results showed no difference in cytotoxic activity between oxygen-releasing hydrogels (with DOX and catalase) and free DOX while omitting catalase and preventing the conversion of hydrogen peroxide to oxygen increased DOX cytotoxicity. Therefore, for cancer therapies, increasing oxidative stress can be desirable either directly or as an adjunct to other therapies [27, 46-50].

Inadequate oxygen levels in tumors also affect the existing photodynamic therapy (PDT) systems [45]. PDT is based on three required components: photosensitizer (PS), oxygen, and light. The PS is activated by light of a specific wavelength and transferred from the ground state to an excited singlet state. The excited triplet state reaction involves two different pathways: pathway I is the reaction between PS excited and substrates, producing unstable radicals through electron or proton transfer, and pathway II is the excited PS reaction with molecular oxygen, forming singlet oxygen through energy transfer [51, 52]. Moreover, oxygen consumption over the PDT process can exacerbate the hypoxic environment [45]. Solid peroxides and solid peroxides/catalysts systems with oxygen release ability can allay hypoxic tumor environment and boost PDT efficiency. In one study, manganese dioxide (MnO_2) has been used as a catalyst to convert hydrogen peroxide release from solid peroxides to oxygen and increase oxygen release rate, leading to relieving tumor hypoxia rapidly. The results demonstrated rapid and sufficient oxygen release from CaO_2/MnO_2

nanoparticles and a high rate of singlet oxygen generation. The *in vivo* impact of catalyzed oxygen release from CaO_2/MnO_2 nanoparticles was also investigated by intravenous MnO_2 nanozyme injection and intratumor CaO_2 and Ce6 injection on tumor-bearing mice. Significantly more apoptotic cells were observed over PDT treatment with Ce6 + CaO_2/MnO_2 than Ce6 alone, confirming improvement of PDT treatment efficiency via relieving tumor hypoxia [44].

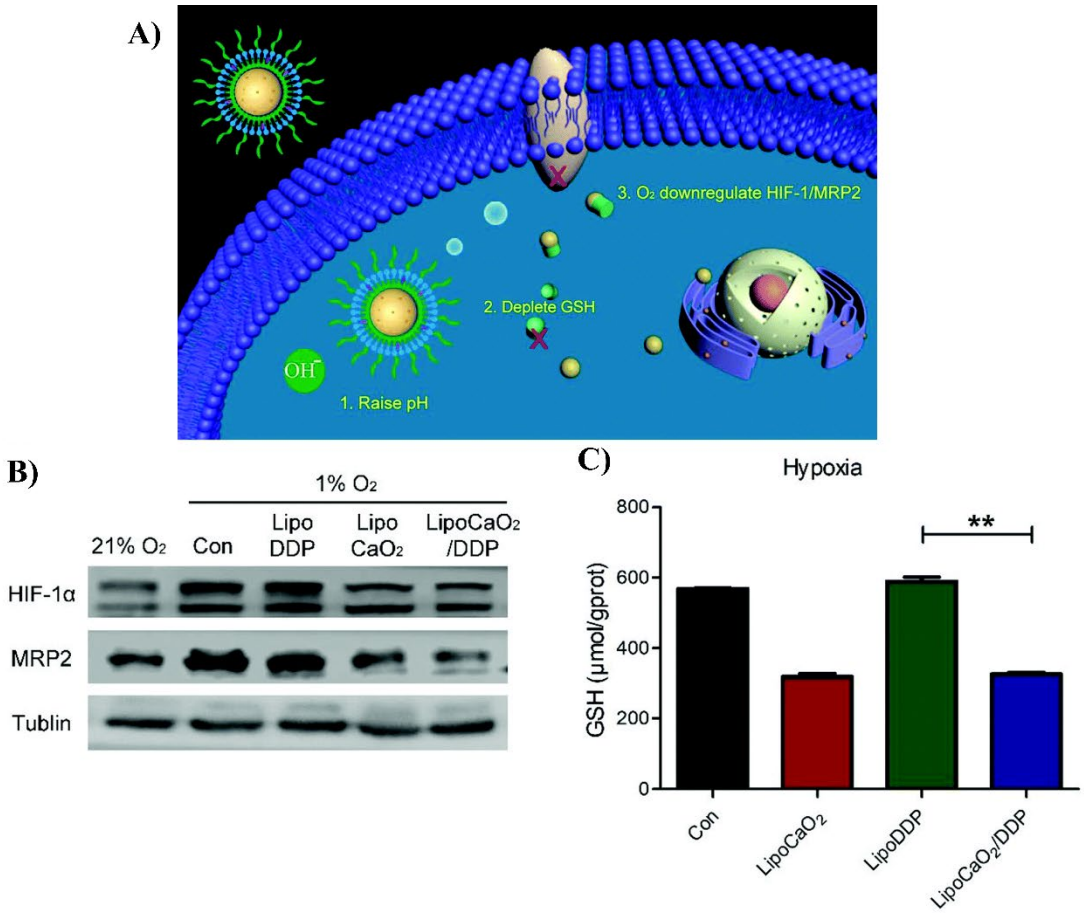

Fig. 2.1. Improvement of cisplatin anticancer efficiency by CaO_2. (A) CaO_2 can improve chemotherapy efficiency by (1) raising the local pH; (2) oxidizing GSH under alkaline conditions and inhibiting cisplatin/GSH binding; and (3) inhibiting the expression of MRP2 by HIF-1 degradation and preventing the excretion of cisplatin–GSH complex. **(B)** Less expression of endogenous HIF-1α and protein MRP2 because of oxygen supply by CaO_2. **(C)** GSH content of hypoxic HepG2 cells under various treatments (LipoCaO₂/DDP is CaO_2 nanoparticles loaded with cisplatin) **p < 0.01. *Reprinted with permission from Royal Society of Chemistry: C. He et al., "Enhancement of cisplatin efficacy by lipid–CaO_2 nanocarrier-mediated comprehensive modulation of the tumor microenvironment," Biomaterials Science, vol. 7, no. 10, pp. 4260-4272, 2019.*

2.1.2. Factors affecting solid peroxides' decomposition

The pH value, particle size, temperature, solubility of peroxides, presence of buffers or catalysts can affect solid peroxides' hydrolysis significantly [9]. According to Table 2.3, calcium peroxide hydrolysis rate, the amount of released hydrogen peroxide, and the stability of hydrogen peroxide increase with decreasing pH values. For example, there is no measurable hydrogen peroxide generation for CaO_2 in water with a pH of 12-13 after 160 hours, but CaO_2 was completely dissolved at pH of 8 over 52 hours. Reduced hydrogen peroxide production and increased O_2 released as a result of growing pH values can come from hydrogen peroxide disproportionation at alkaline pH values or directly from CaO_2 decomposition [53]. Decreasing particle size also increases the hydrolysis reaction rate of CaO_2. Khodaveisi et al. increased the oxidation reaction between silver nanoparticles and CaO_2 by the synthesis of nanosized CaO_2. The reaction rate of nanosized CaO_2 was more rapid than that of CaO_2 in microsize with silver nanoparticles, so nanoparticles provided more hydrogen peroxide for silver compared to microparticles [54].

Compared to magnesium and calcium peroxide, zinc peroxide can retain its peroxide over a wide pH range and will decompose in the acidic pH (around 4-6). In other words, calcium and magnesium peroxide released 50% of the peroxide content around pH 9, while zinc peroxide dissolved 50% of its peroxide content at pH 5 [55]. Therefore, oxygen release from zinc peroxide is controllable by the pH value of the dispersion media, and released oxygen increases by decreasing pH values [56]. In addition to the influence of pH, particle size and temperature affect zinc peroxide decomposition. The amount of released oxygen and oxygen release rate from synthesized ZnO_2 is more than bulk particles because of the larger surface area [57]. There is a negative correlation between temperature and ZnO_2 solubility; higher temperatures can lead to less solubility of ZnO_2 [55].

$Na_2CO_3.1.5H_2O_2$ exhibits the highest oxygen release rate from solid peroxides. Oxygen release kinetics from $Na_2CO_3.1.5H_2O_2$ is dependent on temperature, pH, catalysts, and incorporation of particles within biomaterials. A study showed that incorporating $Na_2CO_3.1.5H_2O_2$ in silicon films can delay oxygen release rate from $Na_2CO_3.1.5H_2O_2$ about tenfold [58]. Zehra et al. [59] entrapped $Na_2CO_3.1.5H_2O_2$ particles within electrospun nanofibers to provide a sustained oxygen release for a minimum 4 days in diabetic wounds. The results showed that hydrophobic fibers could control oxygen release for up to 10 days and also can induce blood vessel formation [59].

Table 2.3. Hydrogen peroxide yield from a 0.2% (w/v) slurry of CaO_2 in water and the time required for complete CaO_2 dissolution at different pH values [53].

pH	Hydrogen peroxide yield (%)	Oxygen yield (%)	Time required for dissolution
6	82	18	4h
7	74	26	20h
8	65	35	52h
9	47	53	6 days
12-13	0	100	62 days

2.2. Ischemic Skin Flaps

Flap is a part of the skin, subcutaneous tissue, and sometimes underlying fascia that is excised and transferred with its own blood supply to the defect site located adjacent to or near the flap [10, 11], in contrast to graft, which is transferred from one region to another without blood supply immediately restored [10]. Skin flap as a reconstructive surgery originated from northern India around 600 BC, when Susruta developed an early version of flap rhinoplasty after amputation of the nose [60]. Then by spreading syphilis to Europe, Tagliacozzi developed a technique to reconstruct the nose with a pedicle flap from the arm, but his work was disregarded by the church and his peers [61]. However, the need for the advancement of reconstructive surgery because of extending traumatic amputation and excessive burn wounds during world war I and II led to the redevelopment of skin flap methods [60].

Skin flaps are divided into two different groups: pedicled and free skin flap. Pedicled flaps are connected to the intrinsic blood supply and the site of origin [62], while vascular supply of free flaps needs to be detached from isolated tissue and be joined to the recipient's vessels after transplantation of flap to some other part of the body [63]. Skin flap can also be classified based on the vascular supply to the flap as musculocutaneous, fasciocutaneous, axial, and random flaps (Fig. 2.2). Musculocutaneous and fascioctaneous flaps include muscle and fascia (the connective tissue covering muscles) in the flap base [64]. Axial flaps are a type of pedicled flaps which are based on identifiable blood sources, making them reliable flaps with reliable blood supply [11]. The survival length of axial flaps is dependent on the included artery length [10]. The blood supply for random skin flaps is not derived from a named and reliable artery, but they are supported by

subdermal and intradermal plexuses [65]. The positive correlation between viable length and width of random flaps was one of the established principles in plastic surgery [66]. The classical concept was greater width of the flap with more blood supply which can support more flap length. Milton [66] studied the impact of changing the width on the viable length of flap. There was no proportional relation between width and survival length and survival length under similar conditions of blood supply was constant, regardless of flap width. Physical properties of the vascular supply and perfusion pressure are key factors in random flap survival. A perfusion pressure lower than the critical closing pressure of the capillary bed will cease nutritional blood flow and cause flap necrosis at the distal area. Although widening the flap incorporates additional blood vessels, it does not change the perfusion and critical closing pressure and thus survival length (Fig. 2.3) [10].

Aherrera et al. [67] also investigated the impact of increasing flap length on skin flap survival while keeping the width identical. The hypothesis was the reduction of flap survival by a greater length-to-width ratio. The results showed no significant difference in survival area/length of random flaps with length-to-width ratios of 3:1, 4:1, and 5:1. Therefore, the same degree of skin flap necrosis confirmed that relation between length-to-width ratio and flap survival might not be rigid and uncompromised as conventionally thought. There is a recommendation for length-to-width ratios of the random flap in severe areas of the body, such as 3:1 for random flaps of face and 2:1 for flaps on the trunk and the leg. It originates from the regional difference of blood supply to the skin. However, it should not imply that widening the flap base can improve the survival length.

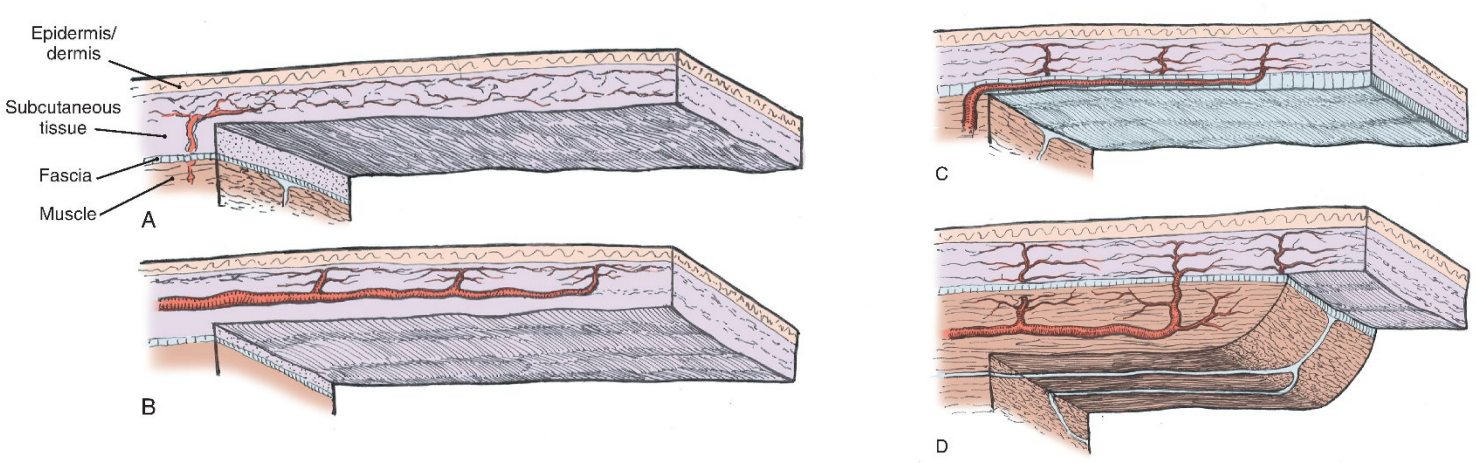

Fig. 2.2. Skin flap classification based on blood supply. A) Random, **B)** Axial. **C)** Fasciocutaneous and **D)** Musculocutaneous. *Reprinted with permission from Elsevier Books: S. R. Baker, Local Flaps in Facial Reconstruction. Elsevier Health Sciences, 2007.*

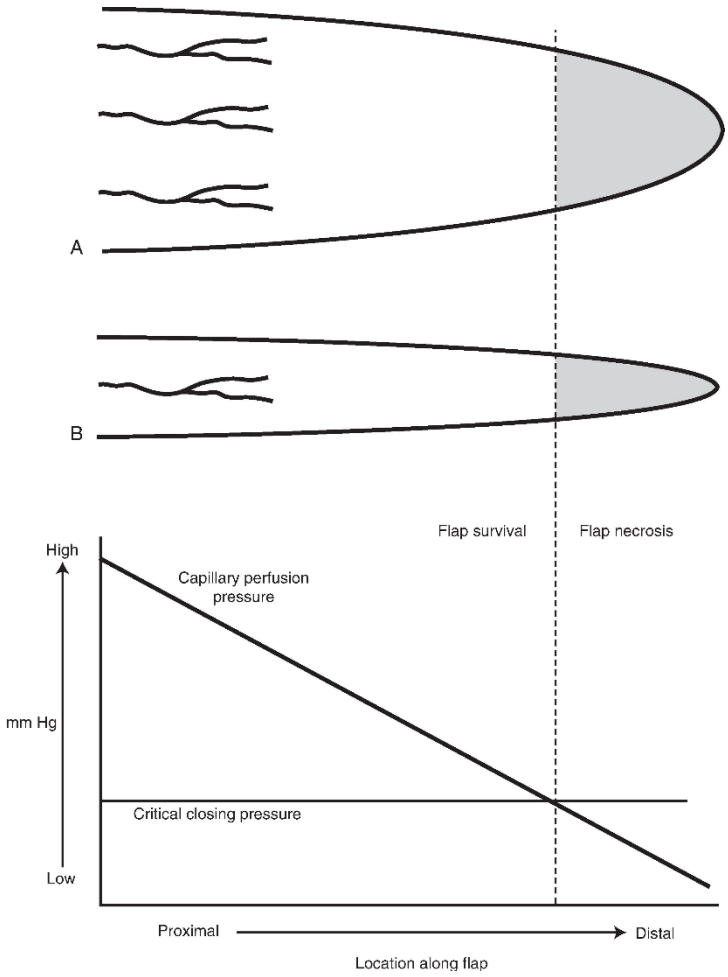

Fig. 2.3. No change in survival length by increasing the flap width. Due to lack of alternation in perfusion pressure and critical closing pressure. Perfusion pressure less than critical closure pressure can cause flap necrosis. *Reprinted with permission from Elsevier Books: S. R. Baker, Local Flaps in Facial Reconstruction. Elsevier Health Sciences, 2007.*

2.2.1. Ischemia and flap necrosis

Ischemia is caused by the inadequate blood supply to tissues due to total or partial, permanent, transient, or cyclical obstruction of arterial inflow [68], impaired venous return, vasospasm, and thrombosis [69]. In oxygen absence, cells switch to respiring via the anaerobic metabolism glycolysis, which results in a decrease in cellular pH and ATP production. To buffer this rapid accumulation of hydrogen ions, excretion of substantial hydrogen ions and influx of sodium ions in turn occurs by Na^+/H^+ exchanger [68]. Intracellular ATP depletion as a result of anaerobic ATP production inactivates Na^+/K^+ ATPase, ATP dependent Ca^{2+} excretion, and Ca^{2+} reuptake into the endoplasmic reticulum. This leads to calcium accumulation inside the cells [68, 70, 71]. Thereby, hyperosmolarity occurs due to overloaded calcium and sodium ions in the cells, which leads to water flow into the cytoplasm and cell swelling and ultimately rupture [72]. Moreover, the mitochondrial membrane potential is disrupted by the opening of the mitochondrial permeability transition pore (MPT), which also impairs ATP production [68]. Prompt reperfusion reintroduces oxygen and substrates to previously ischemic tissue required for aerobic ATP production and can also normalize extracellular pH through washout. Although rapid reoxygenation reduces ischemia-induced injuries, it can cause a phenomenon known as reperfusion injury in parallel via excessive reactive oxygen species (ROS) generation (mainly superoxide), calcium overload, and MPT pore opening [68, 71]. Physiologically, ROS are inactivated by catalase and converted to oxygen and water, but excessive ROS production is beyond the catalytic response of antioxidants in ischemic cells [71, 73]. Therefore, oxidative stress because of ROS promotes endothelial dysfunction, DNA damage, and pronounced inflammatory responses [73]. During the reperfusion stage, neutrophils are also recruited to the site and produce a host of inflammatory factors, including interleukins and free radicals in response to tissue injury. Endothelial cells also release cytokines and pro-adhesive molecules to adjust the inflammatory response [74]. Insufficient blood supply, oxidative stress, and inflammatory response are then the three main factors leading to flap necrosis [15]. However, these are not the exclusive causes of flap necrosis. Venous congestion frequently occurs after skin flap transplantation. It can result in thrombosis in tissue microcirculation and can negatively impact tissue nutrition. Flap necrosis and surgical failure are often the consequences of not diagnosing and treating venous congestion in time [75, 76]. Aside from accidental cell death caused by physical damage, cells can undergo several programmed cell death modes, including apoptosis, necroptosis, and autophagy [70]. While causes of cell death are reasonably well studied,

the impact on cell death mode and any subsequent clinical relevance of programed death modes are only recently being evaluated.

2.2.1.1. Apoptosis

Apoptosis as a form of regulated cell death (RCD) can occur through two main apoptotic pathways: the intrinsic or mitochondrial pathway and extrinsic or death receptor pathway [77]. Apoptosis is induced by hypoxic stress in ischemic injury and high ROS generation in reperfusion injury.

Extrinsic Pathway

The extrinsic pathway is driven by death receptors, including Fas cell surface death receptor (Fas) and tumor necrosis factor (TNF) receptor superfamily [78]. In their extracellular domain, they have one to five cysteine-rich repeats, and in the cytoplasmic domain they include a 60 to 80 amino acid cytoplasmic sequence which is named the death domain (DD) [79]. Activation of death receptors can cause the formation of the death inducing signalling complex (DISC) and initiate the death signal (Fig. 2.4) [80]. In more detail, the binding between the Fas receptor and the Fas ligand causes oligomerization of receptors and makes a homotypic interaction between the DD of these receptors and the DD of Fas-associated protein with DD (FADD). FADD as adapter proteins may also contain a death effector domain (DED). FADD recruits inactive initiator caspases-8 and -10 and inhibitory protein (cFLIP) through homotypic interactions between their death effector domains (DEDs) and then drives DISC [77]. This interaction between FADD and caspases induces the cleavage and activation of the downstream executioner caspases, such as caspase-3 [80].

Intrinsic Pathway

Intrinsic apoptosis is non-receptor mediated and is based on mitochondria. The intrinsic pathway can be initiated by intracellular signals. Signals such as radiation, toxins, hypoxia, hyperthermia, viral infections, and free radicals can initiate apoptosis [81]. Apoptotic cell death induced by ischemia/reperfusion injury is not as common as necrosis [70].

This pathway is based on mitochondrial outer membrane permeabilization (MOMP), with the release of pro-apoptotic proteins like cytochrome c that are stored in the intermembrane space of mitochondria into the cytosol [82]. The regulation of cytochrome c release occurs through protein of Bcl-2 (B-cell lymphoma 2), family. They are divided into three different subsets, pro-survival members (Bcl-2, Bcl-xL, Bcl-w, Mcl-1, and A1), pro-apoptotic members (BAX and BAK) and 'BH3-only' proteins [78]. Upon a death signal, pro-apoptotic 'BH3-only' proteins activate BAK

and BAX, thereby inducing MOMP and release of apoptogenic protein (cytochrome c) [82]. Released cytochrome c, Apaf-1, Caspase-9 and dATP/ATP form a complex (apoptosome) which is responsible for Caspase-9 (initiator caspase) activation, which subsequently activates the effector caspases, caspase-3 and -7. The effector caspases regulate the proteolytic degradation of a broad spectrum of cellular targets that ultimately lead to cell death [83] (Fig. 2.5).

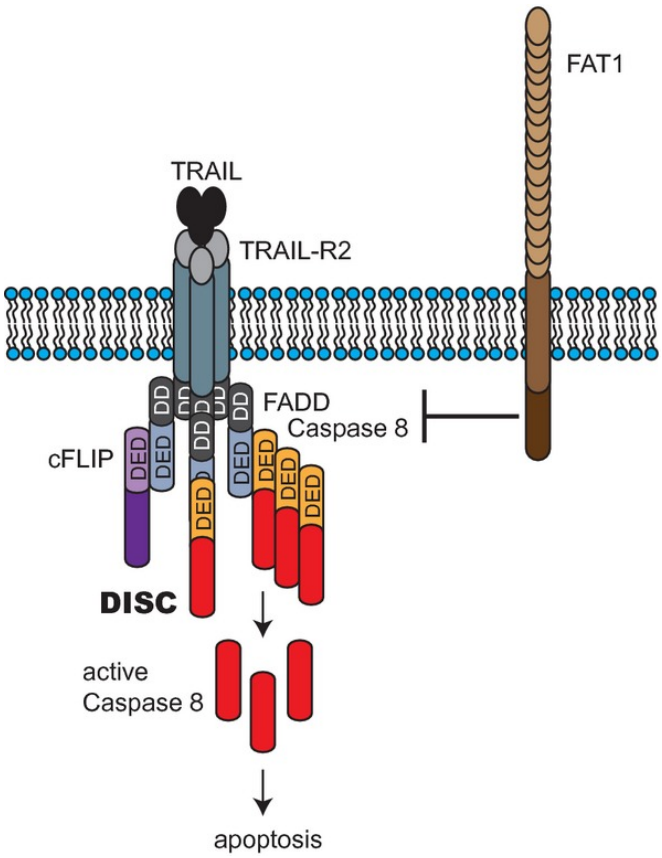

Fig. 2.4. The death inducing signalling complex. After dead receptor ligation, death receptors recruit FADD through their cytosolic DD. Then, FADD recruits caspase-8 (or caspase-10) via its DED to form the death-inducing signalling complex (DISC) and activate caspase-8. Death receptor-mediated apoptosis can be inhibited through a protein called c-FLIP, which binds to FADD and caspase-8. FAT1 also inhibits the binding of caspase-8. *Reprinted with permission from John Wiley and Sons: D. Kranz and M. Boutros, "A synthetic lethal screen identifies FAT1 as an antagonist of caspase-8 in extrinsic apoptosis," The EMBO Journal, vol. 33, no. 3, pp. 181-197, 2014.*

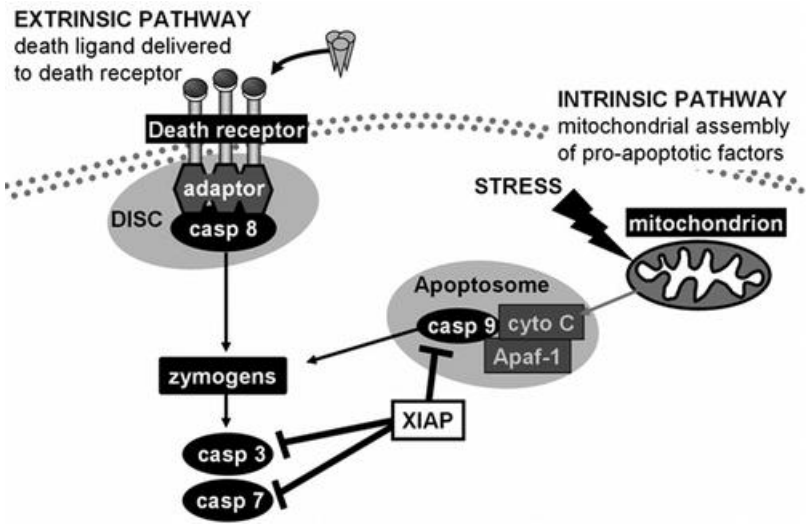

Fig. 2.5. Simplified extrinsic and intrinsic apoptosis pathways. Formation of the death-inducing signaling complex (DISC) upon receptor-ligand binding, recruiting adaptor molecules, and caspase-8. This is termed the extrinsic pathway. In the intrinsic pathway, the mitochondria release cytochrome c from the intermembrane space into the cytosol. This induces the formation of the apoptosome, which activates caspase-9. Active caspase-8 and -9 can cleave and activate the caspases-3 and -7 effectors. X-linked inhibitor of apoptosis protein (XIAP) inhibits caspases-3, -7, and -9. *Reprinted with permission from Springer Nature: S. J. Riedl and F. L. Scott, "Caspases: Activation, Regulation, and Function," in Essentials of Apoptosis: Springer, 2009, pp. 3-24.*

2.2.1.2. Autophagy

Autophagy (self-digestion) is characterized by the disposal of damaged organelles and protein aggregates by packaging into double or multimembrane structures (autophagosome), followed by degradation of the contents by fusing to lysosomes [84, 85].

This process also occurs in ischemia when cells are starved of nutrients and oxygen to promote cell survival by generating substrates for maintenance of cell function [70]. Therefore, autophagy is considered a cell survival process instead of cell death. However, uncontrolled autophagy may ultimately contribute to cell death and ischemia/reperfusion injury [68].

The autophagy process involves 4 consecutive steps (1) sensing of autophagy ‘‘triggers’’ and induction of autophagy; (2) autophagosomes assembly and formation; (3) autophagosomal fusion with the lysosomal membrane; and (4) degradation of the autophagic body [85]. Autophagy is regulated by the mammalian target of rapamycin (mTOR), which inhibits the mechanism. However, ischemic/reperfusion-associated conditions like nutrient withdrawal and oxidative stress can inactivate mTOR [70].

2.2.1.3. Necroptosis

Necrosis originates from the Greek kernel 'necros', meaning dead [86], and is considered an accidental, unprogrammed death of cells that occurs under total ATP depletion [87]. Necrosis, as a passive process, does not require new protein synthesis and is not dependent on any homeostatic mechanism. In humans, cell death by necrosis results from severe changes in physiological conditions, including hypoxia, ischemia, hypoglycemia, exposure to reactive oxygen species, toxin exposure, extreme temperature alterations and nutrient deprivation [86]. Although necrosis has historically been considered as a passive and ''accidental'' process that occurs accidentally, experimental evidence in mammalian cells shows some forms of necrosis which are regulated (necroptosis) [88]. Necroptosis is a form of RCD initiated during impaired apoptosis by ligation of specific death receptors, including FAS and TNFR1 (tumor necrosis factor receptor), or pathogen recognition receptors (PRRs), including TLR3, TLR4, and Z-DNA binding protein 1 [77]. TNF-driven necroptosis is regulated by receptor-interacting protein kinases 1 and 3 (RIPK1 and RIPK3), which interact by virtue of intrinsic RIP homotypic-interacting motifs (RHIMs). The interaction between RIPK1 and RIPK3 leads to autophosphorylation, transphosphorylation, and "necrosome" complex assembly. RIPK3-mediated MLKL (mixed-lineage kinase domain–like) phosphorylation plays a crucial role in necroptosis execution. The pseudokinase MLKL domain phosphorylation uncovers a latent N-terminal 4–helix bundle (4HB) domain, necessary for cell lytic activity. MLKL interaction with phosphatidylinositol phosphates can promote the membrane pore opening, and MLKL assimilation at the plasma membrane can also recruit ion channels, inducing Ca^{2+}, Na^{+}, and K^{+} ions flux [89, 90]. MLKL-dependent necroptotic membrane permeabilization afterward results in releasing cellular cytoplasmic components and necroptosis-related DAMPs (damage-associated molecular patterns) that can promote inflammation in distal tissues [89] (Fig. 2.6).

In next section, we investigated the morphological features of apoptosis and necrosis in hematoxylin and eosin (H&E) stained sections to differentiate them in experimental results.

2.2.2. Morphological characteristics of apoptosis in H&E-stained tissue sections

In the absence of experimental induction, apoptotic cells occur as either single and noncontiguous cells or small cells clusters alone or scattered inside a tissue section (Fig. 2.7A). However, massive apoptosis of most cells can occur as a result of experimental induction [88]. In apoptosis, cell size

is reduced, the cytoplasm is hypereosinophilic and dense [91]. The nucleus may be fragmented into two or more fragments (karyorrhexis). The apoptotic cells show considerable membrane blebbing, which is followed by breaking the dead cells into apoptotic bodies, composed of cytoplasm, tightly packed cytoplasmic organelles and with or without fragmented nuclei (Fig. 2.7A) [91]. The cytoplasmic apoptotic bodies can be engulfed by tingible body macrophages [88] (Fig. 2.7B).

2.2.3. Morphological characteristics of necrosis in H&E-stained tissue sections

Necrotic cell death is characterized morphologically by loss of cell membrane integrity, which modulates an influx of extracellular ions and fluid, leading to cell swelling and its organelles. Another cellular mechanism of necrosis is based on the compromise of organelle membranes, which allows the proteolytic enzymes to flow into the cytoplasm and digest the cell [88].

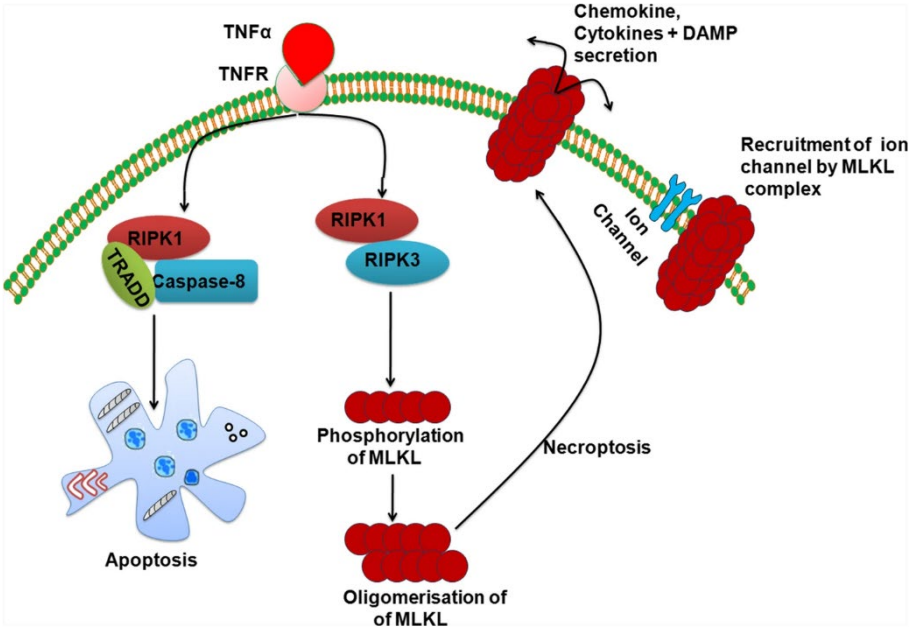

Fig. 2.6. Molecular mechanism of apoptosis and necroptosis. Death receptor controls both extrinsic apoptosis and necroptosis; RIPK1 plays a pivotal role in apoptosis and necroptosis. Caspase-8 activation triggers the pathway towards apoptosis while its inhibition resulting in necroptosis. *Reprinted with permission from Springer Nature: Y. K. Dhuriya and D. Sharma, "Necroptosis: a regulated inflammatory mode of cell death," Journal of Neuroinflammation, vol. 15, no. 1, p. 199.*

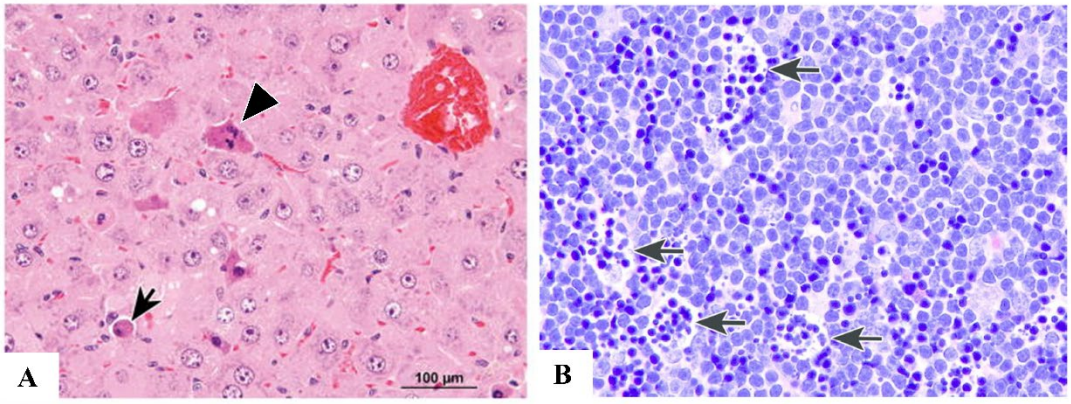

Fig. 2.7. Apoptosis in H&E-stained sections. (A) Example of apoptosis in the liver, arrowhead: apoptotic cells with hypereosinophilic cytoplasm (cytoplasmic condensation) and small pyknotic and fragmented nuclei, which are smaller than surrounding unaffected hepatocytes, arrow: apoptotic bodies. *Reprinted with permission from SAGE Publications: S. A. Elmore et al., "Proceedings of the 2013 National Toxicology Program Satellite Symposium," Toxicol Pathol, vol. 42, no. 1, pp. 12-44.*
(B) the cytoplasmic apoptotic bodies engulfed by tingible body macrophages. *Reprinted with permission from SAGE Publications: S. A. Elmore et al., "Recommendations from the INHAND Apoptosis/Necrosis Working Group," (in eng), Toxicol Pathol, vol. 44, no. 2, pp. 173-88, Feb 2016.*

The increased cellular swelling results in disruption of the plasma membrane and leakage of the cytoplasmic contents into the extracellular space. The release of cellular contents of necrotic cells acts as signals that trigger the production of cytokines and thereby induce inflammation. Some specific substances released from necrotic cells have been known as damage-associated molecular patterns (DAMPs) [91]. The most significant distinction between programmed cell death (i.e., apoptosis and autophagy) and necrosis is plasma membrane disruption and the consequent activation of inflammation in the affected tissue induced by the leakage of intracellular substances [87].

Necrotic cells are characterized by cell and nuclear swelling and increased eosinophilia in H&E-stained sections (Fig. 2.8). This is in contrast to the smaller and shrunken apoptotic cell. Necrotic cells can also show three nuclear patterns, 1) karyolysis (breakdown of DNA because of enzymatic degradation by endonuclease, 2) pyknosis (nuclear shrinkage and increased basophilia) and 3) karyorrhexis (pyknotic nucleus fragmentation) [91]. In case of cell membrane rupture, adjacent cellular debris and inflammatory cells (neutrophils, macrophages, etc.) may also be present. Similarly, contiguous cells containing the same characteristics as single necrotic cells may be seen in focal or diffuse areas of necrosis [88].

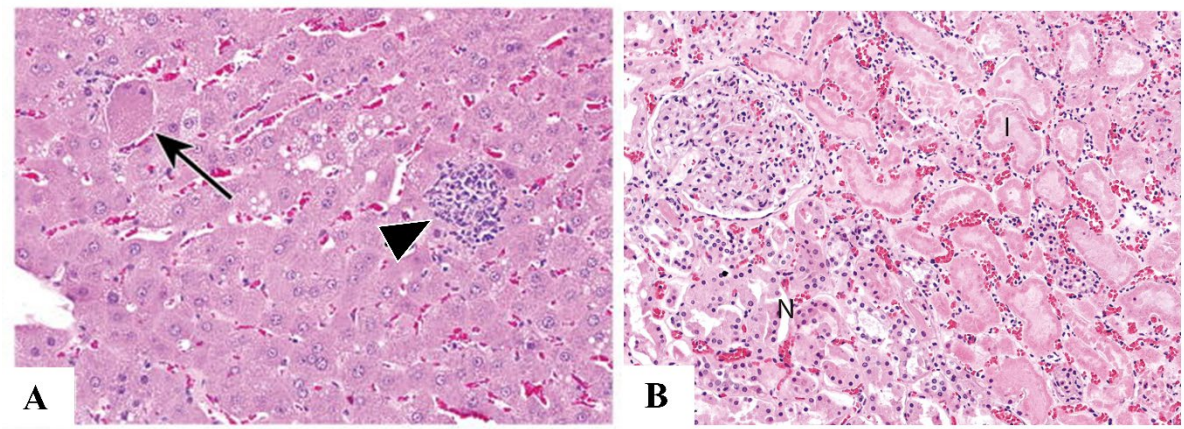

Fig 2.8. Necrosis in H&E-stained sections. (A) Example of single cell necrosis in a necrotic hepatocyte, arrow: marked cell swelling and karyorrhexis and arrowhead: inflammation. *Reprinted with permission from SAGE Publications: S. A. Elmore et al., "Proceedings of the 2013 National Toxicology Program Satellite Symposium," Toxicol Pathol, vol. 42, no. 1, pp. 12-44.*
(B) The histology slide of the kidney. N, shows the healthy cells that are less pink and have nuclei present. I, indicates the necrotic portion with preserved cellular outlines without nuclei and presence of inflammatory cells in between necrotic tubules. *Reprinted with permission from Elsevier: V. Kumar, A. K. Abbas, and J. C. Aster, Robbins & Cotran Pathologic Basis of Disease E-Book. Elsevier Health Sciences, 2020.*

2.2.4. Current approaches for enhancing skin flap viability

2.2.4.1. Clinical methods

Improving blood flow to the skin flap area through pharmaceutical drugs has been proposed as a method to increase skin flap viability. Vasodilators theoretically should enhance blood flow to a hypoperfused distal portion of the skin flap. Sildenafil is a phosphodiesterase inhibitor (PDE 5) that acts on phosphodiesterase enzymes. The crucial role of these enzymes is the separation of a phosphate group from the target cell and inactivation of cyclic adenosine monophosphate (cAMP) or cyclic guanosine monophosphate (cGMP) [92]. Phosphorylation of the smooth muscle contractile protein myosin by cGMP contributes to myosin relaxation and vessel dilation. PDE 5 inhibitors have a prevention role in the dephosphorylation of myosin, thus exhibiting vasodilation to be sustained for a longer period of time. This may cause mitigating the detrimental secondary effects of vasoconstriction such as reduced flap perfusion, free radical-mediated injury, venous insufficiency, and edema [93]. In addition, Nitroglycerin (NTG) functionally boosts local blood flow by dilating both arteries and veins without changing precapillary to postcapillary resistance ratio [94]. Topical NTG can also lead to synthesizing prostacyclin by endothelial cells, which can suppress platelet activation. Prostacyclin is considered a functional vasodilator, which may improve flap survival by diminishing the thrombosis of smaller vessels [95].

The impacts of NTG and Sildenafil as vasodilators on skin flap necrosis are widely studied. Hart et al. [93] reported that intraperitoneal (IP) injection of Sildenafil significantly reduced flap necrosis at earlier postoperative time points (1 and 3 days), while the reduction was not as significant at time periods of 5 and 7 days against control. A study by Sarifakioglu et al. [96] showed a dose-dependent relationship between flap survival and oral sildenafil administration, which survival area in the sildenafil-treated group receiving 3mg/kg/day was statistically identical to control group. In contrast, Barral et al. revealed that subdermally use of Sildenafil was associated with higher necrotic areas over the control group. This contrast in results may be owing to using different doses or various administration routes. Most publications have concluded that systemic delivery of Sildenafil, orally and IP administrations, is more beneficial in reducing skin flap necrosis than local application [97].

Ellabban et al. [97] investigated the combined administration of Sildenafil (orally) and NTG (topically) on skin flap necrosis. The results showed a significant increase in skin flap viability, less apoptotic index, and greater epidermal thickness. Similarly, a human study revealed the positive impact of the low-dose application of NTG ointment on the viability of skin flap after immediate breast reconstruction [95]. Nevertheless, there was no augmentation of skin flap viability as a result of using NTG in studies of Smith et al. [98] and Sá et al. [99]. These controversial results can be because of systemic hypotension consequences of using vasodilators which seems to be detrimental to blood flow and skin flap survival [100]. Therefore, adjusting the doses, administration route, and treatment duration is a principle to avoid the possible hypotensive effects of vasodilators [97].

2.2.4.2. Preclinical methods

Growth factors and pharmaceutical approaches

Skin regeneration is a dynamic process involving the sequential expression of several growth factors and cytokines in order to regulate the critical cellular processes for regeneration. The growth factors which are expressed over the wound healing process include vascular endothelial growth factor (VEGF), platelet-derived growth factor (PDGF), epidermal growth factor (EGF), and transforming growth factor-β (TGF-β) [101]. The expression of VEGF family in injury-based hypoxia is significantly up-regulated, while its production is negligible in normal skin. The growth factors like TGF-β1, fibroblast growth factor-2 (FGF-2), and platelet-derived growth factor-BB

(PDGF-BB) are also able to activate VEGF in addition to hypoxic conditions. Over the wound healing process, different cells like fibroblast, keratinocytes, platelets, and macrophages secrete VEGF, which activates and supports angiogenesis through acting in a paracrine fashion on endothelial cells [102]. VEGF as the most widely investigated growth factor in skin flap, indicated improvement of skin flap survival by both preoperative and intraoperative administration. Simman et al. [103] showed an increased rate of survival as a result of administration of VEGF and endothelial progenitor cells (EPCs) 14 days before the flap elevation. Flap viability increased significantly from 68% in control to 91% following dual injection of VEGF and stem cells. Kryger et al. [104] investigated the delivery method of VEGF on skin flap viability and examined local injections like topical, subdermal, subcutaneous, and systemic injection in the femoral vein. The most effective route of delivery was multiple systemic injections with a 91% survival area compared to 66% in control and 78% in topical delivery. Delivering VEGF over a prolonged period significantly improved the viable area. Therefore, scientists conducted research on developing other delivery vehicles like genes and polymer-based carriers to release growth factors in a sustained and localized manner. These are requirements for wound healing acceleration because of short half-lives of growth factors, rapid dilution in the body and undesirable side effects at high systemic concentration.

Different delivery methods have been developed to provide controlled release of growth factors like hydrogels, micro/nanoparticles, and porous scaffolds [105]. However, various challenges have been posed by many of these delivery methods, including reduced bioactivity of released growth factors, high initial burst release and poor loading efficiency [106]. For example, VEGF was loaded into gelatin microspheres through the water in oil emulsion method. 25% of VEGF was burstly released from microspheres in the initial 24 hours. The heparin-based coacervate delivery system has been developed by scientists to release growth factors based on heparin-binding ability. This platform induces high loading efficiency of growth factors, sustained and controlled release and greater bioactivity over free growth factors [105]. The release rate of growth factors from polycation-heparin coacervate is relevant to electrostatic interaction between heparin and growth factors and also the degradation of polycation [107]. In one study, VEGF and TGF-β3 were coacervated and prepared a coating layer on electrospun nanofibers resembling extracellular matrix (ECM). Different binding affinity between growth factors (VEGF and TGF-β3) and heparin induced sustained release of VEGF and burst TGF-β3 release. Negative charge of TGF-β3 at

physiological pH values due to less isoelectric point inhibits the electrostatic reaction between TGF-β3 and heparin and causes the burst release. The coacervated-coated nanofibers were implanted on top of the defect after flap elevation with 1.5 × 4 cm^2 size. The results exhibited the synergistic effect of VEGF and TGF-β3, such as lower necrotic area and greater neovascularization level in the middle of a flap than control flaps [107].

Drugs and compounds can also improve flap survival by accelerating VEGF expression, microvessel density, and reducing the inflammatory response and oxidative stress like Azadirachtin-A [108], Asiaticoside [109], Nobiletin [110], and Calcitriol [15]. Although the experimental studies confirmed the positive impact of these drugs on skin flap survival, the drugs' mechanism of action is unclear, and more experiments need to be done.

Increasing oxygenation:

Oxygen has been proven to positively impact wound healing, and through the years, many ways have been developed to deliver oxygen to wounds. Hyperbaric oxygen therapy is considered a method to deliver oxygen to wound area and prevent necrosis. Although studies have shown the positive impact of hyperbaric oxygen (HBO) therapy on improving flap survival by increasing oxygen tension and angiogenesis, early recognition of flap compromise is necessary to prevent tissue loss. The positive correlation between flap survival and early HBO therapy confirmed the impact of prompt HBO, while the study showed 100% graft loss following starting HBO therapy after 3 days [16]. Because HBO is not available and practical in every situation [17], oxygen delivery to the tissues following the surgical procedure and skin flap surgery can be an addressable method to prevent skin flap failure until perfusion reestablishment. Several studies used engineered biomaterials with oxygen release ability topically or subdermally to reduce skin flap necrosis.

Zellner et al. [17] used a dissolved oxygen dressing (OxyGenesys) incorporating oxygen gas to reduce skin flap necrosis and compared it with control group similar in formulation to OxyGenesys. Porcine random skin flaps were created and covered topically with OxyGenesys dressing and control sample. The skin flaps were ischemic, 16cm × 4cm in size with 4:1 aspect ratio. The OxyGenesys-treated group showed less dermal fibrosis and necrosis than the control sample, while subcutaneously there was more necrosis and fibrosis in skin flap treated with

OxyGenesys samples. Therefore, OxyGenesys partially succeeded in improving the ischemic wound repair and confirmed the impact of localized oxygen delivery on tissue necrosis.

Solid peroxides have also been used in oxygen delivery studies to provide prolonged oxygen and prevent necrosis before the tissue was sufficiently vascularized [19]. Harrison et al. [1] for the first-time used oxygen generating biomaterials (OGB) to prevent skin flap necrosis. In this work, sodium percarbonate (SPC) was encapsulated within PLGA by solvent casting method. The film was able to release oxygen over a 70h period. The films were tested in a skin flap model 10 mm × 30 mm size on mice and necrotic tissue was examined histologically after 2, 3, and 7 days. OGB showed less necrotic tissue, lower lactase concentration and levels of apoptotic cells over 3 days. However, after 7 days, there was no significant difference between OGB and control in the amount of tissue necrosis. Therefore, OGB was able to delay the onset of necrosis just for 3 days. Prolonging oxygen release from OGB to days and weeks can delay necrosis until revascularisation occurs.

Encapsulation of solid peroxides within hydrophobic polymers can extend oxygen release until perfusion is re-established. A. Shiekh et al. [4] generated CaO_2 (CP)-encapsulated antioxidant polyurethane (PUAO) and implanted it in a skin flap of 30 mm × 10 mm size on the backs of mice. In this study, PUAO was chosen due to its hydrophobic and antioxidant properties to control oxygen release from CP and reduce oxidative stress as a result of hypoxia and H_2O_2 production by CP. A sustained oxygen release was observed from CP-PUAO for 10 days. The scaffold showed around 90% antioxidant capacity over 180 minutes. CP-PUAO group demonstrated more skin flap survival when compared to the PU scaffold without CP. Histologically, preserved dermis and epidermis were observed for CP-PUAO after 3 and 7 days, while the skin completely degenerated in the PU group after 7 days. Although the results confirmed less tissue necrosis through incorporating CP into PUAO polymer compared with PU alone, no significant difference was reported in skin flap survival (histologically and visually) between no scaffold and CP-PUAO scaffold (Fig. 2.9). Mimicking ischemic situations via placing silicon sheets underneath the flaps may possibly show a significant difference between skin flap necrosis of CP-PUAO and PU.

Steg et al. [18] used a hydrophobic carrier for encapsulating CP particles and prepared poly(trimethylene carbonate) (PTMC)-CP microspheres using the solvent evaporation method.

PTMC-CP microspheres were then implanted subcutaneously in a skin flap of 3 cm × 1cm size in mice, and the levels of necrosis were measured at different time points. It was observed that oxygen-generating microspheres delayed skin flap necrosis for up to 10 days while could not prevent flap necrosis. Therefore, the key finding of these studies was that providing oxygen in skin flap cannot hamper tissue necrosis and is just able to reduce the amount of necrosis and also delay the necrosis progression. Maybe lack of oxygen is not the only cause of flap necrosis and in order to prevent the formation of necrotic tissue, delivering substrate levels to the ischemic area with poor blood supply is probably necessary.

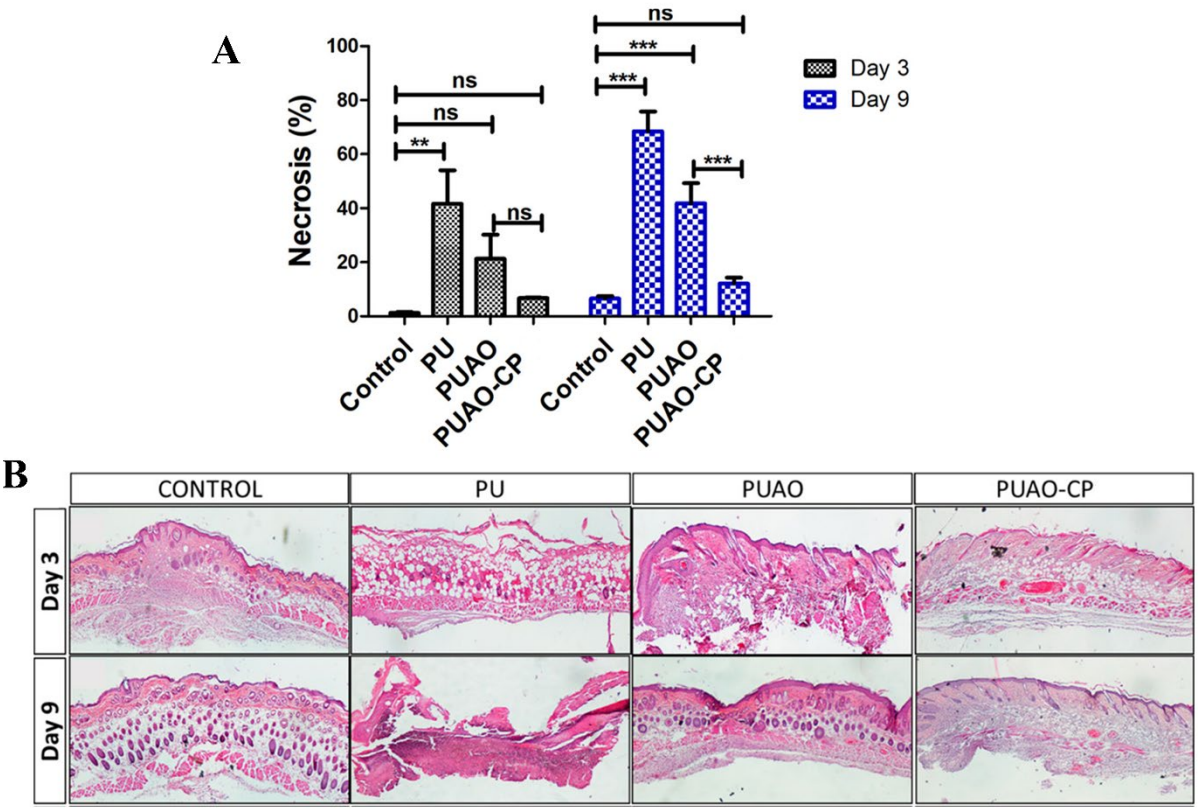

Fig. 2.9. Calcium peroxide-encapsulated antioxidant polyurethane (PUAO) (A) Quantification of necrosis area after 3 and 9 days. **p ≤ 0.01, ***p ≤ 0.001, ns: nonsignificant. **(B)** H&E staining of skin flaps at day 3 and day 9, showing increased necrosis in the PU group compared to PUAO and PUAO-CP groups. *Reprinted with permission from American Chemical Society: P. A. Shiekh, A. Singh, and A. Kumar, "Oxygen-Releasing Antioxidant Cryogel Scaffolds with Sustained Oxygen Delivery for Tissue Engineering Applications," ACS Applied Materials & Interfaces, vol. 10, no. 22, pp. 18458-18469, 2018.*

CHAPTER 3. INTRODUCTION TO MANUSCRIPT

AQUEOUS DECOMPOSITION BEHAVIOR OF SOLID PEROXIDES: EFFECT OF pH AND BUFFER COMPOSITION ON OXYGEN AND HYDROGEN PEROXIDE FORMATION

The first paper investigates the effect of pH and buffer composition on oxygen and hydrogen peroxide release from peroxy- compounds for the first time. This study was conducted across a wide pH range (5-9) and compared the impact of different ionic buffers on solid peroxides' decomposition (carbonate, phosphate and citrate). In order to indicate the reaction between peroxides and ionic buffers, X-ray diffraction analysis was carried out. Cytotoxicity of different peroxides was also assessed by live dead assay. This study allowed us to confirm the pH-dependent decomposition of inorganic peroxides which could be exploited to develop pH responsive hydrogen peroxide/ROS and oxygen delivery systems to tissues with an extreme pH range. We also showed catalytic activity of carbonate anion in ionic buffers.

3.1. Authors

Arghavan Rastinfard[a], Benjamin Dalisson[b], Jake Barralet[a,b],

[a] Division of Orthopaedics, Department of Surgery, Faculty of Medicine and Health Sciences, Montreal General Hospital, Montreal, QC, H3G 1A4, Canada

[b] Faculty of Dentistry, McGill University, 2001 McGill College Avenue, Montreal, QC, H3A 1G1, Canada

3.2. Abstract

The ability of solid peroxides to provide sustained release of both oxygen and hydrogen peroxide makes them potentially suitable for oxygen release or antibacterial applications. Most recent reports using solid peroxides to augment oxygen levels do so by compounding solid peroxide powders in polymers to retard the aqueous decomposition. Compounds with peroxidase activity may be added to reduce hydrogen peroxide toxicity. Peroxides are rarely pure and are mixed with oxide and themselves decompose to form hydroxides in water. Therefore, even if buffering strategies are used, locally the pH at the surface of aqueously immersed peroxide particles is

inevitably alkaline. Since pH affects the decomposition of peroxides and hydrogen peroxide stability, this study compared for the first-time the aqueous decomposition products of hydrogen and inorganic peroxides that are in use or have been used for medical applications of have been evaluated preclinically; calcium peroxide (CaO_2), magnesium peroxide (MgO_2), zinc peroxide (ZnO_2), sodium percarbonate ($Na_2CO_3.1.5H_2O_2$) and hydrogen peroxide (H_2O_2). Since plasma can be approximated to be carbonate buffered phosphate solution, we maintained pH using carbonate and phosphate buffers and compared results with citrate buffers. For a given peroxide compound, we identified not only a strong effect of pH but also of buffer composition on the extent to which oxygen and hydrogen peroxide formation occurred. The influence of buffer composition was not previously appreciated, thereby establishing *in vitro* parameters for better design of intentional release of specific decomposition species.
Keywords: Oxygen; Hydrogen peroxide; Carbonate buffers; Solid peroxides.

3.3. Introduction

Solid peroxides are interesting materials for a variety of biological applications because of their ability to efficiently store large amounts of molecular oxygen (O_2) that is released upon decomposition in aqueous conditions [111]. They have found application commercially in aquaculture [112-116] and for seed protection and soil conditioning for agriculture [117-121] where they raise oxygen levels to maintain aquatic life or prevent bacterial or fungal attack of young plants in waterlogged soils.

Their use in medicine, while an active and rapidly expanding area of research, is quite restricted to dental bleaching applications. Antiseptic topical hydrogen peroxide solutions have for a long time been applied to minor cuts for sanitisation [122]. The main issues surrounding translation aside from cost and regulatory hurdles are the potential to harm the patient through failure of buffering causing caustic tissue damage and that the breakdown into oxygen is rarely direct, and often cytotoxic levels of hydrogen peroxide (H_2O_2) and other reactive oxygen species (ROS) [123] are simultaneously released. However, not all solid peroxides are extremely caustic or reactive, zinc peroxide is relatively insoluble and was widely used to control infections and treat a wide variety of internal and external infections [2] in the era of pre-antibiotic surgery and medicine (~pre 1945). Its oxygen release was considered effective for disrupting anaerobic infections. Today the use of solid peroxides in dentistry persists as a bleaching agent with an alkaline buffering

capacity to offset acid erosion caused by oral bacteria [124-126], that can occur at pH <4.5 [127] but can initiate at pH as high as 5.5 [128]. The overuse of antibiotics has created resistant bacterial strains, and interest in pre-antibiotic bactericidal materials has grown [49, 129-135].

There has been a dramatic increase in interest in these compounds to deliver oxygen to cells and tissues. Mostly reports focus on new routes to control decomposition by polymer encapsulation [6, 28, 136] and routes to control hydrogen peroxide release to minimize cytotoxicity by combining peroxidases such as catalase [34, 35] or inorganic catalysts such as manganese dioxide (MnO_2) [33, 44, 137]. These formulations have been employed to treat skin flaps [3], tissue engineered constructs [5], tissue cultures [21], and isolated islets [58]. Recently manipulation of oxygenation and ROS level of tumors has become an area of active research, and there have been several reports of formulations of nanoperoxides that can modify tumor microenvironment [7, 8, 46, 49]. Oxygenating scaffolds and modifying material research has largely focused on the reduction of cytotoxic hydrogen peroxide generation [33, 35, 138]. However, for cancer therapies, increasing oxidative stress can be desirable either directly or as an adjunct to other therapies [27, 46-50]. Indeed, it is becoming appreciated that hydrogen peroxide and other ROS are important for signalling in a wide variety of biological processes [139-142] and there have already been studies into harnessing the controlled release of ROS from solid peroxides for therapeutic outcomes [143, 144].

While alkali metal hydroxides can be caustic, there can often be little evidence of tissue damage or irritation, depending on the amount and rate of formation, because carbonates and phosphates form *in situ*. A good example being the biocompatibility of magnesium metal that in water would ultimately raise pH to 10.3 [145], yet in extracellular fluid and blood are well tolerated for orthopaedic applications [146].

There are several inorganic compounds that can decompose to form oxygen or hydrogen peroxide; most commonly studied are per-oxides, per-borates, and per-carbonates [21]. While general principles behind their biological application are common, no comparative study has been performed to compare the reaction of solid peroxides at fixed pH in order to better understand results obtained in more complex composites and *in vivo*. We sought to determine to what extent buffering might affect decomposition of peroxy- compounds of low toxicity metals (sodium, zinc,

calcium, and magnesium). Furthermore, we sought to establish whether the buffering ion had any effect or whether pH alone was the more critical factor. In particular, we aimed to assess whether carbonate and phosphate buffers, that would be likely to form insoluble precipitates of zinc, magnesium and calcium, would result in differing decomposition than a citrate buffer that forms more soluble salts. We compared our results with hydrogen peroxide solution decomposition because understanding how the stability of this decomposition product of inorganic peroxy-compounds is altered by the environment could help interpret longer term hydrogen peroxide production measurements. In other words, this enabled us to determine if low levels of hydrogen peroxide were due to low levels of production or just low stability at those experimental conditions.

Whether a peroxide forms mostly oxygen or hydrogen peroxide upon decomposition has not been compared in biological buffers and yet is an important foundation for designing an intended biological effect and so we determined hydrogen peroxide: oxygen ratio as a comparative tool to compare peroxides. It is important to understand how non-formulated peroxides behave in isolation from other materials as their behaviour is complex and highly dependent on the measurement environment. Most recent reports on their medical use, present data from polymer composites, which are intended to prolong oxygen release and also to minimize cell and tissue contact with peroxide compounds. While these composites may be effective, the rationale for a particular formulation is rarely made. To our knowledge, the potential for buffer composition to introduce artifactual results does not appear appreciated and is important for *in vitro* testing of oxygen and ROS releasing materials.

This study then compared for the first-time decomposition products of calcium, magnesium, and zinc peroxides as well and sodium percarbonate across at pH 5, 7 and 9. These conditions could be feasibly encountered physio- or patho-logically or as a result of solid peroxide decomposition. Bacterial infections have been measured as having pH levels from 5 to 9 [127, 147]. The gastrointestinal (GI) tract begins with a gastric pH of ~1-2.5 that fluctuates between 6.5 and 7.5 [148]. Recently using flexible, double-barreled, ultrafine capillary microelectrodes, the pH in the airway surface liquid (ASL) of human nasal mucosa in healthy subjects was found to oscillate widely between ~7.5 and 9 during exhalation and between ~8.5 and 9 during inhalation [149], and this alkalinity plays a key role in reducing bacterial and viral load of the healthy lung. We also studied the impact of different ionic buffers on hydrogen peroxide and oxygen release and

confirmed the decomposition of hydrogen peroxide by carbonate buffers at alkaline pH values. Comparison between ionic buffers and culture media also indicated the reactivity between hydrogen peroxide and HEPES buffer in culture media.

3.4. Materials and Methods

3.4.1. Materials

Calcium peroxide, CaO_2 (CP) was obtained from FMC Corporation. Magnesium peroxide, MgO_2 (MP), zinc peroxide, ZnO_2 (ZP) and sodium percarbonate $Na_2CO_3.1.5H_2O_2$ (SPC) were purchased from Sigma-Aldrich and hydrogen peroxide was sourced from Merck Millipore.

3.4.2. Decomposition experiments

The experiments were conducted in unsealed 15 mL tubes and at pH 5, 7, and 9. To 5 mL deionised water, 10mM of each peroxide was added, normalised for manufacturer's stated purity (75% for CP, 24-28% for MP, 50-60 % for ZP, 20-30% for SPC, and 30% for H_2O_2). Phosphate (pH 5, 7, and 9), carbonate (pH 7.4 and 9), and citrate (pH 5 and 7) 0.5M buffer solutions were prepared using the formulations shown in Table 3.1 except citrate at pH 7 with 2.5 M molarity. We prepared pH 7.4 carbonate by bubbling carbon dioxide at a flow rate of 0.3 LPM into pH 9 carbonate buffer during the experiment. We did not observe a constant pH, but it fluctuated between 7.4-8.2. Each buffer solution's ability to maintain the desired pH with the addition of peroxides was verified. Table 3.2 shows the pH before and after adding peroxides to the buffer solutions. Additionally, a non-buffered water reference was used as a comparison. The endpoint of the experiment was determined to be the point at which no further change in measured parameters was detected.

Because carbonates are known to be reactive with hydrogen peroxide [150] and body fluid may be approximated to be a carbonate buffered phosphate containing saline, 30, 60 and 120 mM sodium bicarbonate ($NaHCO_3$) was added to phosphate-buffered saline (PBS) containing 10 mM hydrogen peroxide. The pH value was maintained by manually adding either 1 N sodium hydroxide (NaOH) or hydrochloric acid (HCl). The hydrogen peroxide concentration was measured as detailed in section 3.4.3 over a 5-hour period.

The impact of buffer media on hydrogen peroxide stability was also studied. DMEM, HEPES buffer, high glucose media (12430054) and DMEM, no glucose media (11966025) containing 10 mM hydrogen peroxide were chosen. The hydrogen peroxide concentration was measured after 2

hours keeping in a humidified incubator at 37° C and 5% CO_2. We also examined the impact of added glucose to no glucose media (25mM) on hydrogen peroxide concentration after 2 hours.

Table 3.1. Composition of different buffer solutions used for decomposition experiments.

Citrate	pH	$Na_3C_6H_5O_7.2H_2O$ (g/L)	$C_6H_8O_7$ (g/L)
	5	93.35	35.08
	7	731.04	2.75
Phosphate	pH	$Na_2HPO_4.7H_2O$ (g/L)	$NaH_2PO_4.H_2O$ (g/L)
	5	1.99	67.97
	7	80.71	27.45
	9	133.15	0.46
Carbonate	pH	Na_2CO_3 (g/L)	$NaHCO_3$ (g/L)
	9	3.9	38.92

3.4.3. Quantitative analyses

At 1, 10, 24, and 48 hours the amount of released oxygen dissolved in the test solution was determined with a NEOFOX Oxygen Sensor. For calibration, the oxygen sensor was exposed to 0, 10, 20, 30, 40, 60, and 80% dissolved oxygen in water (prepared by bubbling nitrogen and oxygen gas through water) and let the Tau value (fluorescence lifetime) stabilize. As per manufacturer's instructions, a least squares calibration curve was obtained using those oxygen values.

A Thermo Scientific peroxide assay kit was used to measure hydrogen peroxide concentrations in the test buffers. For peroxide standards, a 10mM solution of hydrogen peroxide was prepared by diluting a 30% hydrogen peroxide solution. This sample was diluted with Milli-Q water to achieve 6 standards in the concentration range of 10-600µM. Then, 150µL of the assay working reagent was added to 2µL of hydrogen peroxide standards in microplate wells. After 25 minutes incubation, absorbances were measured at 595nm using a plate reader (Tecan Spark). For samples, the working reagent was added to 2µL of peroxide solution after each time point, and hydrogen peroxide concentration was measured by reference to its assay absorbance compared to the standard curve.

Table 3.2. Experiments confirming adequacy of buffer capacity in this study showing little change in final pH after peroxide addition.

	Initial pH	pH after adding peroxides				
		CP	MP	ZP	SPC	H_2O_2
Citrate	5.02	5.05 ± 0.01	5.18 ± 0.02	5.07 ± 0.01	5.20 ± 0.01	5.18 ± 0.02
	7.00	7.55 ± 0.05	7.50 ± 0.05	7.10 ± 0.01	7.24 ± 0.02	6.96 ± 0.02
Phosphate	5.00	5.30 ± 0.02	5.66 ± 0.01	5.04 ± 0.02	5.41 ± 0.01	4.98 ± 0.02
	7.05	7.10 ± 0.01	7.29 ± 0.01	7.14 ± 0.01	7.24 ± 0.01	7.19 ± 0.00
	9.11	9.76 ± 0.02	9.64 ± 0.02	9.21 ± 0.02	9.54 ± 0.04	9.02 ± 0.02
Carbonate	9.03	9.20 ± 0.00	9.11 ± 0.01	9.33 ± 0.01	9.16 ± 0.01	9.11 ± 0.01
	7.40	7.85 ± 0.33	7.80 ± 0.29	7.83 ± 0.30	7.71 ± 0.29	7.82 ± 0.24
Unbuffered Water	6.8	11.47 ± 0.06	10.54 ± 0.05	8.63 ± 0.17	10.62 ± 0.03	6.81 ± 0.02

3.4.4. Assessment of Decomposition

The composition of precipitates at the end of experiments was characterized by X-ray diffraction (XRD) (Bruker D8 Discover) using CuK_α radiation (λ=0.154 nm). The patterns were collected in the range of $4^\circ < 2\theta < 100$ with a step size of $2\theta = 0.005^\circ$. The morphology of the precipitates was characterized using scanning electron microscopy (SEM) (Hitachi SU–8230 FE-SEM). The microscope was operated at 1 kV accelerating voltage and 7.7 mm working distance. Elemental composition of representative areas was mapped using energy-dispersive X-ray spectroscopy (EDS).

3.4.5. Cytotoxicity Assay

We were unable to culture cells in direct contact with any solid peroxide since cells detached even at very low doses which introduced artifacts. In order to better determine relative toxicity at low concentrations, we added 1mg/mL of solid peroxide to DMEM for 24 hours and then used serial dilutions until a concentration was reached where viability was maintained. Madin-Darby Canine Kidney (MDCK) were cultured in Dulbecco's Modified Eagle Medium (DMEM, 11995040) supplemented with 1% penicillin/streptomycin and 10% fetal bovine serum. A 1mg/mL suspension of different solid peroxides was initially prepared by mixing 5mg of peroxides with

5mL of culture medium and stored for 24 hours. This sample was diluted with medium as low as 1:6 dilution. MDCK cells were seeded in a 24 well plate at a density of 2×10^4 cells/well. After 24 hours, the medium was removed, and 1 ml of pure or diluted peroxide solutions were added to each well. Cells were treated with 10mM hydrogen peroxide for 30 minutes to obtain a dead control, and cells with no treatment were used as a live control. Live-dead staining was performed on trypsinized cells after a 15 h exposure using a live/dead assay (Molecular Probes TM, LIVE/DEAD Viability/Cytotoxicity Kit). This assay uses Calcein AM to show live cells with green fluorescence and Ethidium homodimer-1 to show dead cells with red fluorescence. Cells were analyzed by fluorescence microscopy (ZEISS Axio Imager 2) after staining.

3.4.6. Statistical Analysis

All data are expressed as mean ± standard deviation (N=3) and p-values <0.01 were considered statistically significant. An independent T-test was used to determine the statistical difference between two groups. Statistical significance of oxygen and hydrogen peroxide release between three or more groups was assessed by one-way ANOVA, followed by a least significant difference (LSD) post hoc test.

3.5. Results

3.5.1. Hydrogen Peroxide release

Hydrogen peroxide as well as oxygen is a potentially cytotoxic byproduct of aqueous metal-peroxide decomposition. Identifying conditions under which predominantly oxygen or hydrogen peroxide was formed allows the development of biomaterials formulations for specific applications. Hydrogen peroxide can itself be aqueously unstable, and certain materials and ions can cause its decomposition, so release studies can not only give information about initial hydrogen peroxide production but can also indicate whether certain cations or buffer anions alter the net amount of hydrogen peroxide produced. The inclusion of a hydrogen peroxide group in each condition informs as to the effect of pH and buffer anion on hydrogen peroxide stability. Fig. 3.1 shows that at pH 5, buffer composition made little difference to peroxide decomposition. Magnesium and zinc peroxide formed increasing amounts of hydrogen peroxide in an approximately linear fashion. Hydrogen peroxide itself was stable at pH 5, as indicated by the lack of significant change in concentration over the study period. The other peroxides had an almost immediate burst release with little change thereafter. At pH 7 there was little difference in

decomposition behaviour between citrate and phosphate buffers except for zinc peroxide that produced no hydrogen peroxide after 10 hours in citrate but produced up to 10mM in phosphate buffers. In carbonate buffer, hydrogen peroxide was clearly not stable being nearly completely degraded in 2 days. This was seen in the hydrogen peroxide levels from solid peroxide decomposition being least pronounced in calcium peroxide. At pH 9, the behaviours were similar to pH 7, zinc peroxide barely released any hydrogen peroxide; carbonate appeared to destabilise hydrogen peroxide even more than pH 7. Further evidence for this is seen in the rapid drop in hydrogen peroxide levels even in phosphate buffer from sodium percarbonate. The carbonate in the material itself then reacting with hydrogen peroxide. This compound being the most soluble generally reacted the fastest in all conditions.

3.5.2. Oxygen Release

Water, when saturated with air at our laboratory conditions (~24°C), had a measured 261 ± 10 µM of dissolved oxygen. Lower values are obtained when salts are dissolved in the water as has been extensively characterised. This salting out effect can reduce dissolved gasses to reduce oxygen contents below that of pure water. When water was saturated with pure oxygen, this value increased to 1250µM. Decreasing values represent diffusion of oxygen out of the water into the air. As this is dependent on surface area and volume, all experiments were performed in identical 15mL centrifuge tubes that were open to the air; Fig. A1 shows a typical change in oxygen content of oxygen saturated water as a function of time in laboratory conditions. Near constant oxygen levels indicate that oxygen evolution approximately matched the diffusion of oxygen out of the system whilst increasing levels show that the rate of oxygen evolution exceeded that of oxygen diffusion out of the system. We did not include data from carbon dioxide buffered experiments (pH 7.4) because intermittent bubbling with CO_2 to maintain pH introduced artifactual changes in dissolved oxygen. Fig. 3.2 compares the oxygen release of hydrogen peroxide and solid peroxide in different buffer compositions. In all but one condition (Zinc peroxide in citrate buffer pH 5), maximal oxygen levels were attained within less than 24 hours. At pH 5, it was highly notable that phosphate prevented oxygen formation from all compounds except zinc and calcium peroxides in the first 10 hours. In citrate buffer sustained oxygen release was achieved from Zinc, Magnesium and Calcium peroxides. At pH 7, the sustained release was attained from all compounds. Sodium and calcium compounds showed an initial burst profile. At pH 9 phosphate, results were similar, but sodium and calcium compounds decomposed more increasing oxygen levels by nearly four

and two times over baseline conditions, respectively. Carbonate buffer appeared to accelerate decomposition such that peak values were at least 2.5 times higher than ambient for all materials except zinc peroxide that was stable in alkaline conditions and did not appreciably decompose.

3.5.3. Effect of buffer composition on peroxide decomposition

Fig. 3.3 compares the decomposition product formation of different peroxy compounds at pH 5 and 7 in either citrate or phosphate buffers. To eradicate the effect of any burst release and loss of oxygen from slowly releasing systems, the average dissolved oxygen content at 1, 5, 10 and 24 hours was used for comparison. It is apparent that decomposition of the more soluble peroxy compounds, hydrogen peroxide, sodium percarbonate (maximum solubility of 120 g/L in water at 20°C [151]), and calcium peroxide (solubility of 1.65 g/L in water at 20°C [120]) was not affected by pH or buffer. The least soluble compounds, zinc (insoluble) and magnesium peroxide (0.86 g/L at 18°C [152]) were not affected by buffer composition at pH 5, but at pH 7, citrate greatly reduced hydrogen peroxide formation (Fig. 3.3a).

For oxygen production, again the most soluble peroxy compounds (sodium, hydrogen, and calcium) were not sensitive to buffer composition at pH 5, but pH 7 caused increased oxygen formation relative to pH 5, by approximately two-fold for the moderately soluble solid compounds (sodium percarbonate and calcium peroxide), this indicates that the increased oxygen came from compound decomposition and not from hydrogen peroxide decomposition. At pH 7 the effect of buffer composition of the less soluble compounds (zinc and magnesium) was not marked, but at pH 5 citrate buffer clearly increased oxygen formation relative to phosphate buffer.

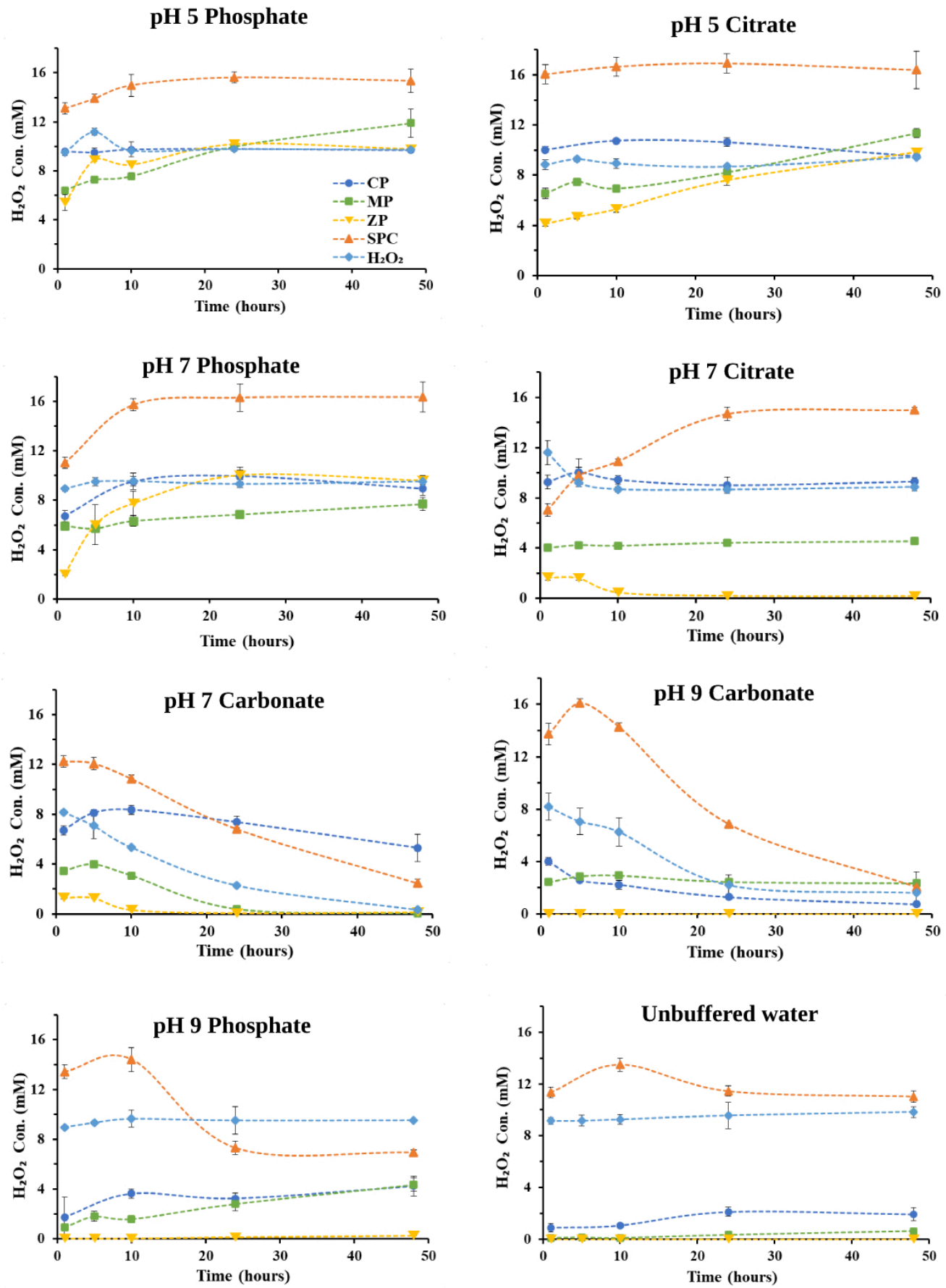

Fig. 3.1. The hydrogen peroxide release with time from different peroxy- compounds at pH 5, 7 and 9 (phosphate, citrate and carbonate buffers) (N = 3). Dotted lines are a visual aid to clarify distinction of different data groups.

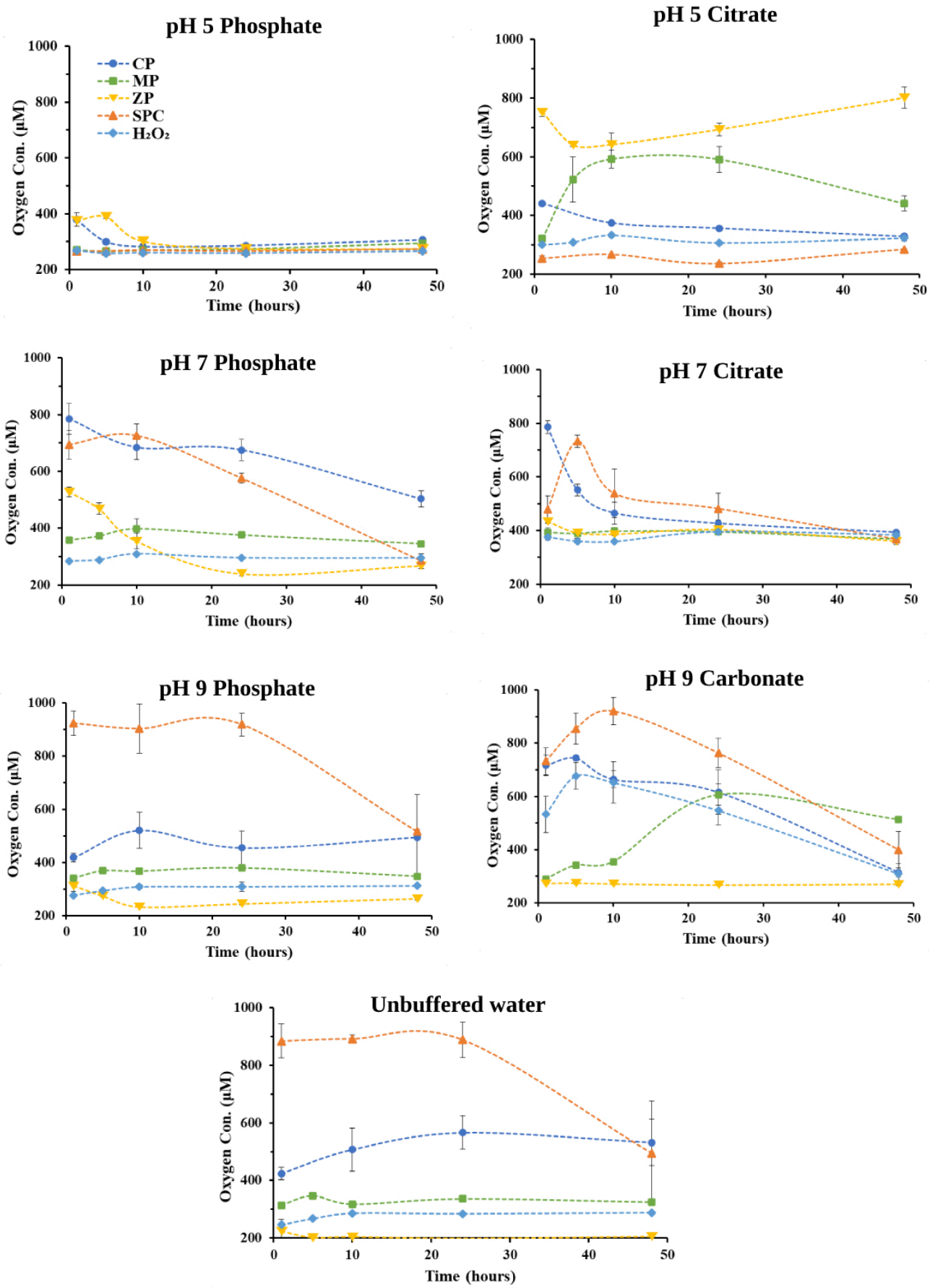

Fig. 3.2. The oxygen release with time from different peroxy- compounds at pH 5, 7 and 9 (phosphate, citrate and carbonate buffers) (N = 3). Dotted lines are a visual aid to help distinction of different data sets.

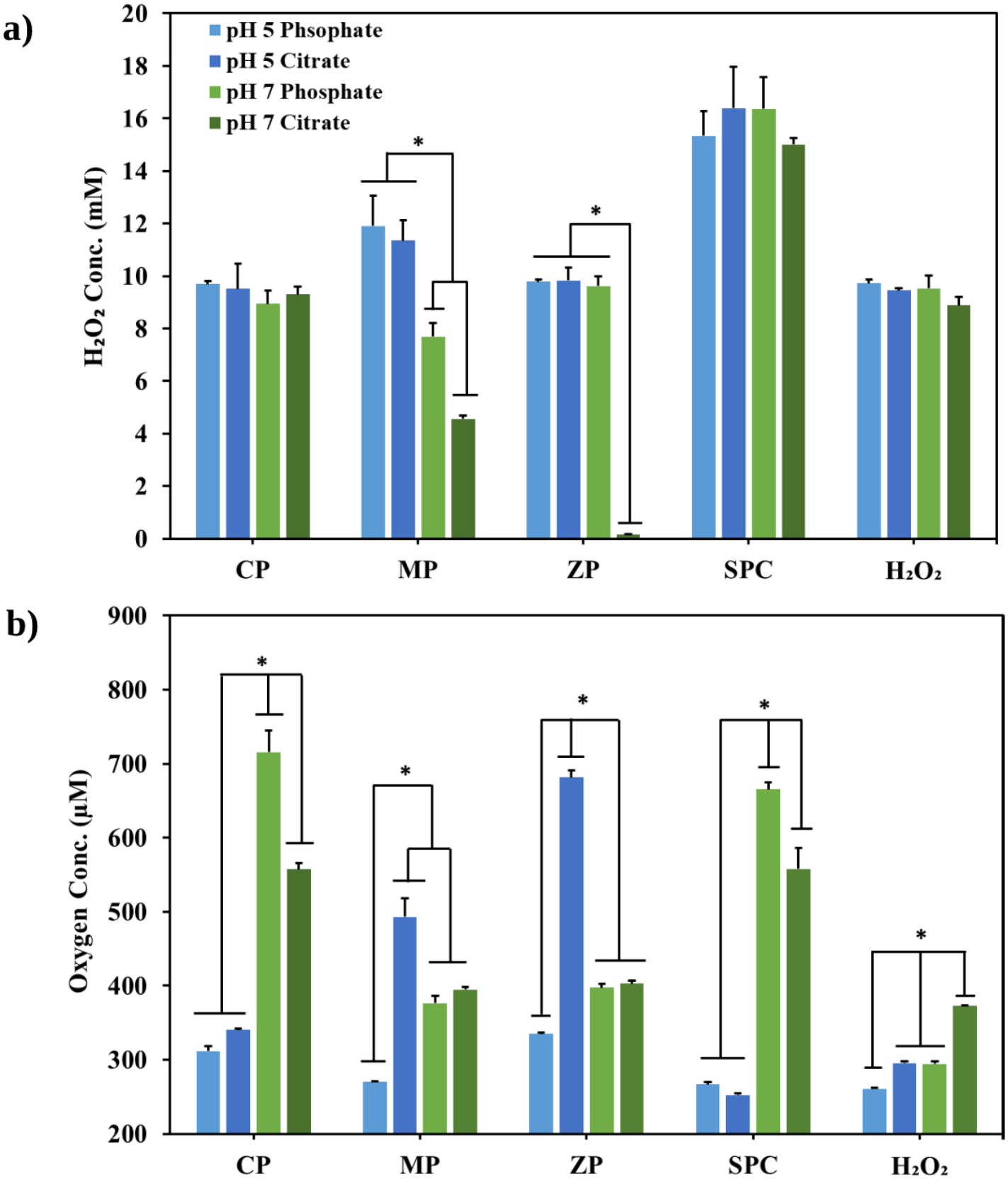

Fig. 3.3. (a) Comparison of hydrogen peroxide levels measured after 48h at pH 5 and 7 in either phosphate or citrate buffers, and **(b)** the average dissolved oxygen content at 1, 5, 10 and 24 hours following peroxy compounds decomposition at pH 5 and 7 in either phosphate or citrate buffers. * indicates $p<0.01$, $N = 3$.

3.5.4. Hydrogen Peroxide: Oxygen ratio

The hydrogen peroxide: oxygen ratio was calculated by dividing the total amount of hydrogen peroxide release by the average dissolved oxygen content at 1, 5, 10 and 24 hours (Fig. 3.4). The ratios were generally higher in each buffer at pH 5 than at pH 7. A significant reduction in the ratio was observed by increasing pH values from 7 to 9. Sodium percarbonate generally showed the highest ratio at a given condition because of releasing high/moderate doses of hydrogen peroxide over the total pH range (Table 3.3). This is except for pH 9 that there was a rapid drop in hydrogen peroxide levels from sodium percarbonate. Except for magnesium peroxide, other peroxides had the lowest H_2O_2/O_2 release at pH 9 carbonate among all other buffers. Interestingly, calcium, magnesium peroxide, and sodium percarbonate decomposition at pH 9 carbonate produced a high amount of oxygen with low hydrogen peroxide (Table 3.3). As the body is buffered with carbonate and all solid peroxides are alkaline in water, it suggests that this is one mechanism by which the damaging effects of hydrogen peroxide are inadvertently minimised.

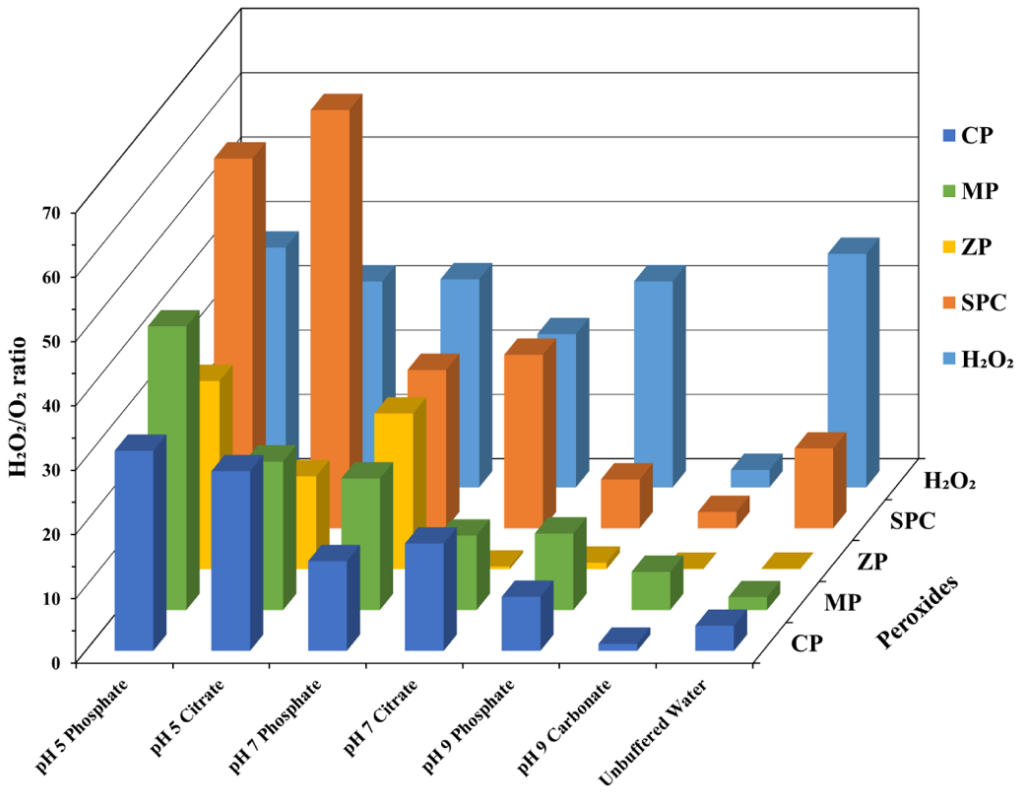

Fig. 3.4. Average H_2O_2/O_2 ratios formed by decomposition of peroxy- compounds in different buffers.

Table 3.3. Peroxides categorised according high, intermediate or low levels of H_2O_2 and O_2 release at acidic, neutral, and alkaline pH of phosphate, citrate and carbonate buffers.

	Acid (phosphate)		Acid (citrate)		Neutral (phosphate)		Neutral (citrate)		Alkaline (phosphate)		Alkaline (carbonate)	
	O_2	H_2O_2	O_2	H_2O_2	O_2	H_2O_2	O_2	H_2O_2	O_2	H_2O_2	O_2	H_2O_2
CP												
MP												
ZP												
SPC												
H_2O_2												

Legend	
O_2	**H_2O_2**
High: >500µM	High: >8mM
Intermediate: 400µM< <500µM	Intermediate: 4mM< <8mM
Low: <400µM	Low: <4mM

3.5.5. X-ray Diffraction of decomposition products

Fig. 3.1 indicates that unbuffered water significantly decreased hydrogen peroxide release, except for sodium percarbonate as the most soluble compound with the fastest reactivity in all conditions. Sodium percarbonate produced about 65% of the maximum theoretical amount of H_2O_2 in sodium percarbonate at unbuffered water, while calcium, magnesium and zinc peroxide released 19, 5 and 0% of H_2O_2 theoretical amount over 48 hours. Moreover, sodium percarbonate decomposition yielded about 81% of theoretical maximum of H_2O_2 over 1 hour at pH 9 carbonate buffer, while calcium, magnesium and zinc released just 39%, 20% and 0%. It was 79%, 17%, 8% and 0% at pH 9 phosphate for sodium percarbonate, calcium, magnesium, and zinc peroxide respectively. Such significant differences were not observed at acidic and neutral conditions. This may be caused by the reaction between solid peroxides, medium, environment and buffer components at alkaline pH values, producing insoluble reaction products and a barrier layer. There is no barrier formation for sodium percarbonate because of high solubility at all conditions and lack of precipitation formation at the end of experiments. Therefore, we examined the surface of calcium, magnesium, and zinc peroxide (Figs. 3.5, A2 and A3) in phosphate and carbonate buffers at pH 7 and 9 and also unbuffered water by XRD analysis.

The XRD measurements (Fig. 3.5) of decomposed calcium peroxide confirmed the formation of insoluble decomposition products from peroxides. Hydroxyapatite (HA) was formed at pH 7 and 9 phosphates. Although the formation of HA preferred at alkaline pH values and increase in pH can help the precipitation of HA [153], the peaks at pH 7 were matched with the HA phase. Using buffers can control pH change due to reaction but the medium near the particles surface layer has higher pH values even at pH 7 because of the caustic product formation (calcium hydroxide $Ca(OH)_2$). The peaks at pH 9 phosphate are sharper than pH 7, due to more concentration of phosphate ions at pH 9, which can increase the reaction rate. The XRD results showed the production of two different polymorphs of calcium carbonate, $CaCO_3$ (calcite and vaterite), after exposure of calcium peroxide in water and pH 9 carbonate. At pH 9 carbonate and water, unreacted calcium peroxides and/or calcium hydroxide product was converted to calcium carbonate, calcite at pH 9 and calcite and vaterite composition in water. The EDS results at pH 9 phosphate (Fig. 3.6a) indicate the co-existence of Ca and P elements in a precipitate which can be attributed to the formation of a calcium phosphate phase. The EDS results from pH 9 carbonate buffer also suggested the existence of Ca and Na elements that can be assigned to $NaHCO_3$ and $CaCO_3$ as two separate phases. The rhombic shape at SEM image also revealed the formation of calcite (Fig. 3.6b). Figs. A2 and A3 also confirmed the formation of phosphate and carbonate products form magnesium and zinc peroxides at pH 7 and 9, but they were stable at unbuffered water.

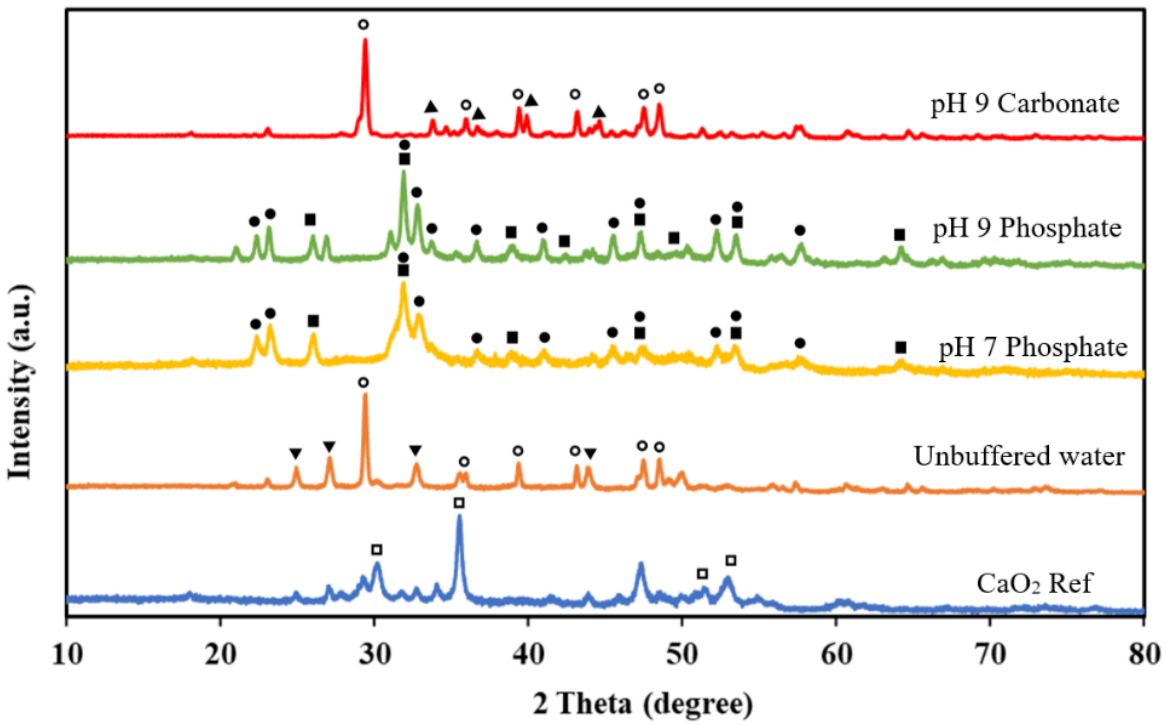

Fig. 3.5. X ray diffraction patterns showing phase composition of calcium peroxide immersed in different buffers for 7 days (□) CaO_2, (○) Calcite, (▼) Vaterite, (■) HA, (●) Na_2HPO_4 and (▲) $Na_3H(CO_3)_2.2H_2O$.

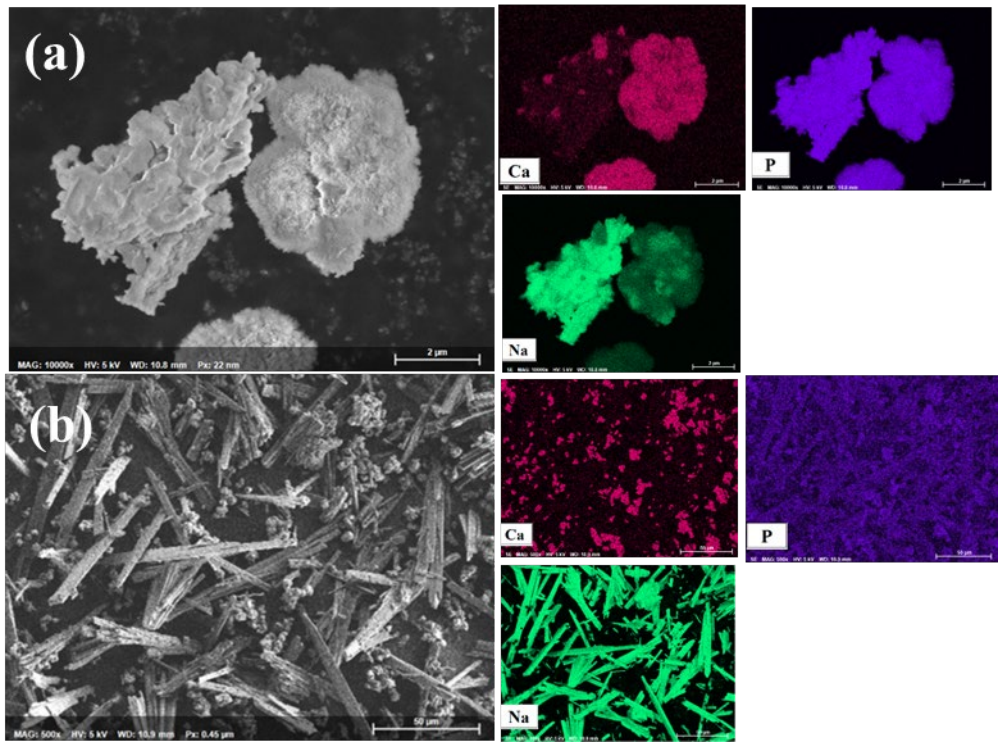

Fig. 3.6. Scanning electron micrographs and corresponding EDX elemental mapping of calcium, phosphorus and sodium in calcium peroxide after 7 days exposure to **(a)** pH 9 phosphate and **(b)** carbonate buffers, showing the precipitation of carbonate and phosphate compounds as a result of peroxide decomposition and the presence of unreacted peroxides.

3.5.6. Cytotoxicity

The cytotoxicity of solid peroxides was examined to determine the relative factors like alkalinity, oxygen, and hydrogen peroxide release rate and cation type with cell viability. The least cytotoxic solid peroxide was magnesium peroxide, since it was the only solid peroxide that when supernatant saturated with its degradation products formed over 24 hours added directly to culture, could support any cell viability (in this case ~50%), near full viability was restored when this supernatant was diluted 1:2. Calcium and zinc peroxides were considerably more toxic and even when diluted to 1:2, viability was 60% or less, and sodium percarbonate was cytotoxic even at 6x dilution (Fig. 3.7a).

Live/dead staining images showed that MDCK cells survived in 1:2 and 1:3 dilution of calcium and zinc peroxide extracts, 1:6 dilution of extract of sodium percarbonate and undiluted extract of magnesium peroxide (Fig. 3.7b). Lower dilutions were cytotoxic and resulted in either detachment or complete cell death. According to Fig. 3.1, the amount of released hydrogen peroxide at pH 7 phosphate after 24 hours could be expected to be ~6.8, 9.9, 10.0 and 16.3 mM for magnesium, calcium, zinc peroxide, and sodium percarbonate, respectively. This supports more cytotoxicity of sodium percarbonate, followed by zinc, calcium, and finally magnesium peroxide, with the lowest cytotoxicity. However, hydrogen peroxide levels alone did not seem to be the only reason for particular cytotoxicity of zinc peroxide since there was no significant difference between the released hydrogen peroxide from zinc and calcium.

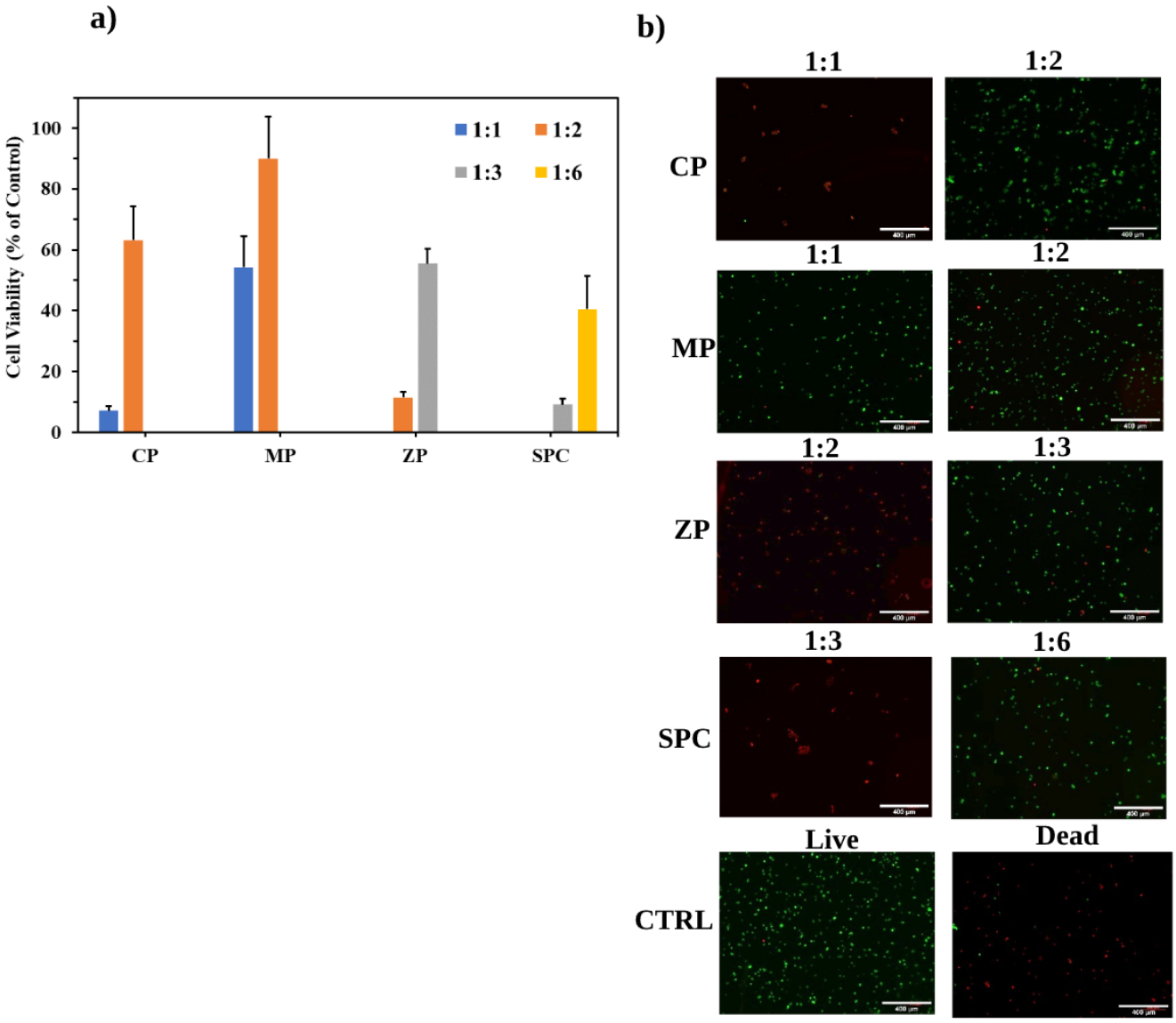

Fig. 3.7. (a) Percentage of cell viability relative to the mean of the live control group **(b)** Fluorescent images of live (green) and dead (red) MDCK cells following exposure to different dilutions of solid peroxide extract (1:1, 1:2, 1:3 and 1:6).

3.6. Discussion

While many prior studies aimed to avoid hydrogen peroxide formation, deliberate induction of bacterial or mammalian cell death clearly has many applications medically [8, 44, 50, 144, 154]. Furthermore, ROS including hydrogen peroxide act as a signaling molecule in inflammation and induce angiogenesis and vascularization [155]. In general, all peroxy compounds showed high hydrogen peroxide release and maximum hydrogen peroxide: oxygen ratio at acidic pH values

(Fig. 3.4). It is well known that the pH of bacterial infections can be lower than surrounding tissues [156], so most of the compounds we studied could feasibly find application as acid-induced hydrogen peroxide release depots. However, it must be recalled that while zinc peroxide was widely employed to treat infections in the pre-antibiotic era [157], it was not as effective as antibiotic treatments and indeed bacteria can become peroxide resistant [158]. Recently there have been efforts to enhance the antibacterial effect and indeed it would seem unlikely that pure peroxides can be immediately beneficial without further materials modification [56]. Accelerated hydrogen peroxide release from peroxy compounds can also be used to kill tumor cells or to radiosensitise them [27, 159, 160].

We observed pH-dependent oxygen release from peroxy compounds. Fig. 3.3 indicated that more oxygen production occurred from sodium percarbonate and calcium peroxide at pH 7 compared to pH 5, while hydrogen peroxide formation was not affected by pH. Therefore, hydrolysis reaction in neutral pH values can form oxygen directly from decomposition of more soluble compounds (calcium peroxide and sodium percarbonate). In contrast, less soluble compounds (magnesium and zinc peroxides) produced lower oxygen at pH 7 relative to pH 5. Increased oxygen release from zinc peroxide by decreasing pH was in consistent with previous studies showing that oxygen release was accelerated by faster zinc peroxide decomposition at acidic pH environment [56]. Moreover, zinc can decompose hydrogen peroxide catalytically in acid solutions [161] and increase oxygen production. Zinc peroxide was also highly affected by buffer composition at acidic and neutral buffers, while other peroxy compounds were not as sensitive to the buffer composition. The differences we observed in decomposition in phosphate and citrate buffers may originate from the buffer effectiveness. The pK_a value for citric acid ($C_6H_7O_7^-$/ /$C_6H_6O_7^{2-}$) and sodium dihydrogen phosphate (HPO_4^{2-}/$H_2PO_4^-$) is 4.76 [162] and 6.86 [163], respectively. The effective range of a buffer is about the pK_a ± one unit pH, so pH 5 citrate and pH 7 phosphate are within the buffer effective range and pH 5 phosphate and 7 citrate are outside the effective range. Therefore, pH 5 phosphate and pH 7 citrate were the conditions with the least buffering capacity and pH near the surface of particles may have been higher.

In evaluation of buffer composition, the lowest hydrogen peroxide: oxygen ratio was measured at pH 9 carbonate and hydrogen peroxide decomposed rapidly over 48 hours, approaching 0mM. The tendency of solutions of hydrogen peroxide to decompose at a faster rate in alkaline conditions is

not due to an increase in the hydroxyl ion concentration alone, but is caused by an increase in the catalytic activity of certain cations/anions present in the solution [164]. Because of significant differences between the amount of hydrogen peroxide released at phosphate and carbonate buffer with the same pH, it is evident that aside from the alkalinity of buffers, there is another factor influencing the stability of hydrogen peroxide most likely HCO_3^-/CO_3^{2-} [150]. Nicoll et al. [164] proposed that bicarbonate ion has more catalytic activity compared to dihydrogen phosphate ions, whereas phosphates can act as stabilizers of hydrogen peroxide [165]. As a result, pH 9 Carbonate can react with hydrogen peroxide (Eqs. 1, 2) [150]. The hydrogen peroxide decomposition rate will be the maximum amount at pH range between 11.5 and 11.7, where both peroxide molecules and perhydroxyl anions are present [166].

$$CO_3^{2-} + H_2O_2 \rightarrow CO_4^{2-} + H_2O \quad (1)$$

$$CO_4^{2-} + HO_2^- \rightarrow HCO_3^- + H_2O + O_2 \quad (2)$$

In order to confirm that carbonate, and not a combination specific cation was responsible for the instability of hydrogen peroxide at high pH, we measured hydrogen peroxide levels in a 0.5M buffer solution of either potassium or sodium carbonate over time (Fig. 3.8). In the presence of both salts, there was an ~80% reduction in peroxide level over 24 hours. At pH 8.5, PBS containing different sodium bicarbonate content, the effect was negligible and only at concentrations of 120mM was a statistically ($p<0.01$) discernable reduction in hydrogen peroxide level noted (~9% after 5 hours (Fig. A4)). However, since solid peroxides are impure mixtures of oxide, they inevitably have high pH microenvironments near the surface of aqueously exposed particles.

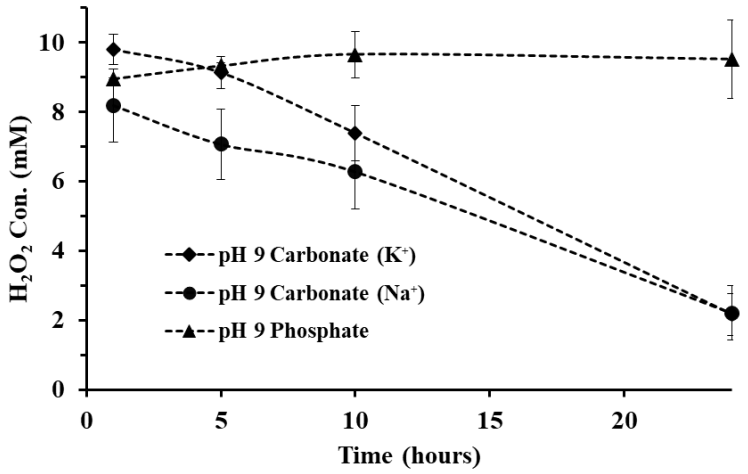

Fig. 3.8. The hydrogen peroxide decomposition at pH 9 (phosphate, carbonate buffers ($NaHCO_3$, $KHCO_3$)) as a function of time (N = 3). Dotted lines are a visual aid to clarify distinction of different data sets.

While the number of buffers investigated was limited, we were curious whether differing buffer compositions in culture media could affect hydrogen peroxide stability. We found measurable differences in hydrogen peroxide just after 2 hours addition to HEPES containing and HEPES free media (Fig. 3.9). This is in consistent with the previous results of Zhao et al. [167], suggesting HEPES oxidation by hydrogen peroxide. This further highlights the capacity for in vitro systems to introduce artefacts into experiments designed to simulate physiological conditions.

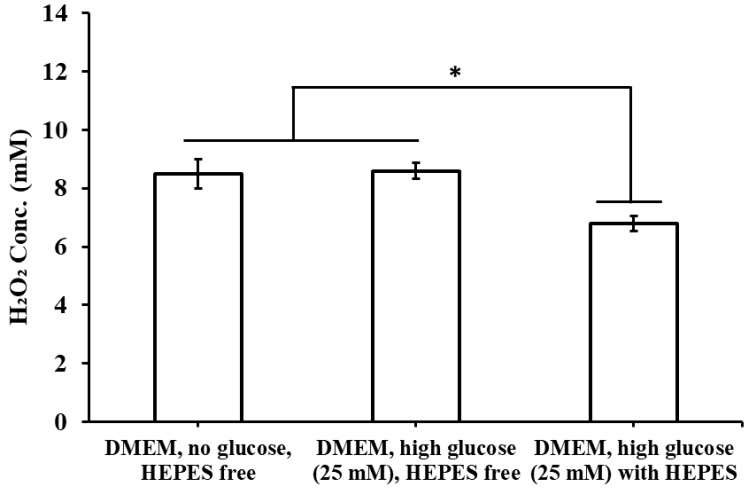

Fig. 3.9. Hydrogen peroxide stability in two different media supplemented with 25 mM glucose (in 5% CO_2, 37°C, 2 hours), * indicates $p<0.01$, N=3.

We found little evidence for the role of insoluble decomposition products playing a significant role in modifying decomposition behavior. The measured hydrogen peroxide concentration released from calcium peroxide over 48 hours in unbuffered water was 19% of the stoichiometric amount of hydrogen peroxide present in calcium peroxide. The slow dissolution of calcium peroxide in unbuffered water can probably be attributed to the formation of a transport barrier on the surface of particles, leading to a reduction in further hydrogen peroxide release. XRD results also confirmed the formation of insoluble carbonates or phosphates in water and buffers as reaction occurs. However, the measured concentrations of released hydrogen peroxide at pH 7 phosphate and citrate were 86% and 89% of hydrogen peroxide amount theoretically released over 48 hours, respectively (Fig. 3.1). Therefore, citrate buffers that form soluble products (no barrier) did not result in faster decomposition and there was no significant difference in hydrogen peroxide release between pH 7 phosphate with deposition products and pH 7 citrate without precipitated products.

Appreciably this deposition cannot change the reaction rate at buffers with the ability to maintain pH at pH 7, while unbuffered buffer and buffers with pH 9 can retain alkaline pH (hydroxide formation) in the vicinity of particles and prevent the reaction acceleration. It is the reason why magnesium and zinc peroxides were stable in unbuffered water (Figs. A2 and A3). Therefore, the pH and solubility of solid peroxides in water seem to be more effective in their decomposition behaviour than barrier formation.

Simultaneous decomposition of solid peroxides into oxygen and hydrogen peroxide enables them suitable for different therapeutic applications. However as solid peroxides decompose, they release basic ions. Most biological systems have some inherent buffering ability and so as shown in Figs. 3.1 and 3.2, pH is one of the most important parameters for decomposition. To some extent the solubility of peroxy compounds and thus released hydrogen peroxide can explain cytotoxicity. Magnesium peroxide with low solubility was the least cytotoxic compound and sodium percarbonate as the most soluble compound induced the highest cytotoxicity. Although solubility of calcium is greater than zinc, zinc peroxide was more toxic than calcium peroxide. 1:2 dilution of calcium extract caused ~63% cell viability, while 1:2 zinc dilution induced around 11% cell viability. Both zinc ions and hydrogen peroxide are considered as the products of zinc peroxide decomposition. Zinc ions can increase mitochondria ROS production and contribute to more oxidative stress [168]. Furthermore, the combination of zinc ions and hydrogen peroxide has been reported to have a synergistic impact on cell cytotoxicity [7], so we observed significantly less cell viability compared to calcium peroxide. Although zinc has quite a low oral toxicity since the uptake of cytotoxic doses of exogenous zinc generally is prevented by systemic homeostasis and efficient regulatory mechanisms, endogenous zinc is of essential importance in cytotoxic events in single cells [169]. *In vitro*, Zn^{2+} is regarded as a dangerous cation and very cytotoxic free ion, such that after intraperitoneal injection, LD_{50} for zinc is only four times higher than cadmium and mercury [170] compared to LD_{50} value for calcium which is about 4,000 times higher [171].
Our study found that there is a dose-dependent cytotoxic effect for solid peroxides (increasing cell viability by increasing the dilution factor). In agreement with this, Fernandez et al. [172] reported more cytotoxicity of sodium percarbonate at higher concentrations or less dilution. Therefore, decreasing hydrogen peroxide release rate and increasing oxygen concentration can improve cell metabolic activity. For example, embedding calcium peroxide in a core-shell structure improved

cell viability that was equivalent to a structure without peroxide by prolonging oxygen release and controlling the amount of released ROS [32].

There are limitations to the study. We did not investigate the impact of particle size on the reaction rate. Increasing the surface area as a result of particle size reduction as they slowly solubalise can cause a faster hydrolysis reaction and a higher concentration of ROS and oxygen [173]. Decomposition profiles in were collected under normoxic laboratory conditions, and solid peroxy compounds may behave differently in hypoxic conditions [174].

3.7. Conclusion

In this study, we examined the impact of pH and buffer composition on the extent of oxygen and hydrogen peroxide release for the first time. The results confirmed pH-dependent decomposition of peroxy compounds like zinc peroxide with accelerated decomposition at acidic environment. This dependence could be exploited to develop pH responsive hydrogen peroxide/ROS and oxygen delivery systems to tissues with an extreme pH range. Buffer composition also affected the decomposition. The accelerated oxygen release in carbonate buffers revealed a catalytic activity of carbonate ions in alkaline solutions. Interestingly, we also found a significant difference in hydrogen peroxide level following decomposition in two different media made with different buffers, this is extremely important since it indicates that *in vitro* systems are unlikely to mimic *in vivo* conditions and are often poor indicators of decomposition in tissues. We found that cytotoxicity was related to solubility and hydrogen peroxide formation but for zinc peroxide, the cation itself was particularly cytotoxic, potentially another factor for it falling out of clinical use. A future research objective will include measuring the bactericidal activity of peroxy compounds as a function of pH and understanding the impact of cation and pH on biocidal activity.

CHAPTER 4. INTRODUCTION TO MANUSCRIPT

The key findings in previous paper helped us to develop a formulation with controlled and prolonged oxygen release in skin flap, which was used and presented in the second manuscript. We could control hydrogen peroxide and hydroxide release by this formulation and as a result provide a cytocompatible film. We hypothesised that subdermal use of oxygen producing materials can improve skin flap survival. Together these two manuscripts provide valuable understanding of the potential use of solid peroxides as therapeutic compounds in skin flap surgeries until perfusion reestablishment.

A PILOT STUDY OF EFFICACY OF OXYGEN DELIVERY BIOMATERIAL FOR ISCHEMIC SKIN PRESERVATION

4.1. Authors

Arghavan Rastinfard[a], Benjamin Dalisson[b], Mirko Gilardino[c], Kevin Watters[d], Yassine Ouhaddi[a], Jake Barralet[a,b]

[a] Division of Orthopaedics, Department of Surgery, Faculty of Medicine and Health Sciences, Montreal General Hospital, Montreal, QC, H3G 1A4, Canada

[b] Faculty of Dentistry, McGill University, 2001 McGill College Avenue, Montreal, QC, H3A 1G1, Canada

[c] Division of Plastic and Reconstructive Surgery, Montreal General Hospital, Montreal, QC, H3G 1A4, Canada

[d] Department of Pathology, Glen Site, McGill University Health Centre, Montreal, Quebec, H4A 3J1, Canada

4.2. Abstract

Impaired or inadequate tissue blood supply (e.g., in a wound or a poorly vascularised graft) can result in tissue ischemia. As revascularization is a slow process relative to the proliferation of bacteria and the onset of tissue necrosis, the limited supply of oxygen and nutrients can result in extensive tissue damage. Additionally, necrosis can spread rapidly, and treatment options are limited such that loss of tissue in ischemic limbs or wounds following necrosis onset is considered unavoidable. There have been several reports of topical oxygen delivery to wounds, but few have attempted subdermal delivery. We developed a biomaterial implantable to sustain delivery of

oxygen directly to tissues and evaluated its preclinical efficacy in preventing ischemic necrosis in full thickness random skin flaps. Necrosis of the distal portion of the skin flap was delayed but not prevented. Necrosis in the middle part of the flap, however, was prevented indicating prolonged survival of skin with restricted blood flow for sufficiently long that the native vascular bed was able to reestablish blood supply. This study indicates that subdermal oxygen delivery alone cannot completely mitigate dermal necrosis. Nonetheless, it provides a compelling proof of concept that implanted materials can improve the survival of tissue at least in the short term to augment conventional treatments or to gain time until surgical intervention.

4.3. Introduction

The skin flap is an important surgical approach to skin reconstruction. When the flap is created, part of the vascularization is cut, which may lead to an inadequate blood supply and induce ischemia. Where a flap is pedicled, and its length exceeds that supplied by a single angiosome, the resulting blood flow path becomes random and is affected by choke vessels that connect discrete angiosomes. These flaps are referred to as random flaps, and the ability of these flaps to survive becomes a function of the length of the pedicle [66]. In addition, comorbidities like diabetes, radiotherapy, etc., may further exacerbate the ability of the blood supply to remodel sufficiently rapidly to prevent tissue death.

Ischemia, a restriction of blood flow to tissues, causes a shortage of oxygen and nutrients that are needed for cellular metabolism [68] and results in loss of tissue homeostasis and can result in damage or dysfunction of tissue when a delivery fails to meet metabolic requirements. In blood, the glucose concentration is regulated between 1.4 mmol/L and 6.2 mmol/L [175] and oxygen concentration between ~100 to 150 μmol/L [176]. Without oxygen, the adenosine triphosphate (ATP) production cycle is limited to a yield of 2 moles of ATP for 1 mole of glucose. In the absence of oxidative phosphorylation, glucose is converted into lactate through glycolysis, and the intracellular pH decreases [68, 71]. The lack of ATP leads to intracellular Na^+, water, and Ca^{2+} accumulation, cell membrane depolarization, protease activation as well as an increased reactive oxygen species (ROS) production [177], all of which can damage cells and lead to necrosis. In addition, in this environment, the mitochondrial membrane is disrupted and opening the permeability transition pore, which further decreases the ATP production and releases apoptotic

factors, and initiates the apoptotic cascade [68, 178]. These alterations and thus the degree of tissue injury varies with the extent and duration of the ischemic period [68].

In addition, necrosis can spread to surrounding tissue, and treatment options are still currently so limited that loss of tissue in ischemic limbs or wounds is considered unavoidable [179]. However, many 'dead' and deliberately cell free acellular tissues are actually used as regenerative allogenic scaffolds [180-182], and so the *in situ* reversibility of tissue death in theory at least seems possible. Calcium peroxide is unstable in aqueous conditions, decomposing to form molecular oxygen and hydrogen peroxide [183]. This and other peroxy- compounds have been widely studied for various oxygen delivery applications, for example, remediating waterlogged soil and in aquaculture [111, 113, 114, 119], and tooth whitening [124-126], but in implantable tissue repair applications, they are still at a research level and have not found application. The main reasons for this are that hydrogen peroxide may also be formed and that caustic hydroxides may be formed. We previously determined that toxic effects could be attributed to hydrogen peroxide generation [183] and pH elevation and so attempted to mitigate this by adding iron oxide as a peroxidase catalyst, adding an acidic buffer to help maintain neutrality, and by reducing the rate of reaction with a polymer diffusion barrier. Since we previously determined that at high pH (as found at the particle surface), carbonate ions can reduce hydrogen peroxide levels, we offset the acidity of calcium monophosphate by adding sodium bicarbonate. This study aimed to evaluate the preclinical efficacy of this simple oxygen generating film to reduce ischemic skin necrosis in full thickness rat random skin flaps.

4.4. Methods

4.4.1. Fabrication of subdermal oxygen generating films

Calcium peroxide (CaO_2, FMC Corporation), iron (II, III) oxide (Fe_3O_4, Sigma-Aldrich), sodium bicarbonate ($NaHCO_3$, Sigma-Aldrich), and calcium dihydrogen phosphate monohydrate, ($Ca(H_2PO_4)_2.H_2O$, abcr GmbH) powders were sieved using 74 μm sieve (ASTM 200 mesh) and then mixed. To fabricate subdermal oxygen releasing films, 10% PCL solution (w/v, M_w 80000, Sigma-Aldrich) was prepared by dissolving PCL in chloroform (Fischer Scientific). The particle mixtures were added to PCL solution (Table 4.1) and stirred for 24 hours to provide homogenous distribution of particles.

In order to produce a control that lacked buffering and peroxidase components, a suspension of 13.7% w/w CaO_2 and 19.7% w/w glass beads (212-300 µm, Sigma-Aldrich) were prepared in a 10%w/v PCL in chloroform. The glass beads acted as a filler so that the amount of particulates in both experimental and control groups was similar since it is well known that polymer permeability to water is strongly affected by filler level [184-186]. They were also sieved through a 74 µm sieve, same as buffering and peroxidase components to approximate the volume of the experimental sample filler. The composite solutions were cast in crystallizing dish, and the solvent was evaporated overnight.

2.3g of cast films were used to prepare the implants for *in vitro* oxygen release measurements and *in vivo* studies. PCL films become malleable around melting point (60 °C), so the dry films were molded into 1.7 × 7 × 0.1 cm^3 implants by heating them on a lab hot plate.

Table 4.1. Weight percentage (%wt) of the components composing experimental and control groups.

Sample	Weight percentage (%wt) of the components					
	CaO_2	Fe_3O_4	$NaHCO_3$	$Ca(H_2PO_4)_2.H_2O$	Glass beads	Total
Experimental	13.7	13.7	3.3	2.7	0	33.4
Control	13.7	0	0	0	19.7	33.4

4.4.2. pH value and hydrogen peroxide measurements

pH and hydrogen peroxide (H_2O_2) measurements were carried out in a sealed chamber for 14 days. Experimental and control containing 0.7 mg CaO_2 were immersed in 2 mL of water. The amount of released H_2O_2 was measured by the Thermo Scientific peroxide assay kit. The pH value of the solution was also measured by a pH meter (Mettler Toledo InLab Microelectrode).

4.4.3. Cytotoxicity of subdermal oxygen generating films

The samples were sterilized in 70% ethanol for 1 hour, washed three times with PBS, and dried under tissue culture hood overnight. 24-well plate and cell culture insert with 0.4µM pore size (PET track-etched membrane, Corning Inc, Corning, NY, USA) were used for cell culture studies. Madin-Darby Canine Kidney (MDCK) cells were cultured in RPMI-1640 (R8758, Sigma-Aldrich)

supplemented with 1% penicillin/streptomycin and 10% fetal bovine serum. MDCK cells were seeded at a seeding density of 2×10^4 cells/well and kept overnight at 37°C and 5% CO_2. Subsequently, each well medium was replaced with a fresh medium (700 µL). Oxygen generating films with the same amount of CaO_2 (0.17 mg) were placed in each culture insert of a 24 well plate, and then 300 µL of the medium was added to the inserts. The cells with no treatment were used as a positive control. After 24 hours, the cell viability was examined.

4.4.4. Live-dead assay

Cell viability was examined using a live-dead assay (Molecular Probes TM, LIVE/DEAD Viability/Cytotoxicity Kit). A dye solution containing 2µM Calcein AM and 2µM Ethidium homodimer-1 was prepared. After 24 hours, the cell culture inserts and medium were removed, and 300µL of dye solution was added to each well and then incubated for 30 min in the incubator. Cells after staining were analyzed by fluorescence microscope (EVOS M5000 Imaging System).

4.4.5. Oxygen and lactate measurements

For *in vitro* measurements, an oxygen generating film ($1.7 \times 7 \times 0.1$ cm^3) was immersed in 40mL phosphate-buffered saline (PBS) at 25°C in an open beaker (Ø=5cm, 2cm liquid depth). The oxygen content of the PBS was assessed using an oxygen probe (AL300 Oxygen Sensor Probe, Ocean Optics). For calibration, the oxygen sensor was exposed to 0, 10, 20, 30, 40, 60, and 80% dissolved oxygen in water (prepared by flushing nitrogen and oxygen gas through water) until the Tau value (fluorescence lifetime) stabilize. For *in vivo* measurements, the probe was inserted through the gaps between sutures under the skin flap at 3 different positions: proximal, middle, and distal. Measurements were performed under anesthesia just after the surgery (day 0) and on days 1, 2, 4, 6, 8, 10. At the moment of euthanasia, sections of the flap were frozen at -80°C and processed [1] to measure the lactate content of the tissues using a Lactate assay kit (Sigma-Aldrich).

4.4.6. Surgical methods

Wistar rats (male, 5 to 6-month-old, 500 to 600g, Charles River Laboratories Inc. Montreal, QC, Canada) were randomized into 2 groups. The control group received no biomaterial, and the experimental groups received oxygen releasing films subdermally (N=9 per group). Surgical procedures were performed after approval from McGill University Animal Care Committee

(UACC, #7899). Animals received carprofen (10mg/kg) 30 min prior to the surgery; all surgeries were performed under general anesthesia using 2% isoflurane. Full depth skin flaps of 9 × 2 cm^2 in size were created on the back [187]. A silicon sheet (SMI, 0.005" NRV M/M 40D) was placed over the muscle to prevent revascularization and reperfusion of the dermal side of the flap from the underlying tissue, then the film was positioned distally, and the skin was re-replaced on top of it and sutured. Animals received carprofen (10mg/kg) every 24 hours for 3 days post-surgery, then slow-release buprenorphine every three days until the experimental endpoint. Animals were allowed free access to food and water and housed in a 12 h day/night cycle. Five animals were sacrificed on day 6, four animals on day 10 using carbon dioxide.

4.4.7. Evaluation of skin flap survival

The skin flap areas were photographed on days 1, 2, 4, 6, 8, and 10 after surgery. On each day, ImageJ software was used to analyze the images and measure the necrotic area. The necrotic tissue was calculated by this formula: necrosis area/flap area × 100. Thermal images were also recorded postoperatively using a smartphone compatible thermal imaging camera (Seek Thermal CompactPRO) in 320x240 resolution and RGB format.

4.4.8. Histology and immunohistochemistry analysis

Flaps sections (proximal, middle, and distal) were cut and divided in half lengthwise. A half sections were used for lactate measurement, and other sections were fixed in 4% paraformaldehyde for 24 hours at 4°C. Samples were placed in a tissue Tek VIP5 Vacuum Infiltration Processor and embedded in paraffin by the Leica EG 1150H. Then, tissues were sectioned with a microtome (RM 2255 microtome Leica Microsystems, Germany) in 4μm of thickness size. Tissue sections were deparaffinized using xylene and stained with Hematoxylin & Eosin (H&E). Immunohistochemical staining was performed with anti-CD34 for blood vessels (1:1000 dilution, ab81289, Abcam), anti-Foxp3 antibody for regulatory T cells (1:200 dilution, ab22510, Abcam), anti-iNOS antibody for M1 polarized macrophages (1:100 dilution, ab3523, Abcam), recombinant anti-Liver arginase antibody for M2 polarized macrophages (1:1000 dilution, ab203490, Abcam), and anti-F4/80 as general macrophage marker (1:500 dilution, EMR1 Antibody (PA5-21399)) using standard procedures. Each slide was washed with PBS (pH 7.4) and incubated with a secondary antibody using the Vectastain ABC kit (Vector Laboratories) according to the manufacturer's instructions. The color was developed with 3,3'-diaminobenzidine (DAB) solution (Vector Laboratories)

containing hydrogen peroxide. The sections were scanned using Aperio scanner ScanScope XT and analyzed by ImageScope software (Leica Biosystems). Tissue necrosis area visible in H&E-stained sections was measured. For microvascular and macrophage markers, DAB staining was quantified within the distal, middle, and proximal areas using the Color Deconvolution algorithm (Aperio). The results were reported as percent total positive × total stained area/total analysis area.

4.5. Results

4.5.1. *In vitro* characterization of subdermal oxygen generating films

First, we examined the ability of oxygen releasing films in offsetting pH values. When immersed in water, the control raised the pH to 10.8 within 2 hours and then continued to increase to 11.4 and 11.6 over 2 and 14 days. In contrast, oxygen releasing films increased pH value to 8.1 within 2 hours and pH was below 10 over 2 days. Then, pH increased gradually to 11.6 within 2 weeks (Fig. 4.1A). These measurements were initially conducted in Eppendorf tubes that were closed in between measurements. Repeating the experiment in tubes that were left open resulted in lower pH for both experimental and control groups. The maximal pH values were obtained in open condition was about 75% and 87% of those in a closed system for experimental and control groups, respectively. The pH value for the control group peaked at 10.1 after 2 hours and then decreased to 8.7 over 24 hours. In contrast, oxygen generating group caused a smaller rise in pH to 8.4 and then stabilized and reached a plateau of 8.7 pH after 24 hours (Fig. 4.1B). This difference was attributed to the reaction with atmospheric carbon dioxide.

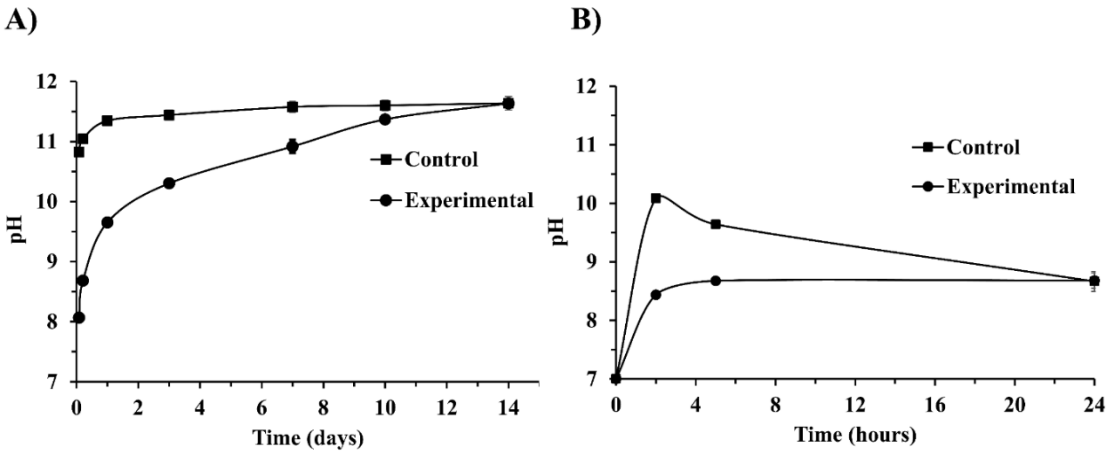

Fig. 4.1. The pH value of water containing control and experimental films **(A)** over two weeks in Eppendorf tubes without air flow **(B)** over 24 hours in open Eppendorf tubes with air contact. The control group is oxygen releasing films formed without iron oxide nanoparticles and buffering components. N=3.

We also attempted to reduce the toxic effect of hydrogen peroxide through incorporating iron oxide with known catalytic activity towards hydrogen peroxide decomposition [53, 188] and sodium bicarbonate since we found that carbonate could also be effective in reducing hydrogen peroxide levels [183]. We confirmed the addition of these compounds significantly ($P<0.05$) decreased the hydrogen peroxide released from the film over the experiment, Fig. 4.2. Both experimental and control groups reached the maximal hydrogen peroxide release after one day (83.3μM for experimental and more than double, 187.7μM for control). Hydrogen peroxide content decreased gradually for both groups, indicating the decomposition rate exceeded the release rate.

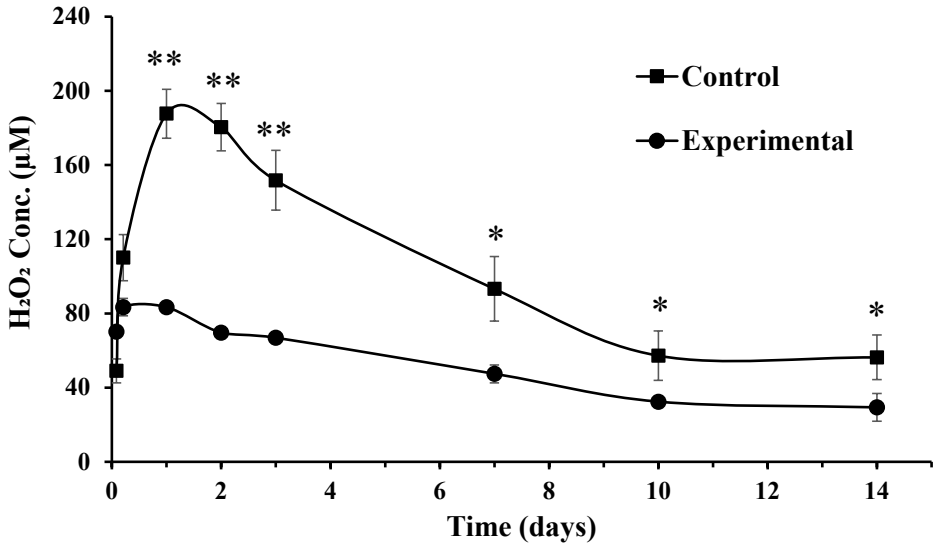

Fig. 4.2. The analysis of hydrogen peroxide release from control and experimental films over two weeks in closed Eppendorf tubes. The control group is oxygen releasing films formed without iron oxide nanoparticles and buffering components. N=4, **P<0.01 and *P<0.05.

Next, we examined the cytotoxicity of experimental and control on MDCK cells after 24 hours. As shown in Fig. 4.3, the control group is significantly cytotoxic with about 34% cell viability. In contrast, the experimental group caused about 81% cell viability through incorporating buffering agents and magnetite. Live/dead assay measurement confirmed higher numbers of viable cells in the experimental group than control. Therefore, oxygen generating films incorporating iron oxide and buffering components enhanced cytocompatibility since iron oxide reduced hydrogen peroxide release and buffers controlled shifting pH values.

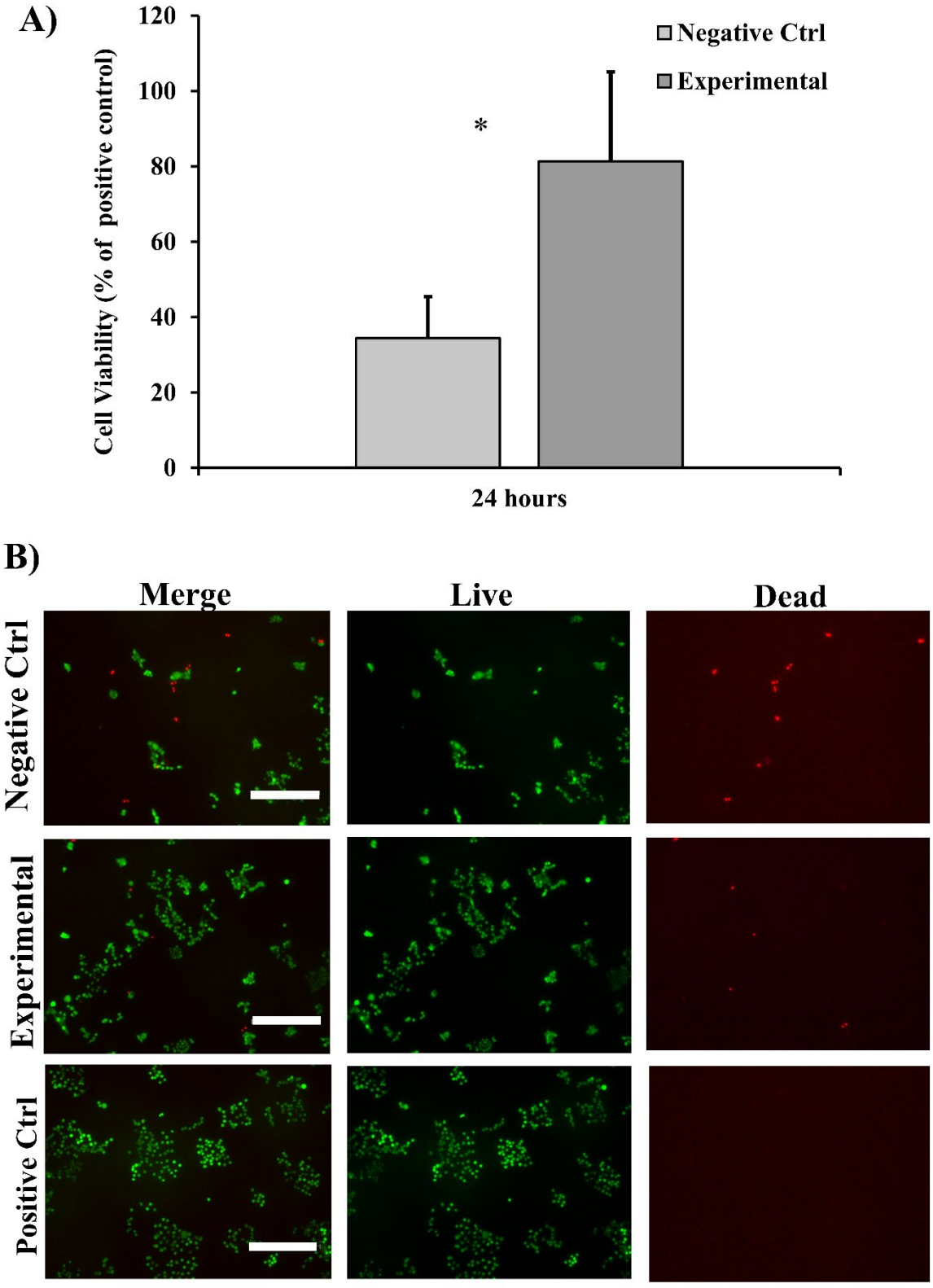

Fig. 4.3. (A) Cytotoxicity of experimental and control group **(B)** Fluorescent microscopic images of the cells after 24 hours using live/dead assay. N=3, * P<0.05. The negative control group is oxygen generating films formed without iron oxide nanoparticles and buffering components. Positive control is cells without any treatment. The scale bar is 300μm.

The oxygen release from experimental was significantly higher compared to that from control baseline remained at about 20% throughout the entire experiment ($P<0.05$), Fig. 4.4. There was a burst release of oxygen at first 15 minutes and oxygen generating films delivered about 35% oxygen. After that, oxygen release raised to about 48% on day 1 and reached the maximum amount of 52% on day 2. Although oxygen levels gradually decreased after day 2, oxygen generating film was able to sustain oxygen release over two weeks.

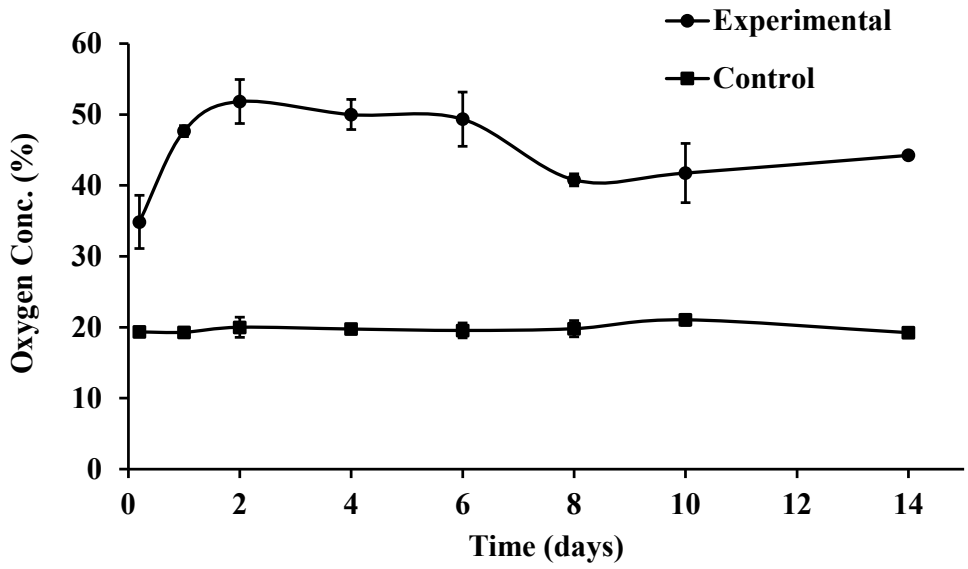

Fig. 4.4. Oxygen release from experimental and control groups in 40 mL PBS at 20°C for two weeks. The control group is films formed without calcium peroxide and iron oxide incorporation.

4.5.2. *In vivo* characterization

At each time point, the skin flaps were photographed, and the necrotic area was evaluated. Immediately after the surgery, the distal part of the flaps of both groups appeared slightly blue (Fig. 4.5A) and dark blue after one day with some necrosis at the extremity. On day 2, the necrosis was obvious in the distal portion of the flap for both groups. The middle and proximal portions were normal in the subdermal oxygen generating group, while in the control group only proximal area appeared normal. On day 4, the dark blue middle portion in control group turned brown and gradually blackened and necrotic over the next few days. The necrotic area in the oxygen releasing group became darker and rougher, starting day 4, but the necrosis did not spread to the middle and proximal area over the experiment.

The extent of skin flap necrosis was significantly greater ($P<0.05$) in the control group than in the experimental group on days 2 and 10 (Fig. 4.5B). In the control group, the necrotic surface area significantly increased after surgery and remained at around 40±10% from day 4 to day 10. In the experimental group, the necrosis increased from about 2±1% on day 1 to 28±11% on day 4 and then remained almost stable at 31±8% until the end of the experiment. Examination of the data revealed that animals developed necrosis at very different rates even within study groups, using analysis of a dichotomous endpoint (did extent of necrosis exceed 40% at any time during healing in a particular subject? (Y/N)), we determined a statistical difference of $P<0.05$ at a power of 98.4% (Table 4.2).

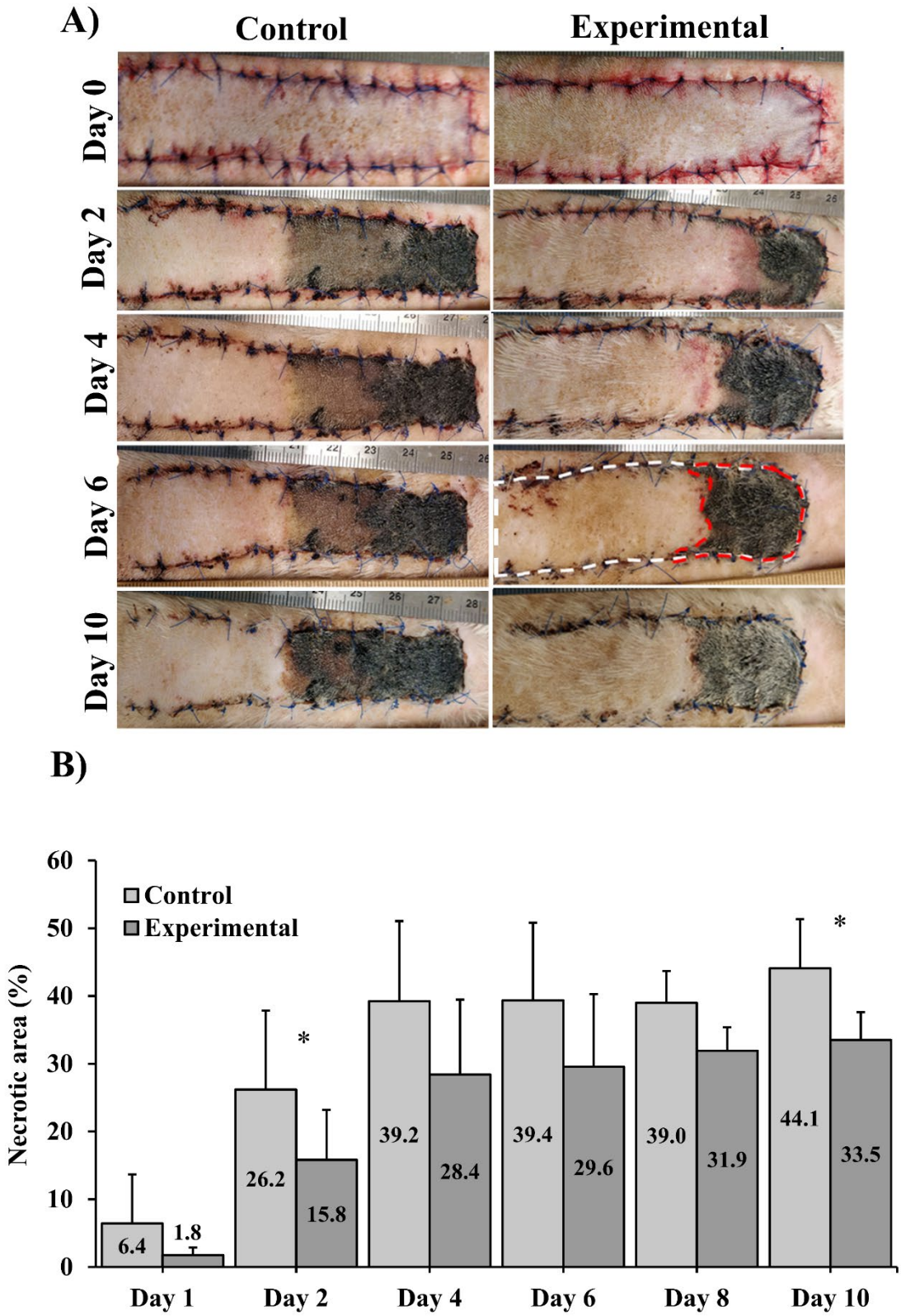

Fig. 4.5. (A) Representative photographs of the skin flap on days 0, 2, 4, 6, and 10 for control and experimental groups, **(B)** Histogram representing the visible relative necrotic area over time, expressed as necrotic area (red dotted line) over total visible flap area (white dotted line). Control group is skin flaps without receiving any materials. Values are expressed as mean ± SD, N=9 per group. *P<0.05.

Table 4.2. Result of dichotomous endpoint analysis.

Sample	Size	Proportion of Necrosis > 40%	Results
Experimental	9	11%	P <0.05
Control	9	89%	Post-hoc power 98.4%

Subcutaneous oxygen concentration was measured immediately after the surgery and on days 1, 2, 4, 6, 8, and 10 post-surgeries in the middle of the proximal, middle and distal third sections. In the control group, no significant differences in subcutaneous oxygen level were observed from day 1 to day 10 at any sections (Fig. 4.6). A similar observation was recorded in the experimental group. Oxygen concentration normally found in tissues (physoxia) is between 2 and 5%, and oxygen levels less than 2% are considered hypoxic [189]. As shown in Fig. 4.6, the oxygen level in the experimental group at any sections of the flap was near physoxic concentration, while there was hypoxia in the control group. The subcutaneous oxygen concentration in the middle and proximal portions was found to be significantly higher in the subdermal oxygen releasing group than in control ($P<0.001$). In the distal portion, the oxygen level was not significantly different ($P<0.05$) between the experimental and control groups. Thermal imaging revealed the temperature gradient over the flap with three different areas (Fig. 4.7): combination of yellow and green (mean temperature 27.9°C), orange (30.4°C), and red (31.7°C). As indicated in Fig. 4.7, the proximal area was about 3.8 and 1.3°C warmer than the distal and middle areas, respectively. Therefore, the green/yellow portion with 3.8°C drops of the reference adjacent skin temperature was the least blood flow area. However, the blackness zone was smaller in the visual image and did not correlate with the least temperature area in the thermal image. To further investigate the impact of oxygen delivery on skin flap, we measured lactate levels of flap tissue. Higher lactate production can be an indication of glycolytic metabolism because of less oxygen content in the ischemic flap [1]. Fig. 4.8 showed no significant difference ($P<0.05$) in lactate concentration between experimental and control groups, although oxygen level was significantly greater in experimental than control. Moreover, lactate measurements for each section of the flap did not indicate significant differences in levels between flap regions or with time at days 6 and 10.

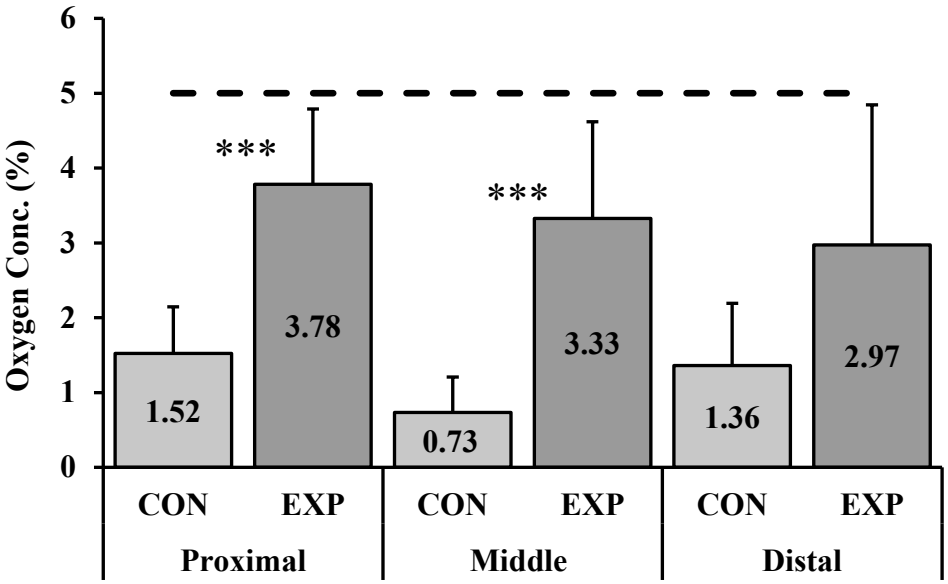

Fig. 4.6. Histogram representing the subcutaneous oxygen concentration of the skin flaps under the proximal, mid-, and distal thirds of the flaps for both the untreated control and the experimental group, all time points combined (the dotted line represents physoxic oxygen concentration for comparison (2-5%)). Values are expressed as mean ± SD, N=8 per group. ***P<0.001. Abbreviations: CON: control, EXP: experimental.

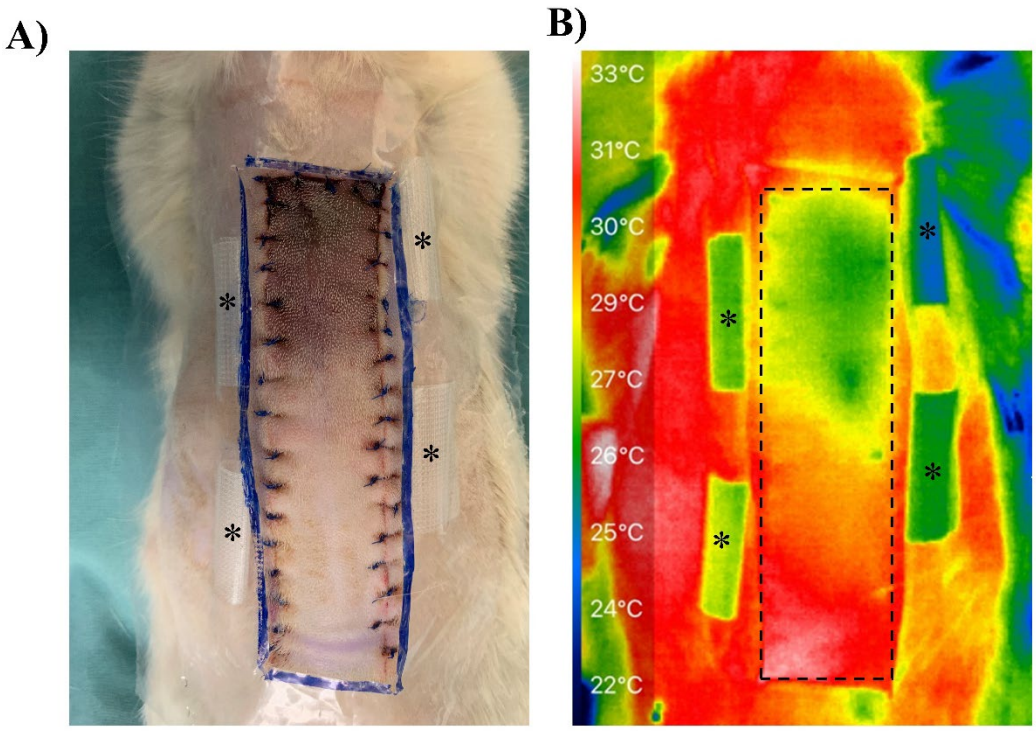

Fig. 4.7. (A) Second day post operative visual and **(B)** IR thermal image of a control flap. The dashed line represents the flap area. Plastic tubes (*) and plastic frame were used as a reference to overlay the thermal and non-thermal images.

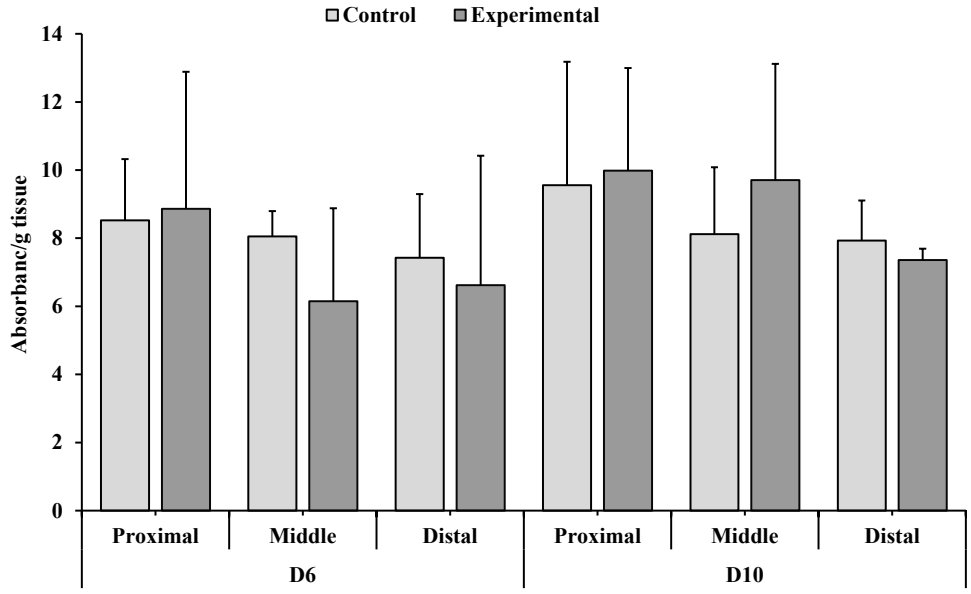

Fig. 4.8. Histogram representing lactate quantification of each section of the flap for untreated control and experimental group at days 6 and 10. Results are expressed as absorbance per gram of tissue and were not significantly different between groups. Values are expressed as mean ± SD, N=3.

Fig. 4.9 shows an H&E-stained cross-section of skin flap tissues from both groups with two different magnifications. Little difference was visible in the tissue architecture of the proximal section when observed under H&E staining between experimental and untreated control groups (Fig. 4.9A, B). Fewer nuclei were discernible (indicative of necrotic non-viable tissue) for both groups as the distance from the proximal section increased. In the midsections, the experimental group exhibited necrosis to a lesser extent than controls, so the interface between live and dead tissue was located at the middle zone for control and distal or middle for the experimental group. Histologically, polymorphonuclear neutrophils (PMN) and also the formation of new epidermis underneath the necrotic tissue were visible at the interface between the necrotic and healthy tissues (Fig. 4.10). The distal portion was the necrotic area for both groups, where disruption of tissue architecture and increased eosinophilia were obvious. In the necrotic portion of the flap, ghost cells were visible around the appendages identified as preserved cell outlines without nuclei. For both groups, the distal sections mostly consisted of necrosed tissues resembling some of the aspects of coagulative necrosis [190, 191] with the disappearance of the nuclei and appendages. Histomorphometric measurement of the relative necrotic area in the skin flaps (epidermis, dermis, and hypodermis) was performed on the H&E-stained sections (Fig. 4.9C). On day 6, the mean necrotic area in the proximal third was 0.0% for both groups and in the distal sections 100.0 ± 0.0% and 85.5 ± 28.5% for the control and experimental group, respectively. In the middle section,

the mean necrotic area was 49.3 ± 37.8% in the control group and 18.9 ± 9.8% for the experimental. There was no significant difference in necrotic area of the three sections between control and oxygen releasing groups.

Four days later on day 10, the necrotic area in the proximal third was 0.0% for both groups, and in the distal area we did not observe a significant difference between groups. In the mid-section, however, necrosis was significantly higher in the control group with 31.1 ± 14.1% of necrotic area versus 6.4 ± 6.1% for experimental ($P<0.05$).

Immunohistochemistry staining was carried out for CD34 to compare blood vessels density in control and experimental groups on day 6. Image analysis of CD34 staining (Fig. 4.11A) exhibited significantly more CD34-positive vessels between the middle and distal area of the experimental group ($P<0.05$), while there was no significant difference between CD34-positive vessels of middle and distal sections in the control group. Measurements of the blood vessel density (mm^2 of blood vessels per mm^2 of tissue) revealed no significant difference between control and experimental groups in three different sections (Fig. 4.11B).

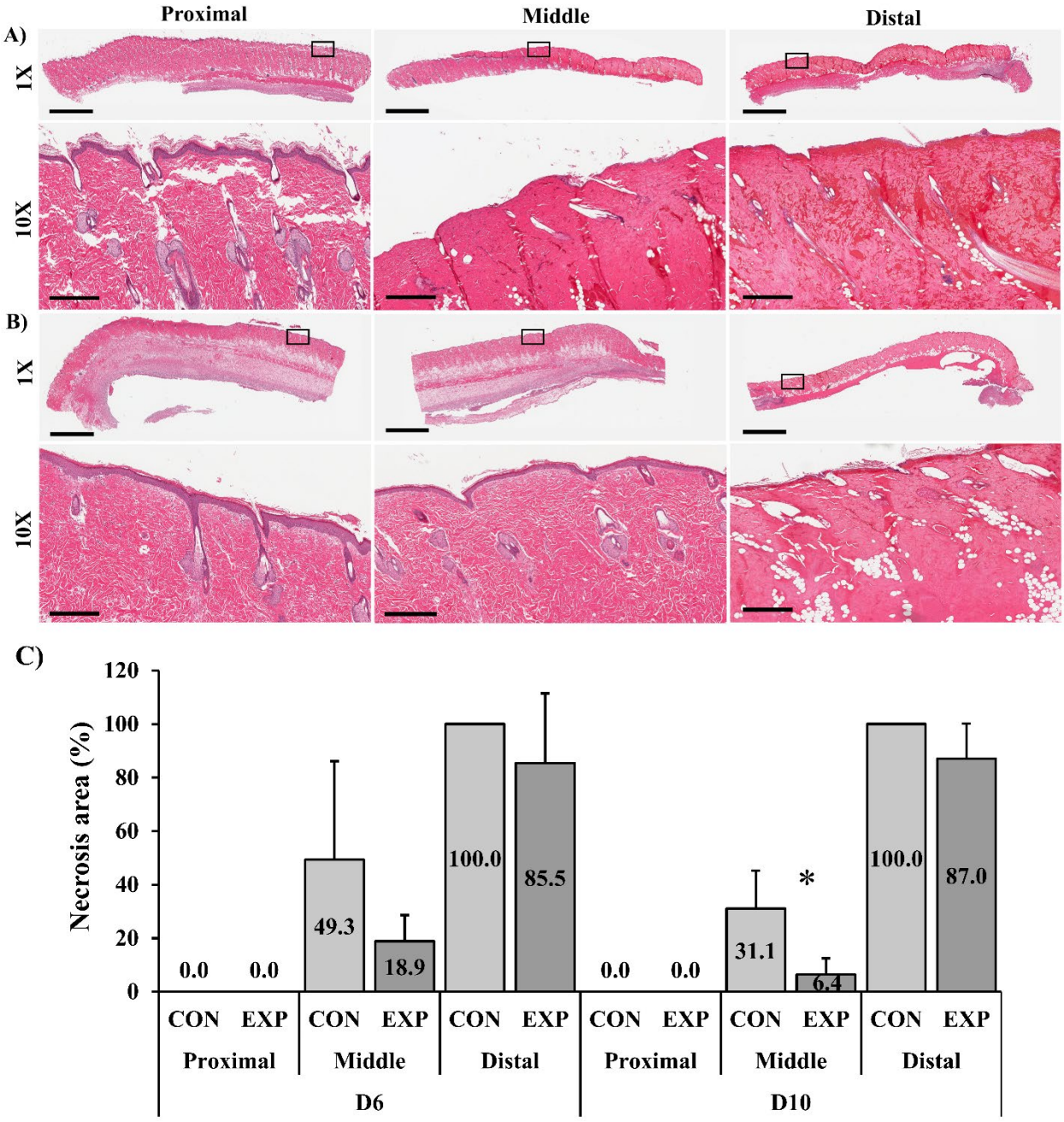

Fig. 4.9. Proximal, middle, and distal area of the H&E-stained sections of skin flap in **(A)** control and **(B)** experimental group after 6 days. Black square boxes indicate the locations examined under higher magnification. The scale bar is 4mm and 400 µm in 1X and 10X magnification, respectively **(C)** Histogram representing relative necrotic area observed histologically with H&E staining of the skin flap sections in control and experimental groups on day 6 and day 10, expressed as necrotic area over total area. Values are expressed as mean ± SD, N=5 per group on day 6 and N=3 on day 10, *P<0.05. Abbreviations: CON: control, EXP: experimental.

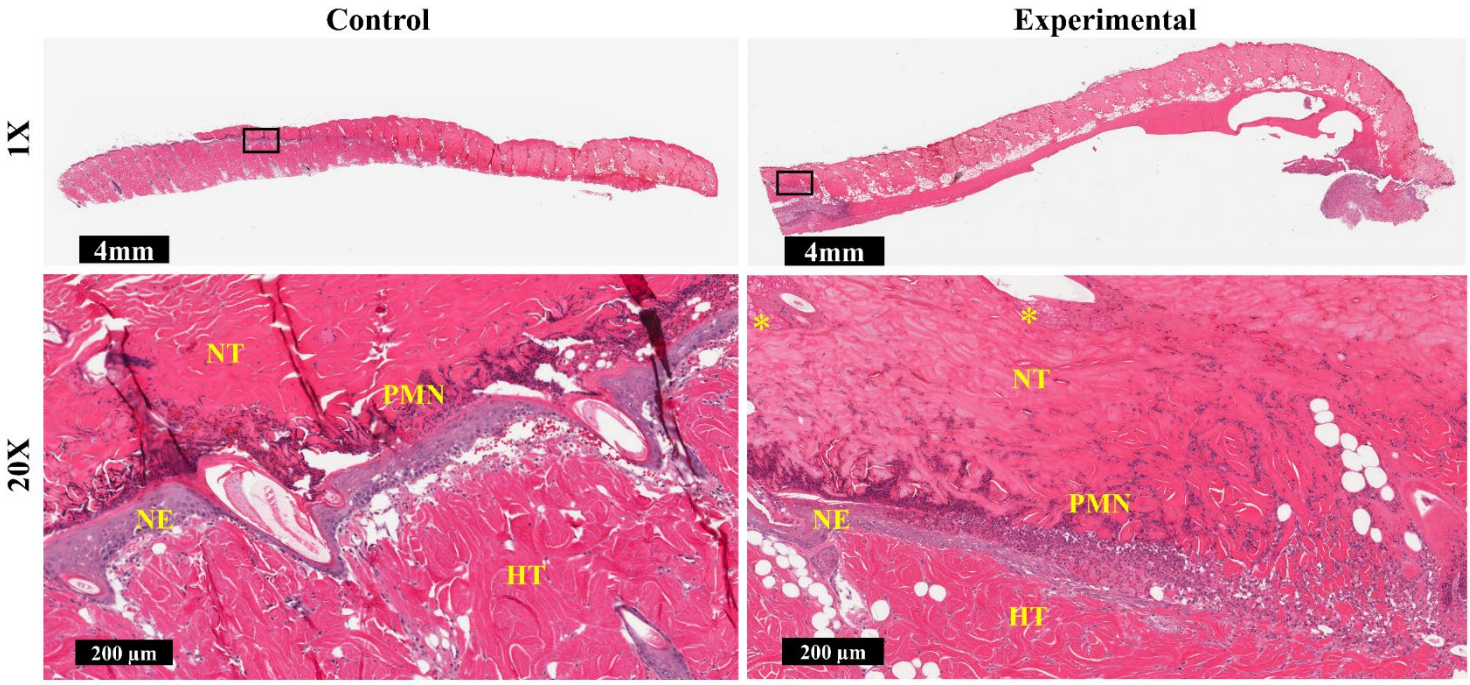

Fig. 4.10. The interface of a healthy and necrotic area of H&E-stained sections of skin flap in control and experimental groups after 6 days. Black square boxes indicate the interface of healthy and necrotic tissue examined under higher magnification. HT: healthy tissue, NT: necrotic tissue, PMN: polymorphonuclear neutrophiles, NE: new epidermis and *: ghost cells.

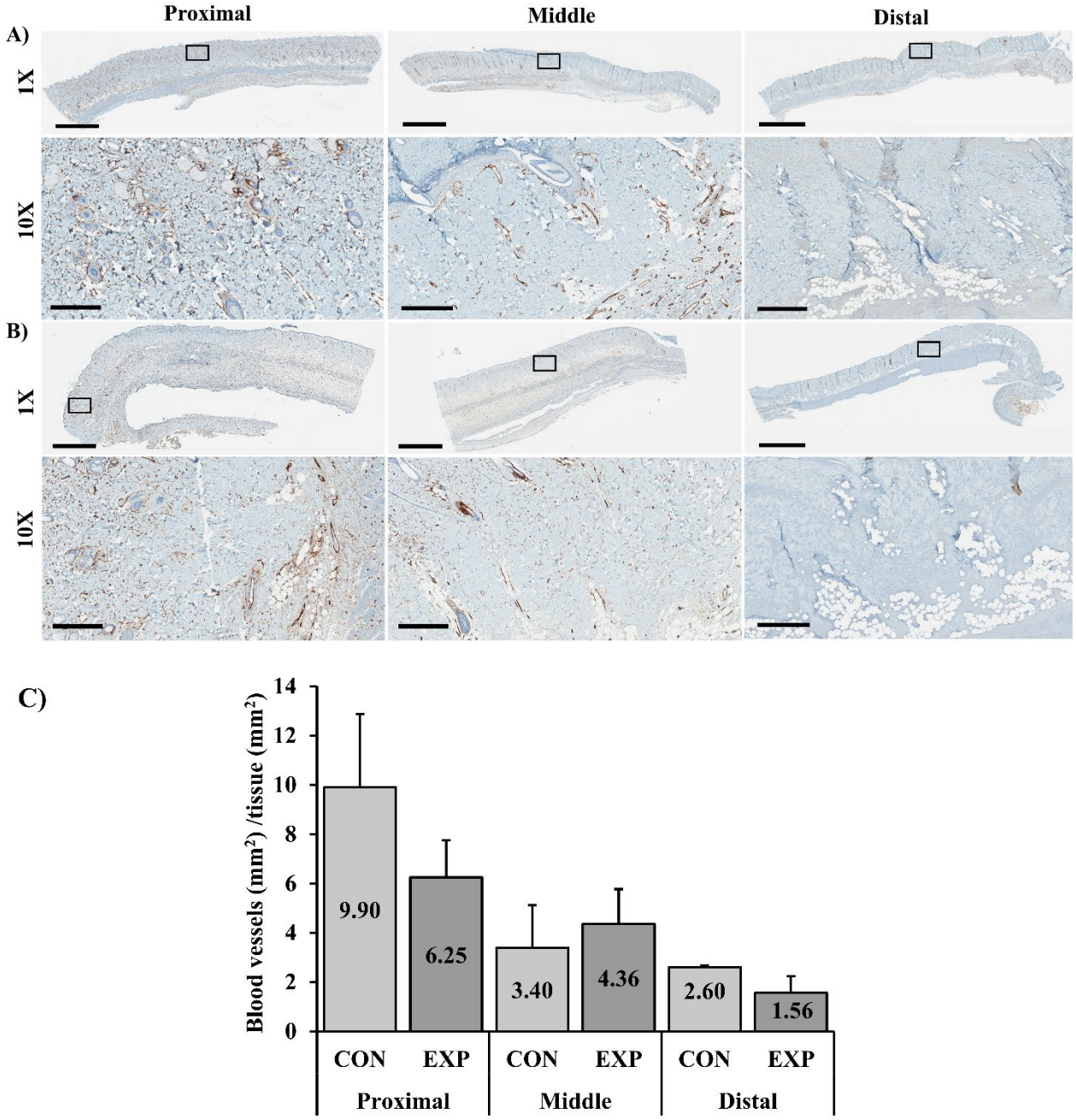

Fig. 4.11. CD34-positive vessels of proximal, middle, and distal skin flap sections in (A) control (B) experimental group. The scale bar is 4mm and 400 µm in 1X and 10X magnification, respectively. (C) Histogram representing relative blood vessel density in epidermis, dermis, and hypodermis, expressed as mm² of blood vessels per mm² of tissue for different skin flap sections in control and experimental groups on day 6. Values are expressed as mean ± SD, N=3 per group. Abbreviations: CON: control, EXP: experimental.

To understand how macrophages participate in skin flap necrosis, we sought to identify the phenotypes of macrophages during tissue repair. Fig. 4.12 shows immunohistochemistry staining of the middle portion of the flap, consisting of the live and dead zone on day 6. Flap sections were stained with a pan-macrophage marker (F4/80), the traditional pro-inflammatory macrophages (M1) marker (iNOS), and anti-inflammatory macrophages (M2) marker (liver arginase). Macrophages present different markers other than iNOS and liver arginase, which are not specific for the identification of M1 or M2 macrophages, and they can be detected in other cells. Therefore, we checked and confirmed the matching between expression of F4/80 as a general macrophage marker and expression of both iNOS and liver arginase (Fig. 4.12A). Analyzing the images showed a significant difference in density of liver arginase with $1.36 \pm 0.45/mm^2$ and $16.01 \pm 8.08/mm^2$ between the control and experimental group, whereas there was no significant difference for the density of iNOS with $5.04 \pm 1.92/mm^2$ and $6.69 \pm 2.27/mm^2$ for the control and experimental group, respectively (Fig. 4.12B).

Since regulatory T cells (Tregs) play a major role in mediating immune homeostasis in the skin, we analysed Foxp3-expressing Tregs to determine whether these cells play a role in alleviating inflammation associated with wounds. Fig. 4.13 shows a significant difference with $0.64 \pm 0.11/mm^2$ and $0.16 \pm 0.07/mm^2$ between the control and experimental group, respectively.

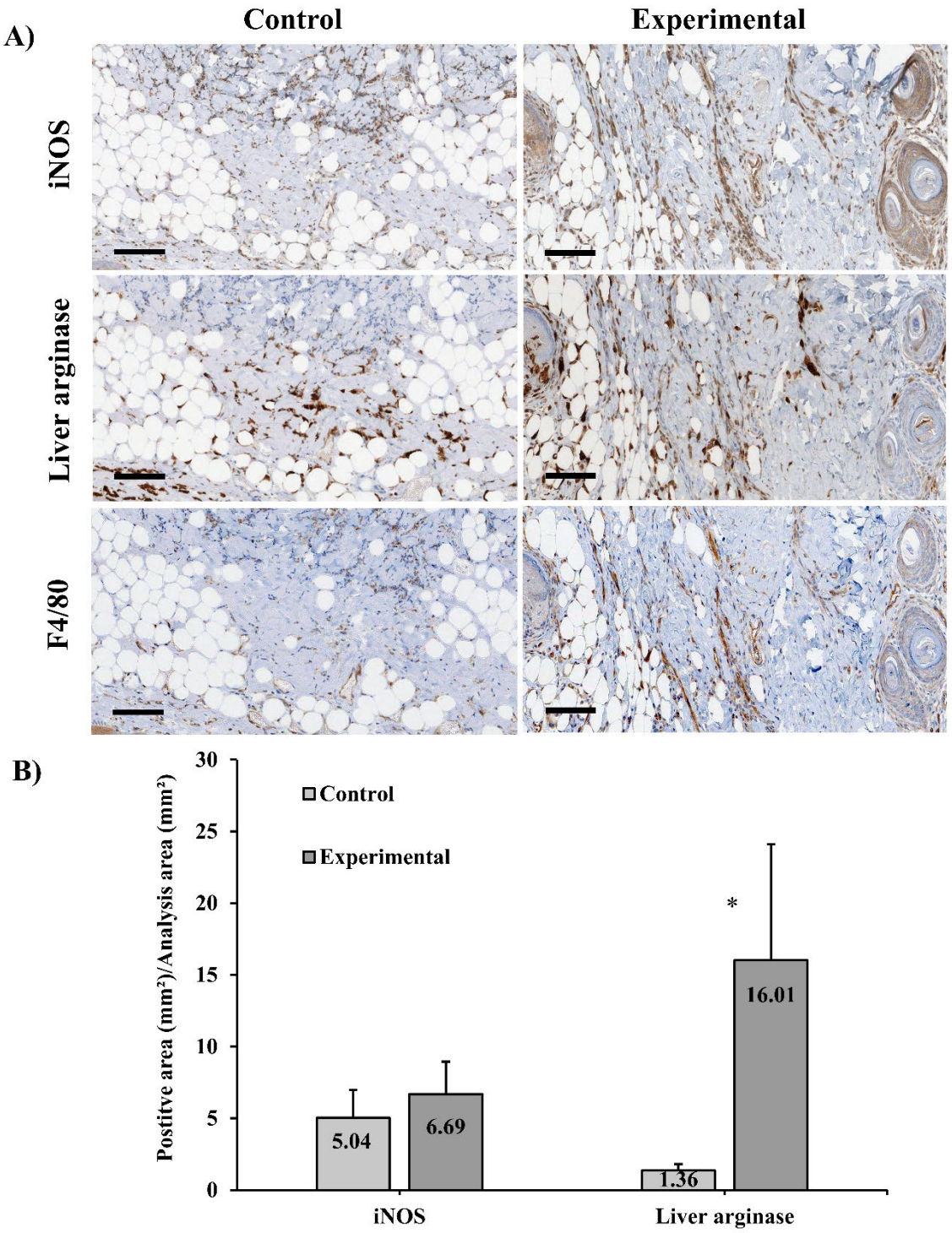

Fig. 4.12. (A) Representative iNOS, liver arginase, and F4/80 immunostaining of skin flap in middle portion for the control and experimental groups on day 6 **(B)** Histogram representing positive stained area (mm^2) per tissue area (mm^2). Values are expressed as mean ± SD, N=3 per group, *P<0.05. The scale bar is 200 µm.

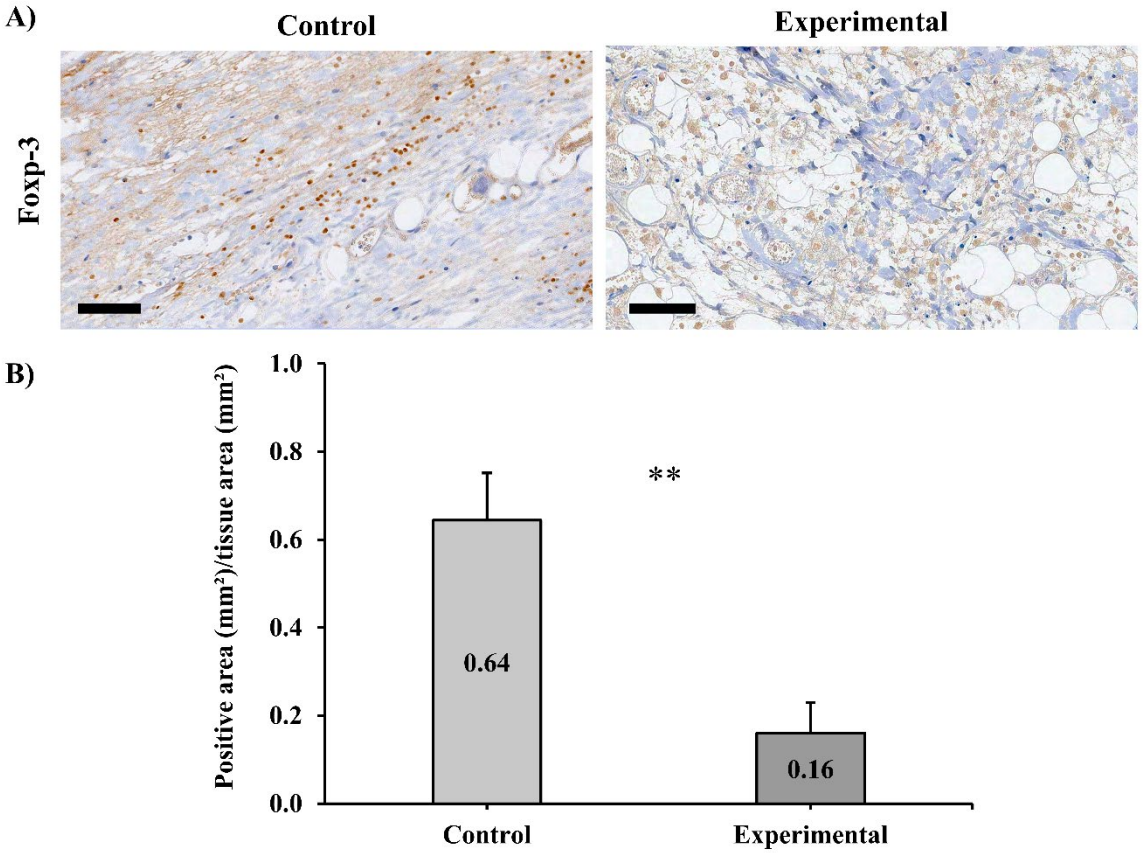

Fig. 4.13. (A) Representative Foxp-3 immunostaining of skin flap in middle portion for the control and experimental groups on day 6. The scale bar is 200 µm. **(B)** Histogram representing Foxp-3 positive stained area (mm^2) per tissue area (mm^2). Values are expressed as mean ± SD, N=3 per group, **P<0.01.

4.6. Discussion

Many different technologies have been developed to address issues encountered when oxygen is insufficient *in vitro* and *in vivo* [19], like hyperbaric oxygen therapy (HBOT), perfluorocarbon (PFC) technologies, hemoglobin based carriers, etc. The particular advantage of the use of peroxy-compounds like hydrogen peroxide, sodium percarbonate, and calcium peroxide is to produce oxygen *in situ*. Indeed to produce one liter of pure oxygen, less than 10 grams of peroxide is required, while it would require several hundredths of grams of red blood cells or several kilograms of PFCs or plasma [192]. In this study, the oxygen producing film was able to release oxygen using the reaction between calcium peroxide and water. Skin oxygen consumption is approximately 0.38µl/h/mg (~0.017µmol/h/mg) [193], such that theoretically 2.6g of calcium peroxide could oxygenate a 7.5g skin flap for 6 days. This amount of peroxide would drastically change the subcutaneous pH and result in skin damage. Much less solid peroxide has typically been previously used preclinically. The first report by Harrison et al. [1] used oxygen generating biomaterials to prevent skin flap necrosis. In this work, sodium percarbonate was encapsulated within Poly (D, L-lactide–co–glycolide) by solvent casting method. The film was able to release oxygen over a 70h period. They showed less necrotic tissue, lower lactase concentration, and levels of apoptotic cells over 3 days. However, after 7 days, there was no significant difference between oxygen producing and control groups in the amount of tissue necrosis. Shiekh et al. [4] generated CaO_2-encapsulated antioxidant polyurethane (PUAO) and implanted it in a skin flap on the backs of mice. A sustained oxygen release was observed from CaO_2-PUAO for 10 days. CaO_2-PUAO group demonstrated more skin flap survival compared to the PU scaffold without CaO_2. Although the results confirmed less tissue necrosis through incorporating CaO_2 into PUAO polymer compared with PU alone, no significant difference was reported in skin flap survival (histologically and visually) between no scaffold and CaO_2-PUAO scaffold.

Here, we reduced hydrogen peroxide generation by adding peroxidase catalysts (iron oxide), a compound known to react with hydrogen peroxide (bicarbonate), and a hydrophobic polymer barrier (polycaprolactone) (Fig. 4.2). We also adjusted pH with an acidic buffer, calcium dihydrogen phosphate (Fig. 4.1). These effects reduced cytotoxicity *in vitro* since iron oxide reduced hydrogen peroxide release and calcium dihydrogen phosphate controlled shifting pH values (Fig. 4.3). We were able to deliver oxygen subcutaneously for 10 days (Fig. 4.6), and we

have shown significant improvement in skin flap survival over those 10 days as compared to control (Fig. 4.5), yet it was not sufficient to prevent necrosis in the distal portion. The results obtained for the control group in this study are consistent with other studies in literature using a similar model, and a similar size [103, 194, 195].

Histomorphometric analysis of the H&E-stained sections on day 6 did not show a significant difference in total necrotic area between control (40.9 ± 14.1%) and oxygen releasing group (27.3 ± 11.6%), like what was observed in macroscopic evaluation of necrotic areas. On day 10, the total necrotic area was significantly different, with 35.6 ± 3.8% and 24.7 ± 5.5% for the control and oxygen generating groups, respectively ($P<0.05$). Interestingly, these numbers were lower than necrotic areas calculated by macroscopic evaluation (Fig. 4.5B). This may be explained by the contraction of the necrotic sections over time. Therefore, contraction is considered a parameter that can affect the results. Previously, Bayramicli et al. [196] showed the higher contraction rate of necrosis tissue compared to the viable portion of an epigastric flap, leading to decreased necrotic area percentage at the experiment endpoint.

Another limitation of this experiment as evidenced by the skin's blue color post-surgery, indicating a venous stasis, a pathology that commonly occurs in skin flaps and that may have participated in necrosis occurrence and spreading [197] and may have hindered the potential benefits of oxygen generating film partially. This pathology is usually addressed clinically using compression methods [198], antithrombotic [199] or leeches [200, 201] One can easily envisage a combination of oxygen releasing materials to other techniques to extend further skin flap survival. The use of leeches has been shown to improve epigastric flap survival during venous congestion [202], and in a similar model the use of some antithrombotic has also been shown to improve skin flap viability [203]. Beyond the prevention of venous congestion, other methods have been shown to increase skin flap survival, like N-acetylcysteine [204, 205], antioxidant scavenging the radicals formed during the ischemic cascade, or vasodilators like nitroglycerine [95] and Sildenafil [93]. However, there are controversial results regarding the advantage of vasodilators. We observed about 50% necrosis by applying nitroglycerine patches topically (Fig. B1). This can be because of systemic hypotension consequences of using vasodilators which seems to be detrimental to blood flow and skin flap survival [100]. Therefore, adjusting the doses,

administration route, and treatment duration is a principle to avoid the possible hypotensive effects of vasodilators [97].

In vivo oxygen measurements showed that oxygen generating films could induce near physoxic oxygen concentration at any section of the flap, but the oxygen level was statistically similar between the experimental and control group at the distal portion (Fig. 4.6). This can be attributed to insufficient blood flow in the distal section, which was confirmed by thermal images (Fig. 4.7). Skin temperature decreased longitudinally by moving from proximal to the distal area as shown in Fig. B2, but there was a fluctuation in skin temperature over time, which can be due mainly to hair growth, changing ambient temperature, and the impact of image registration markers on temperature. Therefore, thermal imaging was prone to artifactual limitations, especially over time. Lack of adequate blood vessels inhibited oxygen diffusion to full skin thickness because oxygen diffusion distance through tissues is rarely more than 200μm [206], yet the thickness of the skin was several millimeters, implying that a part of the flap was not receiving oxygen from the oxygen releasing film. More blood vessels in middle and proximal sections (higher skin temperature in thermal images) could increase oxygen levels in blood vessels and provide oxygen delivery to greater skin thickness through oxygen diffusion between vessels and cell membranes. Therefore, it is possible that the use of split thickness skin flap could result in improved viability in distal area. The lactate concentration, a marker of tissue hypoxia, inside each section of the flap was not significantly different between both groups (Fig. 4.8). This suggests that oxygen delivery alone was not sufficient to maintain aerobic mechanism in the whole skin thickness.

In inflammation, wound macrophages play a key role in the skin flap due to their function in the production of mediators and growth factors at the wound site [207, 208]. Successful healing of skin flap tissue in healthy rats is characterized by the presence of alternately activated macrophages during healing [209]. M1 macrophages play a pro-inflammatory role, present antigens, and function as an immune monitor with the expression of pro-inflammatory cytokines, such as Il-6, iNOS, HLA-DR, and the transcription factors pSTAT1 and RBP -J [210-212]. M2 macrophages mainly secrete Arginase-I, interleukin 10 (IL-10), CD163, and transforming growth factor-β (TGF-β) [213-215] and other anti-inflammatory cytokines, which are responsible for reducing inflammation and play a role in wood healing [216].

Immunostaining (Fig. 4.12A) showed that the expression of iNOS and liver arginase match the localisation of expression of F4/80. Macrophage M2 phenotype is associated with the promotion of tissue repair and pro-angiogenic function [217, 218], suppression of inflammation (by limiting responses dependent on M1), and regulation of wound healing and fibrosis [219].

After the skin lesion, the inflammatory phase occurs early, characterized by strong activation of the innate and adaptive immune systems. Tregs constitute a large percentage of lymphocytes that reside in the skin [220, 221], and they play an essential role in regulating the tissue inflammation. We sought to determine whether Tregs play a role in the healing of skin wounds in our experimental group compared to the control. We found that the number of cells was lower in the tissues of rats with oxygen releasing film compared to the control. Knowing that activated Tregs accumulate in the skin plays a major role in reducing the accumulation of pro-inflammatory macrophages [222], which does not explain the low rate of M1. Maybe the oxygen releasing film increased the transition from M1 to M2 early.

This study's goal was to determine whether oxygen delivery could be effective in reducing necrosis. It did not determine whether macrophage polarisation (and hence immune modulation) is a direct consequence of oxygenation or whether oxygenation improved healing, and hence we observed an associated increase in M2 as part of that healing process. However, previously increased polarization of M2 macrophages has been observed to coincide with the oxygen level in the microenvironment [223, 224]. The sequential occurrence of the two macrophage polarization states has been reported as being necessary for correct resolution of healing [217, 225] and for tissue repair after injury [226]. Given the complexity of the healing, inflammatory and host bed response it appears not unreasonable that elevating oxygen levels in what is otherwise ischemic tissue may have multiple beneficial effects to mitigate conditions that are conducive to ischemic necrosis.

4.7. Conclusion

Here we report the fabrication and use of a non-biodegradable oxygen delivery implant which was able to sustain the release of a large amount of oxygen over 14 days. Although we demonstrate its efficacy to prevent necrosis, the study is inherently limited by the oxygen amount delivered and by the ischemic model used because oxygen is not the only factor of necrosis onset and venous

congestion that may have played a non-negligible role. This situation is not uncommon, and clinically relevant and oxygen delivery is here shown as a tool to help prevent necrosis onset.

CHAPTER 5. DISCUSSION AND FURTHER WORK

Our first paper showed that the relationship between pH and peroxides' decomposition could not be explained as a general statement like faster decomposition by decreasing pH because other factors also influence this dependence, such as buffer composition and type of solid peroxides. For example, we observed the accelerated oxygen release in carbonate buffers and confirmed the catalytic activity of carbonate ions in alkaline solutions. Buffer effectiveness impacted oxygen and hydrogen peroxide release from less soluble peroxy- compounds and pH 5 citrate buffer clearly increased oxygen formation relative to pH 5 phosphate buffer. Interestingly, we also found a significant difference in hydrogen peroxide level following decomposition in two different cell culture media made with different buffers, this is extremely important since it indicates that *in vitro* systems are unlikely to mimic *in vivo* conditions and are often poor indicators of decomposition in tissues. These were the key findings of first paper which we used in developing the formulation of subdermal oxygen releasing films for skin flap. A future research objective will include designing a combination of different peroxides with antimicrobial effects and at the same time oxygen generation in the wound. The requirement of this research is to measure the bactericidal activity of peroxy- compounds as a function of pH and understand the impact of cation and pH on biocidal activity.

We developed a new formulation for oxygen releasing films. We used sodium bicarbonate in formulation because of its ability to reduce hydrogen peroxide levels at high pH and offset the acidity of calcium monophosphate. Oxygen releasing films reduced hydrogen peroxide generation and prevented pH elevation and as a consequence, improved cell viability. They were able to deliver oxygen subcutaneously for 10 days and improve skin flap survival over 10 days as compared to control. However, the previous studies did not report a significant difference in skin flap survival between oxygen producing and control flaps more than 3 days [1, 4]. Interestingly, we observed higher expression of M2 macrophages in oxygen releasing films than control. Oxygen delivery could impact M2 polarization at the wound site and improve the flap survival by reducing inflammation and contributing to wood healing, because the presence of alternatively activated macrophages is necessary for healing of skin flap tissue in healthy mice [69]. Therefore, in this

study insufficient blood supply due to obstruction of arterial inflow and impaired venous outflow, and inflammatory response were effective in necrotic loss of skin flap tissue. Although we demonstrate the efficacy of oxygen delivery to reduce necrosis, we could not prevent necrosis totally. Necrosis appeared multifactorial; and combined strategies would seem required to sustain skin integrity in which there is no blood flow like preventing venous congestion, suppressing inflammatory reactions, and reducing oxidative stress. Studying the synergistic impact of oxygen releasing materials and clinical methods for addressing venous congestion on skin flap survival can be taken into account as a future research objective.

CHAPTER 6. CONCLUSION

Understanding the decomposition behaviour of non-formulated peroxy- compounds in isolation from other materials plays a key role in designing hydrogen peroxide/ROS and oxygen delivery systems as their behaviour is complex and highly dependent on the measurement environment. Therefore, we examined the release profiles of peroxides as a pre-requisite study and used its key findings in designing oxygen releasing films in the ischemic skin flap model. The results clearly showed controlling hydrogen peroxide release and offsetting pH changes by the developed oxygen delivery formulation. However, delivering oxygen to ischemic tissue was just an example of therapeutic applications of peroxy- compounds, and they can be used in many different medical applications, so our comparative study of peroxides' decomposition seems functional to formulate a system for any intended biological effect.

References

[1] B. S. Harrison, D. Eberli, S. J. Lee, A. Atala, and J. J. Yoo, "Oxygen producing biomaterials for tissue regeneration," *Biomaterials,* vol. 28, no. 31, pp. 4628-4634, 2007/11/01/ 2007, doi: https://doi.org/10.1016/j.biomaterials.2007.07.003.

[2] F. L. Meleney, "Present role of zinc peroxide in treatment of surgical infections," (in eng), *J Am Med Assoc,* vol. 149, no. 16, pp. 1450-3, Aug 16 1952, doi: 10.1001/jama.1952.02930330018006.

[3] S. Tripathi, B. N. Singh, S. Divakar, G. Kumar, S. P. Mallick, and P. Srivastava, "Design and evaluation of ciprofloxacin loaded collagen chitosan oxygenating scaffold for skin tissue engineering," *Biomedical Materials,* vol. 16, no. 2, p. 025021, 2021/02/23 2021, doi: 10.1088/1748-605x/abd1b8.

[4] P. A. Shiekh, A. Singh, and A. Kumar, "Oxygen-Releasing Antioxidant Cryogel Scaffolds with Sustained Oxygen Delivery for Tissue Engineering Applications," *ACS Applied Materials & Interfaces,* vol. 10, no. 22, pp. 18458-18469, 2018/06/06 2018, doi: 10.1021/acsami.8b01736.

[5] C. Y. C. Montesdeoca *et al.*, "Oxygen-generating smart hydrogels supporting chondrocytes survival in oxygen-free environments," *Colloids and Surfaces B: Biointerfaces,* vol. 194, p. 111192, 2020/10/01/ 2020, doi: https://doi.org/10.1016/j.colsurfb.2020.111192.

[6] E. Pedraza, M. M. Coronel, C. A. Fraker, C. Ricordi, and C. L. Stabler, "Preventing hypoxia-induced cell death in beta cells and islets via hydrolytically activated, oxygen-generating biomaterials," *Proceedings of the National Academy of Sciences of the United States of America,* Article vol. 109, no. 11, pp. 4245-4250, 2012, doi: 10.1073/pnas.1113560109.

[7] L.-S. Lin *et al.*, "Cooperation of endogenous and exogenous reactive oxygen species induced by zinc peroxide nanoparticles to enhance oxidative stress-based cancer therapy," (in eng), *Theranostics,* vol. 9, no. 24, pp. 7200-7209, 2019, doi: 10.7150/thno.39831.

[8] Y. Sheng *et al.*, "Oxygen generating nanoparticles for improved photodynamic therapy of hypoxic tumours," (in eng), *J Control Release,* vol. 264, pp. 333-340, Oct 28 2017, doi: 10.1016/j.jconrel.2017.09.004.

[9] M. Gholipourmalekabadi, S. Zhao, B. S. Harrison, M. Mozafari, and A. M. Seifalian, "Oxygen-Generating Biomaterials: A New, Viable Paradigm for Tissue Engineering?," (in eng), *Trends Biotechnol,* vol. 34, no. 12, pp. 1010-1021, Dec 2016, doi: 10.1016/j.tibtech.2016.05.012.

[10] S. R. Baker, *Local Flaps in Facial Reconstruction*. Elsevier Health Sciences, 2007.

[11] N. B. Semer, *Practical Plastic Surgery for Nonsurgeons*. Hanley & Belfus, 2001.

[12] A. C. Society, "Breast Cancer Facts & Figures 2019-2020," American Cancer Society, Inc, Atlanta, 2019.

[13] Aetna. "BRCA Testing, Prophylactic Mastectomy, and Prophylactic Oophorectomy." http://www.aetna.com/cpb/medical/data/200_299/0227.html (accessed November 23, 2021).

[14] S. A. Robertson, J. A. Jeevaratnam, A. Agrawal, and R. I. Cutress, "Mastectomy skin flap necrosis: challenges and solutions," (in eng), *Breast Cancer (Dove Med Press),* vol. 9, pp. 141-152, 2017, doi: 10.2147/BCTT.S81712.

[15] K. L. Zhou, Y. H. Zhang, D. S. Lin, X. Y. Tao, and H. Z. Xu, "Effects of calcitriol on random skin flap survival in rats," (in eng), *Sci Rep,* vol. 6, p. 18945, Jan 6 2016, doi: 10.1038/srep18945.

[16] A. Francis and R. C. Baynosa, "Hyperbaric Oxygen Therapy for the Compromised Graft or Flap," (in eng), *Adv Wound Care (New Rochelle),* vol. 6, no. 1, pp. 23-32, 2017, doi: 10.1089/wound.2016.0707.

[17] S. Zellner, R. Manabat, and D. F. Roe, "A dissolved oxygen dressing: a pilot study in an ischemic skin flap model," (in eng), *J Int Med Res,* vol. 43, no. 1, pp. 93-103, Feb 2015, doi: 10.1177/0300060514541826.

[18] H. Steg, "Oxygen-releasing biomaterials," University of Groningen, 2018.

[19] A. L. Farris, A. N. Rindone, and W. L. Grayson, "Oxygen Delivering Biomaterials for Tissue Engineering," (in eng), *J Mater Chem B,* vol. 4, no. 20, pp. 3422-3432, 2016, doi: 10.1039/C5TB02635K.

[20] W. C. Schumb, *Hydrogen Peroxide, by Walter C. Schumb, Charles N. Satterfield [and] Ralph L. Wentworth*. Reinhold Publishing Corporation, 1955.
[21] H. Zhang and J. E. Barralet, "Mimicking oxygen delivery and waste removal functions of blood," *Adv. Drug Deliv. Rev.,* Review vol. 122, pp. 84-104, 2017, doi: 10.1016/j.addr.2017.02.001.
[22] A. L. Farris, A. N. Rindone, and W. L. Grayson, "Oxygen delivering biomaterials for tissue engineering," *Journal of Materials Chemistry B,* vol. 4, no. 20, pp. 3422-3432, 2016.
[23] I. I. Vol'nov and A. W. Petrocelli, *Peroxides, Superoxides, and Ozonides of Alkali and Alkaline Earth Metals*. Plenum Press, 1966.
[24] G. Camci-Unal, N. Alemdar, N. Annabi, and A. Khademhosseini, "Oxygen-releasing biomaterials for tissue engineering," *Polymer international,* vol. 62, no. 6, pp. 843-848, 2013.
[25] H. Wang, Y. Zhao, T. Li, Z. Chen, Y. Wang, and C. Qin, "Properties of calcium peroxide for release of hydrogen peroxide and oxygen: a kinetics study," *Chemical Engineering Journal,* vol. 303, pp. 450-457, 2016.
[26] P. L. Thi, Y. Lee, D. L. Tran, T. T. Hoang Thi, K. M. Park, and K. D. Park, "Calcium peroxide-mediated in situ formation of multifunctional hydrogels with enhanced mesenchymal stem cell behaviors and antibacterial properties," (in eng), *J Mater Chem B,* vol. 8, no. 48, pp. 11033-11043, Dec 23 2020, doi: 10.1039/d0tb02119a.
[27] M. Zhang *et al.*, "Calcium-Overload-Mediated Tumor Therapy by Calcium Peroxide Nanoparticles," *Chem,* vol. 5, no. 8, pp. 2171-2182, 2019/08/08/ 2019, doi: https://doi.org/10.1016/j.chempr.2019.06.003.
[28] S. Khorshidi, A. Karkhaneh, and S. Bonakdar, "Fabrication of amine-decorated nonspherical microparticles with calcium peroxide cargo for controlled release of oxygen," *Journal of Biomedical Materials Research - Part A,* Article vol. 108, no. 1, pp. 136-147, 2020, doi: 10.1002/jbm.a.36799.
[29] P. K. Chandra *et al.*, "Peroxide-based oxygen generating topical wound dressing for enhancing healing of dermal wounds," *Wound Repair and Regeneration,* vol. 23, no. 6, pp. 830-841, 2015, doi: https://doi.org/10.1111/wrr.12324.
[30] Z. W. Zehra M, Hasan A, Butt H, Ramzan A, Azam M, Mehmood A, Falahati M, Chaudhry AA, Rehman IU, Yar M., "Oxygen Generating Polymeric Nano Fibers That Stimulate Angiogenesis and Show Efficient Wound Healing in a Diabetic Wound Model," *Int J Nanomedicine,* vol. 15, pp. 3511-3522, 2020.
[31] J. I. Kang, K. M. Park, and K. D. Park, "Oxygen-generating alginate hydrogels as a bioactive acellular matrix for facilitating wound healing," *Journal of Industrial and Engineering Chemistry,* vol. 69, pp. 397-404, 2019/01/25/ 2019, doi: https://doi.org/10.1016/j.jiec.2018.09.048.
[32] X. Lv *et al.*, "Structural and functional evaluation of oxygenating keratin/silk fibroin scaffold and initial assessment of their potential for urethral tissue engineering," *Biomaterials,* vol. 84, pp. 99-110, 2016/04/01/ 2016, doi: https://doi.org/10.1016/j.biomaterials.2016.01.032.
[33] T.-E. Hsieh, S.-J. Lin, L.-C. Chen, C.-C. Chen, P.-L. Lai, and C.-C. Huang, "Optimizing an Injectable Composite Oxygen-Generating System for Relieving Tissue Hypoxia," (in English), *Frontiers in Bioengineering and Biotechnology,* Original Research vol. 8, no. 511, 2020-May-26 2020, doi: 10.3389/fbioe.2020.00511.
[34] T. Abudula *et al.*, "Oxygen-Releasing Antibacterial Nanofibrous Scaffolds for Tissue Engineering Applications," *Polymers,* vol. 12, no. 6, p. 1233, 2020. [Online]. Available: https://www.mdpi.com/2073-4360/12/6/1233.
[35] E. Mohseni-Vadeghani, R. Karimi-Soflou, S. Khorshidi, and A. Karkhaneh, "Fabrication of oxygen and calcium releasing microcarriers with different internal structures for bone tissue engineering: Solid filled versus hollow microparticles," (in eng), *Colloids Surf B Biointerfaces,* vol. 197, p. 111376, Jan 2021, doi: 10.1016/j.colsurfb.2020.111376.
[36] Z. Zhang *et al.*, "Gelatin-CaO2/SAP/PLGA composite scaffold enhances the reparation of critical-sized cranial defects by promoting seed cell survival," *Applied Materials Today,* vol. 22, p. 100960, 2021/03/01/ 2021, doi: https://doi.org/10.1016/j.apmt.2021.100960.

[37] M. M. Coronel, J. P. Liang, Y. Li, and C. L. Stabler, "Oxygen generating biomaterial improves the function and efficacy of beta cells within a macroencapsulation device," *Biomaterials,* vol. 210, pp. 1-11, 2019/07/01/ 2019, doi: https://doi.org/10.1016/j.biomaterials.2019.04.017.
[38] H. Steg *et al.*, "Oxygen-releasing poly(trimethylene carbonate) microspheres for tissue engineering applications," *Polymers for Advanced Technologies,* vol. 28, no. 10, pp. 1252-1257, 2017, doi: https://doi.org/10.1002/pat.3919.
[39] M. Zhang, T. Kiratiwongwan, and W. Shen, "Oxygen-releasing polycaprolactone/calcium peroxide composite microspheres," *Journal of Biomedical Materials Research Part B: Applied Biomaterials,* vol. 108, no. 3, pp. 1097-1106, 2020, doi: https://doi.org/10.1002/jbm.b.34461.
[40] Z. Lu, X. Jiang, M. Chen, L. Feng, and Y. J. Kang, "An oxygen-releasing device to improve the survival of mesenchymal stem cells in tissue engineering," *Biofabrication,* vol. 11, no. 4, p. 045012, 2019/08/13 2019, doi: 10.1088/1758-5090/ab332a.
[41] C.-C. Huang *et al.*, "An Implantable Depot That Can Generate Oxygen in Situ for Overcoming Hypoxia-Induced Resistance to Anticancer Drugs in Chemotherapy," *Journal of the American Chemical Society,* vol. 138, no. 16, pp. 5222-5225, 2016/04/27 2016, doi: 10.1021/jacs.6b01784.
[42] B. Newland, M. Baeger, D. Eigel, H. Newland, and C. Werner, "Oxygen-Producing Gellan Gum Hydrogels for Dual Delivery of Either Oxygen or Peroxide with Doxorubicin," *ACS Biomaterials Science & Engineering,* vol. 3, no. 5, pp. 787-792, 2017/05/08 2017, doi: 10.1021/acsbiomaterials.7b00078.
[43] C. He *et al.*, "Enhancement of cisplatin efficacy by lipid–CaO2 nanocarrier-mediated comprehensive modulation of the tumor microenvironment," *Biomaterials Science,* 10.1039/C9BM00797K vol. 7, no. 10, pp. 4260-4272, 2019, doi: 10.1039/C9BM00797K.
[44] Y. Hu, X. Wang, P. Zhao, H. Wang, W. Gu, and L. Ye, "Nanozyme-catalyzed oxygen release from calcium peroxide nanoparticles for accelerated hypoxia relief and image-guided super-efficient photodynamic therapy," *Biomaterials Science,* 10.1039/D0BM00187B vol. 8, no. 10, pp. 2931-2938, 2020, doi: 10.1039/D0BM00187B.
[45] Q. Yu *et al.*, "Oxygen self-sufficient NIR-activatable liposomes for tumor hypoxia regulation and photodynamic therapy," *Chemical Science,* 10.1039/C9SC03161H vol. 10, no. 39, pp. 9091-9098, 2019, doi: 10.1039/C9SC03161H.
[46] C. He, X. Zhang, and G. Xiang, "Nanoparticle facilitated delivery of peroxides for effective cancer treatments," *Biomaterials Science,* 10.1039/D0BM01265C vol. 8, no. 20, pp. 5574-5582, 2020, doi: 10.1039/D0BM01265C.
[47] Y. Huang, Y. Shao, and Y. Zhu, "Sustained reactive oxygen species generation from percarbamide nanomedicine via a mechanism of X-Ray-initiated free radical chain reactions," (in eng), *J Biomater Appl,* vol. 34, no. 5, pp. 728-738, Nov 2019, doi: 10.1177/0885328219868851.
[48] M. Suo *et al.*, "Development of a novel oxidative stress-amplifying nanocomposite capable of supplying intratumoral H2O2 and O2 for enhanced chemodynamic therapy and radiotherapy in patient-derived xenograft (PDX) models," *Nanoscale,* 10.1039/D0NR06594C vol. 12, no. 45, pp. 23259-23265, 2020, doi: 10.1039/D0NR06594C.
[49] H. Hu, L. Yu, X. Qian, Y. Chen, B. Chen, and Y. Li, "Chemoreactive Nanotherapeutics by Metal Peroxide Based Nanomedicine," *Advanced Science,* vol. 8, no. 1, p. 2000494, 2021, doi: https://doi.org/10.1002/advs.202000494.
[50] D. Wu *et al.*, "Efficacy-shaping nanomedicine by loading Calcium Peroxide into Tumor Microenvironment-responsive Nanoparticles for the Antitumor Therapy of Prostate Cancer," *Theranostics,* Research Paper vol. 10, no. 21, pp. 9808-9829, 2020, doi: 10.7150/thno.43631.
[51] R. Baskaran, J. Lee, and S.-G. Yang, "Clinical development of photodynamic agents and therapeutic applications," *Biomaterials Research,* vol. 22, no. 1, p. 25, 2018/09/26 2018, doi: 10.1186/s40824-018-0140-z.
[52] D. L. Sai, J. Lee, D. L. Nguyen, and Y.-P. Kim, "Tailoring photosensitive ROS for advanced photodynamic therapy," *Experimental & Molecular Medicine,* vol. 53, no. 4, pp. 495-504, 2021/04/01 2021, doi: 10.1038/s12276-021-00599-7.

[53] A. Northup and D. Cassidy, "Calcium peroxide (CaO2) for use in modified Fenton chemistry," *Journal of Hazardous Materials,* vol. 152, no. 3, pp. 1164-1170, 2008/04/15/ 2008, doi: https://doi.org/10.1016/j.jhazmat.2007.07.096.
[54] J. Khodaveisi, H. Banejad, A. Afkhami, E. Olyaie, S. Lashgari, and R. Dashti, "Synthesis of calcium peroxide nanoparticles as an innovative reagent for in situ chemical oxidation," *Journal of hazardous materials,* vol. 192, no. 3, pp. 1437-1440, 2011.
[55] Y. Wolanov, P. V. Prikhodchenko, A. G. Medvedev, R. Pedahzur, and O. Lev, "Zinc dioxide nanoparticulates: A hydrogen peroxide source at moderate pH," *Environmental science & technology,* vol. 47, no. 15, pp. 8769-8774, 2013.
[56] C. Bergs, L. Brück, R. R. Rosencrantz, G. Conrads, L. Elling, and A. Pich, "Biofunctionalized zinc peroxide (ZnO2) nanoparticles as active oxygen sources and antibacterial agents," *RSC Advances,* 10.1039/C7RA06332F vol. 7, no. 62, pp. 38998-39010, 2017, doi: 10.1039/C7RA06332F.
[57] C. Bergs, P. Simon, Y. Prots, and A. Pich, "Ultrasmall functional ZnO 2 nanoparticles: synthesis, characterization and oxygen release properties," *RSC advances,* vol. 6, no. 88, pp. 84777-84786, 2016.
[58] J. P. McQuilling, S. Sittadjody, S. Pendergraft, A. C. Farney, and E. C. Opara, "Applications of particulate oxygen-generating substances (POGS) in the bioartificial pancreas," *Biomaterials science,* vol. 5, no. 12, pp. 2437-2447, 2017.
[59] M. Zehra *et al.*, "Oxygen Generating Polymeric Nano Fibers That Stimulate Angiogenesis and Show Efficient Wound Healing in a Diabetic Wound Model," *International Journal of Nanomedicine,* vol. 15, pp. 3511-3522, 2020.
[60] A. R. Mundy, J. Fitzpatrick, D. E. Neal, and N. J. R. George, *The Scientific Basis of Urology*. CRC Press, 2010.
[61] P. M. Stell, "The viability of skin flaps," (in eng), *Ann R Coll Surg Engl,* vol. 59, no. 3, pp. 236-241, 1977. [Online]. Available: https://pubmed.ncbi.nlm.nih.gov/324339
[62] M. Z. Siemionow and M. Eisenmann-Klein, *Plastic and Reconstructive Surgery*. Springer London, 2010.
[63] M. Fujioka, "Surgical Reconstruction of Radiation Injuries," (in eng), *Adv Wound Care (New Rochelle),* vol. 3, no. 1, pp. 25-37, Jan 1 2014, doi: 10.1089/wound.2012.0405.
[64] T. E. Rohrer, J. L. Cook, and A. Kaufman, *Flaps and Grafts in Dermatologic Surgery E-Book*. Elsevier Health Sciences, 2017.
[65] A. W. Partin, A. J. Wein, L. R. Kavoussi, C. A. Peters, and R. R. Dmochowski, *Campbell Walsh Wein Urology, E-Book*. Elsevier Health Sciences, 2020.
[66] S. H. Milton, "Pedicled skin-flaps: The fallacy of the length: Width ratio," *BJS (British Journal of Surgery),* vol. 57, no. 7, pp. 502-508, 1970, doi: https://doi.org/10.1002/bjs.1800570705.
[67] A. S. Aherrera, D. J. Pincus, and A. J. Vernadakis, "Investigating the Impact of Flap Overdesign on Viability," (in eng), *Surg J (N Y),* vol. 2, no. 2, pp. e37-e41, Apr 2016, doi: 10.1055/s-0036-1584263.
[68] T. Kalogeris, C. P. Baines, M. Krenz, and R. J. Korthuis, "Cell biology of ischemia/reperfusion injury," (in English), *International review of cell and molecular biology,* vol. 298, pp. 229-317, 2012.
[69] C. Schürmann, O. Seitz, R. Sader, J. Pfeilschifter, I. Goren, and S. Frank, "Role of wound macrophages in skin flap loss or survival in an experimental diabetes model," (in eng), *Br J Surg,* vol. 97, no. 9, pp. 1437-51, Sep 2010, doi: 10.1002/bjs.7123.
[70] T. Kalogeris, C. P. Baines, M. Krenz, and R. J. Korthuis, "Ischemia/Reperfusion," (in eng), *Compr Physiol,* vol. 7, no. 1, pp. 113-170, Dec 6 2016, doi: 10.1002/cphy.c160006.
[71] S. Sanada, I. Komuro, and M. Kitakaze, "Pathophysiology of myocardial reperfusion injury: preconditioning, postconditioning, and translational aspects of protective measures," (in eng), *Am*

J Physiol Heart Circ Physiol, vol. 301, no. 5, pp. H1723-41, Nov 2011, doi: 10.1152/ajpheart.00553.2011.

[72] M. Y. Wu *et al.*, "Current Mechanistic Concepts in Ischemia and Reperfusion Injury," (in eng), *Cell Physiol Biochem,* vol. 46, no. 4, pp. 1650-1667, 2018, doi: 10.1159/000489241.

[73] M. Y. Wu *et al.*, "Current Mechanistic Concepts in Ischemia and Reperfusion Injury," *Cellular Physiology and Biochemistry,* vol. 46, no. 4, pp. 1650-1667, 2018, doi: 10.1159/000489241.

[74] H. J. Kim *et al.*, "Anti-inflammatory effects of anthocyanins from black soybean seed coat on the keratinocytes and ischemia-reperfusion injury in rat skin flaps," (in eng), *Microsurgery,* vol. 32, no. 7, pp. 563-70, Oct 2012, doi: 10.1002/micr.22019.

[75] T. Miyawaki *et al.*, "The effect of low-molecular-weight heparin in the survival of a rabbit congested skin flap," (in eng), *Plast Reconstr Surg,* vol. 109, no. 6, pp. 1994-9, May 2002, doi: 10.1097/00006534-200205000-00032.

[76] N. Xu, S. Guo, Y. Wang, Q. Sun, and C. Wang, "Transplantation of Adipose Tissue-Derived Stromal Cells Promotes the Survival of Venous-Congested Skin Flaps in Rabbit Ear," *Cell Biochemistry and Biophysics,* Article vol. 71, no. 2, pp. 557-563, 2015, doi: 10.1007/s12013-014-0234-8.

[77] L. Galluzzi *et al.*, "Molecular mechanisms of cell death: recommendations of the Nomenclature Committee on Cell Death 2018," *Cell Death & Differentiation,* vol. 25, no. 3, pp. 486-541, 2018/03/01 2018, doi: 10.1038/s41418-017-0012-4.

[78] K. McArthur and B. T. Kile, "Apoptotic Caspases: Multiple or Mistaken Identities?," (in eng), *Trends Cell Biol,* vol. 28, no. 6, pp. 475-493, Jun 2018, doi: 10.1016/j.tcb.2018.02.003.

[79] M. E. Guicciardi and G. J. Gores, "The Death Receptor Pathway," in *Essentials of Apoptosis: A Guide for Basic and Clinical Research*, Z. Dong and X.-M. Yin Eds. Totowa, NJ: Humana Press, 2009, pp. 119-150.

[80] F. Gonzalvez, "The role of cardiolipin in the regulation of mitochondria-dependent apoptosis," PhD, Institute of Cancer Sciences, University of Glasgow, 2008.

[81] S. Elmore, "Apoptosis: a review of programmed cell death," (in eng), *Toxicol Pathol,* vol. 35, no. 4, pp. 495-516, 2007, doi: 10.1080/01926230701320337.

[82] S. Campello and L. Scorrano, "The Mitochondrial Pathway: Focus on Shape Changes," in *Essentials of Apoptosis: A Guide for Basic and Clinical Research*, Z. Dong and X.-M. Yin Eds. Totowa, NJ: Humana Press, 2009, pp. 151-175.

[83] Q. Bao and Y. Shi, "Apoptosome: a platform for the activation of initiator caspases," *Cell Death & Differentiation,* vol. 14, no. 1, pp. 56-65, 2007/01/01 2007, doi: 10.1038/sj.cdd.4402028.

[84] P. Saikumar and M. A. Venkatachalam, "Apoptosis and cell death," in *Basic Concepts of Molecular Pathology*: Springer, 2009, pp. 29-40.

[85] Y. Dong, V. V. Undyala, R. A. Gottlieb, R. M. Mentzer, and K. Przyklenk, "Review: Autophagy: Definition, Molecular Machinery, and Potential Role in Myocardial Ischemia-Reperfusion Injury," *Journal of Cardiovascular Pharmacology and Therapeutics,* vol. 15, no. 3, pp. 220-230, 2010/09/01 2010, doi: 10.1177/1074248410370327.

[86] P. Syntichaki and N. Tavernarakis, "Death by necrosis. Uncontrollable catastrophe, or is there order behind the chaos?," (in eng), *EMBO Rep,* vol. 3, no. 7, pp. 604-609, 2002, doi: 10.1093/embo-reports/kvf138.

[87] O. M. E. a. G. H. V.-N. Ma. Luisa Escobar, *Necrosis as Programmed Cell Death, Cell Death - Autophagy, Apoptosis and Necrosis*. 2015.

[88] S. A. Elmore *et al.*, "Recommendations from the INHAND Apoptosis/Necrosis Working Group," (in eng), *Toxicol Pathol,* vol. 44, no. 2, pp. 173-88, Feb 2016, doi: 10.1177/0192623315625859.

[89] M. E. Choi, D. R. Price, S. W. Ryter, and A. M. K. Choi, "Necroptosis: a crucial pathogenic mediator of human disease," (in eng), *JCI Insight,* vol. 4, no. 15, p. e128834, 2019, doi: 10.1172/jci.insight.128834.

[90] Y. K. Dhuriya and D. Sharma, "Necroptosis: a regulated inflammatory mode of cell death," *Journal of Neuroinflammation,* vol. 15, no. 1, p. 199, 2018/07/06 2018, doi: 10.1186/s12974-018-1235-0.
[91] V. Kumar, A. K. Abbas, and J. C. Aster, *Robbins & Cotran Pathologic Basis of Disease E-Book*. Elsevier Health Sciences, 2020.
[92] T. J. Padda IS. "Phosphodiesterase Inhibitors." Treasure Island (FL): StatPearls Publishing. https://www.ncbi.nlm.nih.gov/books/NBK559276/ (accessed October 30, 2021).
[93] K. Hart *et al.*, "Short- and long-term effects of sildenafil on skin flap survival in rats," (in eng), *Laryngoscope,* vol. 116, no. 4, pp. 522-8, Apr 2006, doi: 10.1097/01.mlg.0000200792.67802.3b.
[94] P. Wang, L. Gu, Z. Qin, Q. Wang, and J. Ma, "Efficacy and safety of topical nitroglycerin in the prevention of mastectomy flap necrosis: a systematic review and meta-analysis," (in eng), *Scientific reports,* vol. 10, no. 1, pp. 6753-6753, 2020, doi: 10.1038/s41598-020-63721-1.
[95] M. H. Yun, E. S. Yoon, B.-I. Lee, and S.-H. Park, "The Effect of Low-Dose Nitroglycerin Ointment on Skin Flap Necrosis in Breast Reconstruction after Skin-Sparing or Nipple-Sparing Mastectomy," (in eng), *Arch Plast Surg,* vol. 44, no. 6, pp. 509-515, 2017, doi: 10.5999/aps.2017.00934.
[96] N. Sarifakioglu, S. Gokrem, L. Ates, U. B. Akbuga, and G. Aslan, "The influence of sildenafil on random skin flap survival in rats: an experimental study," (in eng), *Br J Plast Surg,* vol. 57, no. 8, pp. 769-72, Dec 2004, doi: 10.1016/j.bjps.2004.04.014.
[97] M. A. Ellabban *et al.*, "The Effects of Sildenafil and/or Nitroglycerin on Random-pattern Skin Flaps After Nicotine Application in Rats," *Scientific Reports,* vol. 10, no. 1, p. 3212, 2020/02/21 2020, doi: 10.1038/s41598-020-60128-w.
[98] D. K. Smith and R. W. Dolan, "Effects of vasoactive topical agents on the survival of dorsal skin flaps in rats," *Otolaryngology–Head and Neck Surgery,* vol. 121, no. 3, pp. 220-223, 1999/09/01 1999, doi: 10.1016/S0194-5998(99)70175-0.
[99] J. Z. Sá, J. L. Aguiar, A. F. Cruz, A. R. Schuler, J. R. Lima, and O. M. Marques, "The effects of local nitroglycerin on the surgical delay procedure in prefabricated flaps by vascular implant in rats," (in eng), *Acta Cir Bras,* vol. 27, no. 12, pp. 905-11, Dec 2012, doi: 10.1590/s0102-86502012001200013.
[100] H. Ashrafpour *et al.*, "Vasodilator effect and mechanism of action of vascular endothelial growth factor in skin vasculature," (in eng), *Am J Physiol Heart Circ Physiol,* vol. 286, no. 3, pp. H946-54, Mar 2004, doi: 10.1152/ajpheart.00901.2003.
[101] S. Barrientos, O. Stojadinovic, M. S. Golinko, H. Brem, and M. Tomic-Canic, "PERSPECTIVE ARTICLE: Growth factors and cytokines in wound healing," *Wound Repair and Regeneration,* vol. 16, no. 5, pp. 585-601, 2008, doi: https://doi.org/10.1111/j.1524-475X.2008.00410.x.
[102] T. N. Demidova-Rice, M. R. Hamblin, and I. M. Herman, "Acute and impaired wound healing: pathophysiology and current methods for drug delivery, part 2: role of growth factors in normal and pathological wound healing: therapeutic potential and methods of delivery," (in eng), *Adv Skin Wound Care,* vol. 25, no. 8, pp. 349-370, 2012, doi: 10.1097/01.ASW.0000418541.31366.a3.
[103] R. Simman, Craft, C. & McKinney, B, "Improved Survival of Ischemic Random Skin Flaps Through the Use of Bone Marrow Nonhematopoietic Stem Cells and Angiogenic Growth Factors," *Annals of Plastic Surgery,* vol. 54, no. 5, pp. 546-552, 2005, doi: 10.1097/01.sap.0000158068.86576.73.
[104] Z. Kryger, F. Zhang, W. C. Lineaweaver, T. Dogan, C. Cheng, and H. J. Buncke, "The effects of VEGF on survival of a random flap in the rat: examination of various routes of administration," *British Journal of Plastic Surgery,* vol. 53, no. 3, pp. 234-239, 2000/04/01/ 2000, doi: https://doi.org/10.1054/bjps.1999.3315.
[105] H. Chu and Y. Wang, "Therapeutic angiogenesis: controlled delivery of angiogenic factors," (in eng), *Ther Deliv,* vol. 3, no. 6, pp. 693-714, 2012, doi: 10.4155/tde.12.50.

[106] W. C. W. Chen *et al.*, "Controlled dual delivery of fibroblast growth factor-2 and Interleukin-10 by heparin-based coacervate synergistically enhances ischemic heart repair," *Biomaterials,* vol. 72, pp. 138-151, 2015/12/01/ 2015, doi: https://doi.org/10.1016/j.biomaterials.2015.08.050.
[107] M. S. Lee *et al.*, "Dual delivery of growth factors with coacervate-coated poly(lactic-co-glycolic acid) nanofiber improves neovascularization in a mouse skin flap model," *Biomaterials,* vol. 124, pp. 65-77, 2017/04/01/ 2017, doi: https://doi.org/10.1016/j.biomaterials.2017.01.036.
[108] J. B. He, M. J. Fang, X. Y. Ma, W. J. Li, and D. S. Lin, "Angiogenic and anti-inflammatory properties of azadirachtin A improve random skin flap survival in rats," (in eng), *Exp Biol Med (Maywood),* vol. 245, no. 18, pp. 1672-1682, Dec 2020, doi: 10.1177/1535370220951896.
[109] X. Feng *et al.*, "Effects of Asiaticoside Treatment on the Survival of Random Skin Flaps in Rats," (in eng), *J Invest Surg,* vol. 34, no. 1, pp. 107-117, Jan 2021, doi: 10.1080/08941939.2019.1584255.
[110] R. Jiang, C. Lin, C. Jiang, Z. Huang, W. Gao, and D. Lin, "Nobiletin enhances the survival of random pattern skin flaps: Involvement of enhancing angiogenesis and inhibiting oxidative stress," *International Immunopharmacology,* vol. 78, p. 106010, 2020/01/01/ 2020, doi: https://doi.org/10.1016/j.intimp.2019.106010.
[111] H. F. Zhang and J. E. Barralet, "Mimicking oxygen delivery and waste removal functions of blood," (in English), *Adv. Drug Deliv. Rev.,* Review vol. 122, pp. 84-104, Dec 2017, doi: 10.1016/j.addr.2017.02.001.
[112] A. Biochemists. "Phycomycin® SCP." https://www.appliedbiochemists.com/phycomycin.html (accessed November 18, 2021).
[113] D. N. Hanh, B. K. Rajbhandari, and A. P. Annachhatre, "Bioremediation of sediments from intensive aquaculture shrimp farms by using calcium peroxide as slow oxygen release agent," (in eng), *Environ Technol,* vol. 26, no. 5, pp. 581-9, May 2005, doi: 10.1080/09593332608618543.
[114] S. M. Santander-De Leon *et al.*, "Effect of magnesium peroxide biostimulation of fish feed-loaded marine sediments on changes in the bacterial community," (in eng), *Biocontrol Sci,* vol. 18, no. 1, pp. 41-51, 2013, doi: 10.4265/bio.18.41.
[115] E. R. LLS. "EOx." https://www.eosremediation.com/eox-product-information/?gclid=Cj0KCQiA4feBBhC9ARIsABp_nbWB70kopZfme_x5jK-4vQtMGOmQD-i4iPhfY__On6SbVBHC7FWOsg4aAjBdEALw_wcB (accessed November 11, 2021).
[116] M. Ali *et al.*, "Synthesis of controlled release calcium peroxide nanoparticles (CR-nCPs): Characterizations, H2O2 liberate performances and pollutant degradation efficiency," *Separation and Purification Technology,* vol. 241, p. 116729, 2020/06/15/ 2020, doi: https://doi.org/10.1016/j.seppur.2020.116729.
[117] Chempoint. "Calcium Peroxide." https://www.chempoint.com/industries/agriculture/calcium-peroxide-1 (accessed November 11, 2021).
[118] S. Lu, X. Zhang, and Y. Xue, "Application of calcium peroxide in water and soil treatment: A review," *Journal of Hazardous Materials,* vol. 337, pp. 163-177, 2017/09/05/ 2017, doi: https://doi.org/10.1016/j.jhazmat.2017.04.064.
[119] J. Mei, W. Wang, S. Peng, and L. Nie, "Seed Pelleting with Calcium Peroxide Improves Crop Establishment of Direct-seeded Rice under Waterlogging Conditions," *Scientific Reports,* vol. 7, no. 1, p. 4878, 2017/07/07 2017, doi: 10.1038/s41598-017-04966-1.
[120] T. Bera, K. S. Inglett, and G. D. Liu, "Effects of solid oxygen fertilizers and biochars on nitrous oxide production from agricultural soils in Florida," *Scientific Reports,* vol. 10, no. 1, p. 21754, 2020/12/10 2020, doi: 10.1038/s41598-020-78198-1.
[121] Solvay. "IXPER® calcium peroxide." Solvay. https://www.solvay.com/en/product/ixper-calcium-peroxide-75c (accessed November 11, 2021).
[122] E. C. Murphy and A. J. Friedman, "Hydrogen peroxide and cutaneous biology: Translational applications, benefits, and risks," *Journal of the American Academy of Dermatology,* vol. 81, no. 6, pp. 1379-1386, 2019/12/01/ 2019, doi: https://doi.org/10.1016/j.jaad.2019.05.030.

[123] Y. Ma, B. T. Zhang, L. Zhao, G. Guo, and J. M. Lin, "Study on the generation mechanism of reactive oxygen species on calcium peroxide by chemiluminescence and UV-visible spectra," (in eng), *Luminescence,* vol. 22, no. 6, pp. 575-80, Nov-Dec 2007, doi: 10.1002/bio.1003.
[124] Colgate. "Colgate Baking Soda and Peroxide Whitening Toothpaste, Brisk Mint." https://www.colgate.com/en-us/smartlabel/35000510969 (accessed November 11, 2021).
[125] D. A. Feitosa *et al.*, "Impact of toothbrushing with a dentifrice containing calcium peroxide on enamel color and roughness," (in eng), *Gen Dent,* vol. 63, no. 1, pp. e9-e11, Jan-Feb 2015.
[126] Supersmile. "Professional Whitening Toothpaste." https://www.supersmile.com/products/teeth-whitening-toothpaste-sensitivity-free-remove-coffee-tea-tobacco-red-wine-stains?variant=259920691216 (accessed November 11, 2021).
[127] J. van Houte, J. Lopman, and R. Kent, "The Final pH of Bacteria Comprising the Predominant Flora on Sound and Carious Human Root and Enamel Surfaces," *Journal of Dental Research,* vol. 75, no. 4, pp. 1008-1014, 1996/04/01 1996, doi: 10.1177/00220345960750040201.
[128] Y. M. Dong, E. I. F. Pearce, L. Yue, M. J. Larsen, X. J. Gao, and J. D. Wang, "Plaque pH and Associated Parameters in Relation to Caries," *Caries Research,* vol. 33, no. 6, pp. 428-436, 1999, doi: 10.1159/000016547.
[129] F. Paladini and M. Pollini, "Antimicrobial Silver Nanoparticles for Wound Healing Application: Progress and Future Trends," (in eng), *Materials (Basel),* vol. 12, no. 16, p. 2540, 2019, doi: 10.3390/ma12162540.
[130] T. J. Hall, I. Azoidis, I. A. Barroso, E. A. B. Hughes, L. M. Grover, and S. C. Cox, "Formulation of an antimicrobial superabsorbent powder that gels in situ to produce reactive oxygen," *Materials Science and Engineering: C,* vol. 118, p. 111479, 2021/01/01/ 2021, doi: https://doi.org/10.1016/j.msec.2020.111479.
[131] I. Negut, V. Grumezescu, and A. M. Grumezescu, "Treatment Strategies for Infected Wounds," (in eng), *Molecules,* vol. 23, no. 9, p. 2392, 2018, doi: 10.3390/molecules23092392.
[132] L. Tonoyan, D. Montagner, R. Friel, and V. O'Flaherty, "Antimicrobials offered from nature: Peroxidase-catalyzed systems and their mimics," *Biochemical Pharmacology,* vol. 182, p. 114281, 2020/12/01/ 2020, doi: https://doi.org/10.1016/j.bcp.2020.114281.
[133] R. Pachaiappan, S. Rajendran, P. L. Show, K. Manavalan, and M. Naushad, "Metal/metal oxide nanocomposites for bactericidal effect: A review," *Chemosphere,* vol. 272, p. 128607, 2021/06/01/ 2021, doi: https://doi.org/10.1016/j.chemosphere.2020.128607.
[134] K. Fröber, C. Bergs, A. Pich, and G. Conrads, "Biofunctionalized zinc peroxide nanoparticles inhibit peri-implantitis associated anaerobes and Aggregatibacter actinomycetemcomitans pH-dependent," *Anaerobe,* vol. 62, p. 102153, 2020.
[135] S. S. Ali, R. Morsy, N. A. El-Zawawy, M. F. Fareed, and M. Y. Bedaiwy, "Synthesized zinc peroxide nanoparticles (ZnO(2)-NPs): a novel antimicrobial, anti-elastase, anti-keratinase, and anti-inflammatory approach toward polymicrobial burn wounds," (in eng), *International journal of nanomedicine,* vol. 12, pp. 6059-6073, 2017, doi: 10.2147/IJN.S141201.
[136] H. Steg *et al.*, "Control of oxygen release from peroxides using polymers," *Journal of Materials Science: Materials in Medicine,* Article vol. 26, no. 7, 2015, Art no. 207, doi: 10.1007/s10856-015-5542-z.
[137] W. Zhu *et al.*, "Modulation of Hypoxia in Solid Tumor Microenvironment with MnO2 Nanoparticles to Enhance Photodynamic Therapy," *Advanced Functional Materials,* vol. 26, no. 30, pp. 5490-5498, 2016, doi: https://doi.org/10.1002/adfm.201600676.
[138] C.-W. Chang and M.-J. Wang, "Preparation of Microfibrillated Cellulose Composites for Sustained Release of H2O2 or O2 for Biomedical Applications," *ACS Sustainable Chemistry & Engineering,* vol. 1, no. 9, pp. 1129-1134, 2013/09/03 2013, doi: 10.1021/sc400054v.
[139] J. Zheng *et al.*, "It takes two to tango: coupling of Hippo pathway and redox signaling in biological process," (in eng), *Cell Cycle,* vol. 19, no. 21, pp. 2760-2775, Nov 2020, doi: 10.1080/15384101.2020.1824448.

[140] P. Jia, C. Dai, P. Cao, D. Sun, R. Ouyang, and Y. Miao, "The role of reactive oxygen species in tumor treatment," *RSC Advances,* 10.1039/C9RA10539E vol. 10, no. 13, pp. 7740-7750, 2020, doi: 10.1039/C9RA10539E.
[141] M. Schieber and N. S. Chandel, "ROS function in redox signaling and oxidative stress," *Current biology,* vol. 24, no. 10, pp. R453-R462, 2014.
[142] C. Caliceti, P. Nigro, P. Rizzo, and R. Ferrari, "ROS, Notch, and Wnt signaling pathways: crosstalk between three major regulators of cardiovascular biology," (in eng), *Biomed Res Int,* vol. 2014, p. 318714, 2014, doi: 10.1155/2014/318714.
[143] S. Gao *et al.*, "Self-evolved hydrogen peroxide boosts photothermal-promoted tumor-specific nanocatalytic therapy," *Journal of Materials Chemistry B,* 10.1039/C9TB00525K vol. 7, no. 22, pp. 3599-3609, 2019, doi: 10.1039/C9TB00525K.
[144] C. Liu *et al.*, "An open source and reduce expenditure ROS generation strategy for chemodynamic/photodynamic synergistic therapy," *Nature communications,* vol. 11, no. 1, pp. 1-9, 2020.
[145] S. Johnston, Z. Shi, and A. Atrens, "The influence of pH on the corrosion rate of high-purity Mg, AZ91 and ZE41 in bicarbonate buffered Hanks' solution," *Corrosion Science,* vol. 101, pp. 182-192, 2015/12/01/ 2015, doi: https://doi.org/10.1016/j.corsci.2015.09.018.
[146] S. Agarwal, J. Curtin, B. Duffy, and S. Jaiswal, "Biodegradable magnesium alloys for orthopaedic applications: A review on corrosion, biocompatibility and surface modifications," *Materials Science and Engineering: C,* vol. 68, pp. 948-963, 2016/11/01/ 2016, doi: https://doi.org/10.1016/j.msec.2016.06.020.
[147] A. J. Bullock, M. Garcia, J. Shepherd, I. Rehman, and M. Sheila, "Bacteria induced pH changes in tissue-engineered human skin detected non-invasively using Raman confocal spectroscopy," *Applied Spectroscopy Reviews,* vol. 55, no. 2, pp. 158-171, 2020/02/07 2020, doi: 10.1080/05704928.2018.1558232.
[148] D. F. Evans, G. Pye, R. Bramley, A. G. Clark, T. J. Dyson, and J. D. Hardcastle, "Measurement of gastrointestinal pH profiles in normal ambulant human subjects," (in eng), *Gut,* vol. 29, no. 8, pp. 1035-1041, 1988, doi: 10.1136/gut.29.8.1035.
[149] D. Kim *et al.*, "Large pH oscillations promote host defense against human airways infection," *Journal of Experimental Medicine,* vol. 218, no. 4, 2021, doi: 10.1084/jem.20201831.
[150] Z. Zhu, J. J. Noël, and D. W. Shoesmith, "Hydrogen peroxide decomposition on simulated nuclear fuel bicarbonate/carbonate solutions," *Electrochimica Acta,* vol. 340, p. 135980, 2020/04/20/ 2020, doi: https://doi.org/10.1016/j.electacta.2020.135980.
[151] R. Thoo, W. Siuda, and I. Jasser, "The Effects of Sodium Percarbonate Generated Free Oxygen on Daphnia—Implications for the Management of Harmful Algal Blooms," *Water,* vol. 12, no. 5, p. 1304, 2020. [Online]. Available: https://www.mdpi.com/2073-4441/12/5/1304.
[152] S. Suvarnapathaki, X. Wu, D. Lantigua, M. A. Nguyen, and G. Camci-Unal, "Breathing life into engineered tissues using oxygen-releasing biomaterials," *NPG Asia Materials,* vol. 11, no. 1, p. 65, 2019/11/08 2019, doi: 10.1038/s41427-019-0166-2.
[153] O. E. Albertson and W. P. C. F. T. F. o. N. Control, *Nutrient Control* (no. no. 7). Water Pollution Control Federation, 1983.
[154] C. Liu *et al.*, "An open source and reduce expenditure ROS generation strategy for chemodynamic/photodynamic synergistic therapy," *Nature Communications,* vol. 11, no. 1, p. 1735, 2020/04/08 2020, doi: 10.1038/s41467-020-15591-4.
[155] C. Wittmann, P. Chockley, S. K. Singh, L. Pase, G. J. Lieschke, and C. Grabher, "Hydrogen peroxide in inflammation: messenger, guide, and assassin," (in eng), *Adv Hematol,* vol. 2012, p. 541471, 2012, doi: 10.1155/2012/541471.
[156] Y. He *et al.*, "Calcium Peroxide Nanoparticles-Embedded Coatings on Anti-Inflammatory TiO2 Nanotubes for Bacteria Elimination and Inflammatory Environment Amelioration," *Small,* vol. n/a, no. n/a, p. 2102907, doi: https://doi.org/10.1002/smll.202102907.

[157] F. L. Meleney, "Present role of zinc peroxide in treatment of surgical infections," *Journal of the American Medical Association,* vol. 149, no. 16, pp. 1450-1453, 1952.
[158] C. D. Pericone, S. Park, J. A. Imlay, and J. N. Weiser, "Factors contributing to hydrogen peroxide resistance in Streptococcus pneumoniae include pyruvate oxidase (SpxB) and avoidance of the toxic effects of the fenton reaction," (in eng), *J Bacteriol,* vol. 185, no. 23, pp. 6815-25, Dec 2003, doi: 10.1128/jb.185.23.6815-6825.2003.
[159] Y. Ogawa *et al.*, "Phase I study of a new radiosensitizer containing hydrogen peroxide and sodium hyaluronate for topical tumor injection: a new enzyme-targeting radiosensitization treatment, Kochi Oxydol-Radiation Therapy for Unresectable Carcinomas, Type II (KORTUC II)," (in eng), *Int J Oncol,* vol. 34, no. 3, pp. 609-18, Mar 2009, doi: 10.3892/ijo_00000186.
[160] N. R. A. M. Rosli, F. Mohamed, C. K. Heng, I. A. Rahman, A. F. Ahmad, and H. M. K. Mohamad, "Synthesis and radiosensitization properties of hydrogen peroxide and sodium hyaluronate complex," *AIP Conference Proceedings,* vol. 1614, no. 1, pp. 78-81, 2014, doi: 10.1063/1.4895175.
[161] J. Weiss, "The catalytic decomposition of hydrogen peroxide on different metals," *Transactions of the Faraday Society,* 10.1039/TF9353101547 vol. 31, no. 0, pp. 1547-1557, 1935, doi: 10.1039/TF9353101547.
[162] R. Bar and J. L. Gainer, "Acid Fermentation in Water Organic Solvent Tw□ Liquid Phase Systems," *Biotechnology Progress,* vol. 3, 1987.
[163] M. Kreiner and M. C. Parker, "High-activity biocatalysts in organic media: solid-state buffers as the immobilisation matrix for protein-coated microcrystals," (in eng), *Biotechnol Bioeng,* vol. 87, no. 1, pp. 24-33, Jul 5 2004, doi: 10.1002/bit.20101.
[164] W. D. Nicoll and A. F. Smith, "Stability of Dilute Alkaline Solutions of Hydrogen Peroxide," *Industrial & Engineering Chemistry,* vol. 47, no. 12, pp. 2548-2554, 1955/12/01 1955, doi: 10.1021/ie50552a051.
[165] "Kinetics and Stoichiometry of Oxygen Release from Solid Peroxides," *Environmental Engineering Science,* vol. 16, no. 3, pp. 187-199, 1999, doi: 10.1089/ees.1999.16.187.
[166] L. J. Csányi and Z. M. Galbács, "Carbon dioxide-mediated decomposition of hydrogen peroxide in alkaline solutions," *Journal of the Chemical Society, Faraday Transactions 1: Physical Chemistry in Condensed Phases,* 10.1039/F19858100113 vol. 81, no. 1, pp. 113-116, 1985, doi: 10.1039/F19858100113.
[167] G. Zhao and N. D. Chasteen, "Oxidation of Good's buffers by hydrogen peroxide," *Analytical Biochemistry,* vol. 349, no. 2, pp. 262-267, 2006/02/15/ 2006, doi: https://doi.org/10.1016/j.ab.2005.10.005.
[168] K. E. Dineley, L. L. Richards, T. V. Votyakova, and I. J. Reynolds, "Zinc causes loss of membrane potential and elevates reactive oxygen species in rat brain mitochondria," *Mitochondrion,* vol. 5, no. 1, pp. 55-65, 2005/02/01/ 2005, doi: https://doi.org/10.1016/j.mito.2004.11.001.
[169] L. M. Plum, L. Rink, and H. Haase, "The essential toxin: impact of zinc on human health," (in eng), *Int J Environ Res Public Health,* vol. 7, no. 4, pp. 1342-1365, 2010, doi: 10.3390/ijerph7041342.
[170] M. M. Jones, J. E. Schoenheit, and A. D. Weaver, "Pretreatment and heavy metal LD50 values," (in eng), *Toxicol Appl Pharmacol,* vol. 49, no. 1, pp. 41-4, Jun 15 1979, doi: 10.1016/0041-008x(79)90274-6.
[171] H. Inc. "Calcium Chloride Injection." https://723462.app.netsuite.com/core/media/media.nl?id=12035&c=723462&h=411a338ca37616b888c4&_xt=.pdf (accessed 19 November, 2021).
[172] M. R. Fernández, R. V. Carvalho, F. A. Ogliari, F. A. Beira, A. Etges, and M. Bueno, "Cytotoxicity and genotoxicity of sodium percarbonate: a comparison with bleaching agents commonly used in discoloured pulpless teeth," *International Endodontic Journal,* vol. 43, no. 2, pp. 102-108, 2010, doi: https://doi.org/10.1111/j.1365-2591.2009.01648.x.

[173] S. Shen *et al.*, "Synthesis of CaO2 nanocrystals and their spherical aggregates with uniform sizes for use as a biodegradable bacteriostatic agent," *Small,* vol. 15, no. 36, p. 1902118, 2019.
[174] H. Newland, D. Eigel, A. E. Rosser, C. Werner, and B. Newland, "Oxygen producing microscale spheres affect cell survival in conditions of oxygen-glucose deprivation in a cell specific manner: implications for cell transplantation," *Biomaterials Science,* 10.1039/C8BM00490K vol. 6, no. 10, pp. 2571-2577, 2018, doi: 10.1039/C8BM00490K.
[175] M. Güemes, S. A. Rahman, and K. Hussain, "What is a normal blood glucose?," *Archives of Disease in Childhood,* vol. 101, no. 6, pp. 569-574, 2016, doi: 10.1136/archdischild-2015-308336.
[176] K. Jungermann and T. Kietzmann, "Oxygen: modulator of metabolic zonation and disease of the liver," *Hepatology (Baltimore, Md.),* vol. 31, no. 2, pp. 255-60, 2000.
[177] A. Görlach, K. Bertram, S. Hudecova, and O. Krizanova, "Calcium and ROS: A mutual interplay," *Redox Biology,* vol. 6, pp. 260-271, 2015/12/01/ 2015, doi: https://doi.org/10.1016/j.redox.2015.08.010.
[178] R. Jennings, "The Cell Biology Of Acute Myocardial Ischemia," *Annual Review of Medicine,* vol. 42, no. 1, pp. 225-246, 1991, doi: 10.1146/annurev.med.42.1.225.
[179] P. F. Petrasek, S. Homer-Vanniasinkam, and P. M. Walker, "Determinants of ischemic injury to skeletal muscle," (in English), *Journal of vascular surgery,* vol. 19, no. 4, pp. 623-31, 1994.
[180] J. E. Mayer, "In search of the ideal valve replacement device," *The Journal of Thoracic and Cardiovascular Surgery,* vol. 122, no. 1, pp. 8-9, 2001/07/01/ 2001, doi: https://doi.org/10.1067/mtc.2001.115926.
[181] G. Steinhoff *et al.*, "Tissue Engineering of Pulmonary Heart Valves on Allogenic Acellular Matrix Conduits," *Circulation,* vol. 102, no. suppl_3, pp. Iii-50-Iii-55, 2000, doi: doi:10.1161/circ.102.suppl_3.III-50.
[182] J. Sun, J. Lyu, F. Xing, R. Chen, X. Duan, and Z. Xiang, "A biphasic, demineralized, and Decellularized allograft bone-hydrogel scaffold with a cell-based BMP-7 delivery system for osteochondral defect regeneration," *Journal of Biomedical Materials Research Part A,* vol. 108, no. 9, pp. 1909-1921, 2020.
[183] A. Rastinfard, B. Dalisson, and J. Barralet, "Aqueous decomposition behavior of solid peroxides: effect of pH and buffer composition on oxygen and hydrogen peroxide formation," **Submitted** to *Acta Biomaterialia,* 2021.
[184] G. Wypych, "11 - EFFECT OF FILLERS ON EXPOSURE TO DIFFERENT ENVIRONMENTS," in *Handbook of Fillers (Fourth Edition)*, G. Wypych Ed.: ChemTec Publishing, 2016, pp. 571-587.
[185] C. Y. Tang, D. Z. Chen, T. M. Yue, K. C. Chan, C. P. Tsui, and P. H. F. Yu, "Water absorption and solubility of PHBHV/HA nanocomposites," *Composites Science and Technology,* vol. 68, no. 7, pp. 1927-1934, 2008/06/01/ 2008, doi: https://doi.org/10.1016/j.compscitech.2007.12.003.
[186] C. P. L. Chow, X. S. Xing, and R. K. Y. Li, "Moisture absorption studies of sisal fibre reinforced polypropylene composites," *Composites Science and Technology,* vol. 67, no. 2, pp. 306-313, 2007/02/01/ 2007, doi: https://doi.org/10.1016/j.compscitech.2006.08.005.
[187] R. M. McFarlane, G. Deyoung, and R. A. Henry, "THE DESIGN OF A PEDICLE FLAP IN THE RAT TO STUDY NECROSIS AND ITS PREVENTION," (in eng), *Plast Reconstr Surg,* vol. 35, pp. 177-82, Feb 1965, doi: 10.1097/00006534-196502000-00007.
[188] S.-S. Lin and M. D. Gurol, "Catalytic Decomposition of Hydrogen Peroxide on Iron Oxide: Kinetics, Mechanism, and Implications," *Environmental Science & Technology,* vol. 32, no. 10, pp. 1417-1423, 1998/05/01 1998, doi: 10.1021/es970648k.
[189] D. B. Cybyk *et al.*, "Biodegradable oxygen biosensors via electrospinning," *MEDICAL DEVICES & SENSORS,* vol. 4, no. 1, p. e10149, 2021, doi: https://doi.org/10.1002/mds3.10149.
[190] A. B. Yadav, S. K. Yadav, A. Narwal, and A. Devi, "A Contemporary Approach to Classify Ghost Cells Comprising Oral Lesions," (in eng), *J Clin Diagn Res,* vol. 9, no. 9, pp. ZM01-ZM2, 2015, doi: 10.7860/JCDR/2015/13426.6500.

[191] P. K. Mankapure, "Ghost cells and its histogenesis: a narrative review," *IJSS Case Rep Rev,* vol. 2, pp. 35-9, 2015.
[192] P. Cabrales, B. Y. S. VÁZquez, A. C. Negrete, and M. Intaglietta, "Perfluorocarbons as gas transporters for O2, NO, CO and volatile anesthetics," *Transfusion Alternatives in Transfusion Medicine,* vol. 9, no. 4, pp. 294-303, 2007/12/01 2008, doi: 10.1111/j.1778-428X.2007.00085.x.
[193] M. J. Im, C.-T. Su, J. E. Hoopes, R. M. Anthenelli, and J. E. Hoopes, "Skin-Flap Metabolism in Rats: Oxygen Consumption and Lactate Production," *Plastic and Reconstructive Surgery,* vol. 71, no. 5, pp. 685-688, 1983. [Online]. Available: https://journals.lww.com/plasreconsurg/Fulltext/1983/05000/Skin_Flap_Metabolism_in_Rats__Oxygen_Consumption.20.aspx.
[194] T. Kashimura, K. Soejima, T. Asami, T. Kazama, T. Matsumoto, and H. Nakazawa, "The effect of mature adipocyte-derived dedifferentiated fat (DFAT) cells on a dorsal skin flap model," *Journal of Investigative Surgery,* vol. 29, no. 1, pp. 6-12, 2016.
[195] Y. Sawada, T. Yotsuyanagi, I. Hatayama, and K. Sone, "The relationship between Prostaglandin E1 applied area and flap survival rate," *British Journal of Plastic Surgery,* vol. 45, no. 6, pp. 465-468, 1992/01/01/ 1992, doi: https://doi.org/10.1016/0007-1226(92)90211-F.
[196] T. Yavas, M. Serin, and M. Bayramicli, "Calculation of contraction patterns in rat skin flap model," *Journal of plastic surgery and hand surgery,* vol. 51, no. 2, pp. 95-98, 2017.
[197] Q. Qiao *et al.*, "Patterns of flap loss related to arterial and venous insufficiency in the rat pedicled TRAM flap," *Annals of plastic surgery,* vol. 43, no. 2, pp. 167-71, 1999.
[198] R. A. Beach and A. J. Mamelak, "'New' approaches to venous congestion," *Expert Review of Dermatology,* vol. 5, no. 6, pp. 589-591, 2010/12/01 2010, doi: 10.1586/edm.10.64.
[199] M. Reiter, M. Kapsreiter, C. S. Betz, and U. Harréus, "Perioperative management of antithrombotic medication in head and neck reconstruction—a retrospective analysis of 137 patients," *American Journal of Otolaryngology,* vol. 33, no. 6, pp. 693-696, 2012/11/01/ 2012, doi: https://doi.org/10.1016/j.amjoto.2012.05.008.
[200] M. Jose, J. Varghese, and A. Babu, "Salvage of venous congestion using medicinal leeches for traumatic nasal flap," (in eng), *J Maxillofac Oral Surg,* vol. 14, no. Suppl 1, pp. 251-254, 2015, doi: 10.1007/s12663-012-0468-1.
[201] K. Y. Mumcuoglu, "Recommendations for the Use of Leeches in Reconstructive Plastic Surgery," *Evidence-Based Complementary and Alternative Medicine,* vol. 2014, p. 7, 2014, Art no. 205929, doi: 10.1155/2014/205929.
[202] C. Lee, R. J. Mehran, M.-L. Lessard, and C. L. Kerrigan, "Leeches: controlled trial in venous compromised rat epigastric flaps," *British Journal of Plastic Surgery,* vol. 45, no. 3, pp. 235-238, 1992/01/01/ 1992, doi: https://doi.org/10.1016/0007-1226(92)90085-C.
[203] A. M. Fichter *et al.*, "Impact of different antithrombotics on the microcirculation and viability of perforator-based ischaemic skin flaps in a small animal model," *Scientific Reports,* Article vol. 6, p. 35833, 10/21/online 2016, doi: 10.1038/srep35833.
[204] L. E. Abla, H. C. Gomes, S. Percario, and L. M. Ferreira, "Acetylcysteine in random skin flap in rats," *Acta cirurgica brasileira,* vol. 20, no. 2, pp. 121-3, 2005.
[205] O. DESEADCH, "Effects of N-acetylcysteine on random skin flaps in rats," *Wounds,* vol. 25, no. 3, pp. 68-74, 2013.
[206] J. Malda, T. J. Klein, and Z. Upton, "The roles of hypoxia in the in vitro engineering of tissues," (in English), *Tissue engineering,* vol. 13, no. 9, pp. 2153-62, 2007.
[207] P. Martin, "Wound Healing--Aiming for Perfect Skin Regeneration," *Science,* vol. 276, no. 5309, pp. 75-81, 1997, doi: doi:10.1126/science.276.5309.75.
[208] S. A. Eming, T. Krieg, and J. M. Davidson, "Inflammation in Wound Repair: Molecular and Cellular Mechanisms," *Journal of Investigative Dermatology,* vol. 127, no. 3, pp. 514-525, 2007/03/01/ 2007, doi: https://doi.org/10.1038/sj.jid.5700701.
[209] C. Schürmann *et al.*, "Tight spatial and temporal control in dynamic basal to distal migration of epithelial inflammatory responses and infiltration of cytoprotective macrophages determine

healing skin flap transplants in mice," (in eng), *Ann Surg,* vol. 249, no. 3, pp. 519-34, Mar 2009, doi: 10.1097/SLA.0b013e31819a8d6c.
[210] M. H. M. Barros, F. Hauck, J. H. Dreyer, B. Kempkes, and G. Niedobitek, "Macrophage Polarisation: an Immunohistochemical Approach for Identifying M1 and M2 Macrophages," *PLOS ONE,* vol. 8, no. 11, p. e80908, 2013, doi: 10.1371/journal.pone.0080908.
[211] A. Puig-Kröger *et al.*, "Folate receptor beta is expressed by tumor-associated macrophages and constitutes a marker for M2 anti-inflammatory/regulatory macrophages," (in eng), *Cancer Res,* vol. 69, no. 24, pp. 9395-403, Dec 15 2009, doi: 10.1158/0008-5472.Can-09-2050.
[212] K. Movahedi *et al.*, "Different tumor microenvironments contain functionally distinct subsets of macrophages derived from Ly6C(high) monocytes," (in eng), *Cancer Res,* vol. 70, no. 14, pp. 5728-39, Jul 15 2010, doi: 10.1158/0008-5472.Can-09-4672.
[213] S. K. Biswas and A. Mantovani, "Macrophage plasticity and interaction with lymphocyte subsets: cancer as a paradigm," *Nature Immunology,* vol. 11, no. 10, pp. 889-896, 2010/10/01 2010, doi: 10.1038/ni.1937.
[214] L.-Q. Kong *et al.*, "The Clinical Significance of the CD163+ and CD68+ Macrophages in Patients with Hepatocellular Carcinoma," *PLOS ONE,* vol. 8, no. 3, p. e59771, 2013, doi: 10.1371/journal.pone.0059771.
[215] C. A. Ambarus *et al.*, "Soluble Immune Complexes Shift the TLR-Induced Cytokine Production of Distinct Polarized Human Macrophage Subsets towards IL-10," *PLOS ONE,* vol. 7, no. 4, p. e35994, 2012, doi: 10.1371/journal.pone.0035994.
[216] J. A. Van Ginderachter *et al.*, "Classical and alternative activation of mononuclear phagocytes: Picking the best of both worlds for tumor promotion," *Immunobiology,* vol. 211, no. 6, pp. 487-501, 2006/09/14/ 2006, doi: https://doi.org/10.1016/j.imbio.2006.06.002.
[217] S. Gordon, "Alternative activation of macrophages," *Nature Reviews Immunology,* vol. 3, no. 1, pp. 23-35, 2003/01/01 2003, doi: 10.1038/nri978.
[218] S. Gordon and F. O. Martinez, "Alternative Activation of Macrophages: Mechanism and Functions," *Immunity,* vol. 32, no. 5, pp. 593-604, 2010, doi: 10.1016/j.immuni.2010.05.007.
[219] C. L. Karp and P. J. Murray, "Non-canonical alternatives: What a macrophage is 4," *Journal of Experimental Medicine,* vol. 209, no. 3, pp. 427-431, 2012, doi: 10.1084/jem.20120295.
[220] I. K. Gratz *et al.*, "Cutting Edge: Memory Regulatory T Cells Require IL-7 and Not IL-2 for Their Maintenance in Peripheral Tissues," *The Journal of Immunology,* vol. 190, no. 9, pp. 4483-4487, 2013, doi: 10.4049/jimmunol.1300212.
[221] R. Sanchez Rodriguez *et al.*, "Memory regulatory T cells reside in human skin," *The Journal of Clinical Investigation,* vol. 124, no. 3, pp. 1027-1036, 03/03/ 2014, doi: 10.1172/JCI72932.
[222] A. Nosbaum *et al.*, "Cutting Edge: Regulatory T Cells Facilitate Cutaneous Wound Healing," *The Journal of Immunology,* p. 1502139, 2016, doi: 10.4049/jimmunol.1502139.
[223] A. Egners, M. Erdem, and T. Cramer, "The Response of Macrophages and Neutrophils to Hypoxia in the Context of Cancer and Other Inflammatory Diseases," *Mediators of Inflammation,* vol. 2016, p. 2053646, 2016/02/29 2016, doi: 10.1155/2016/2053646.
[224] M. M. Escribese, M. Casas, and A. L. Corbí, "Influence of low oxygen tensions on macrophage polarization," (in eng), *Immunobiology,* vol. 217, no. 12, pp. 1233-40, Dec 2012, doi: 10.1016/j.imbio.2012.07.002.
[225] J. M. Olefsky and C. K. Glass, "Macrophages, Inflammation, and Insulin Resistance," *Annual Review of Physiology,* vol. 72, no. 1, pp. 219-246, 2010, doi: 10.1146/annurev-physiol-021909-135846.
[226] J. S. Duffield *et al.*, "Selective depletion of macrophages reveals distinct, opposing roles during liver injury and repair," *The Journal of Clinical Investigation,* vol. 115, no. 1, pp. 56-65, 01/03/ 2005, doi: 10.1172/JCI22675.

APPENDICES

Appendix A. Supplemental figures of chapter 3

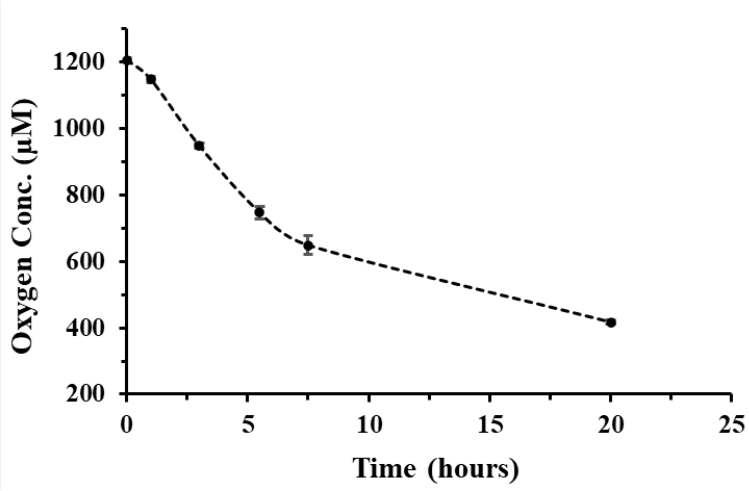

Fig. A1. Typical change in oxygen content of oxygen saturated water as a function of time in laboratory conditions (N=3).

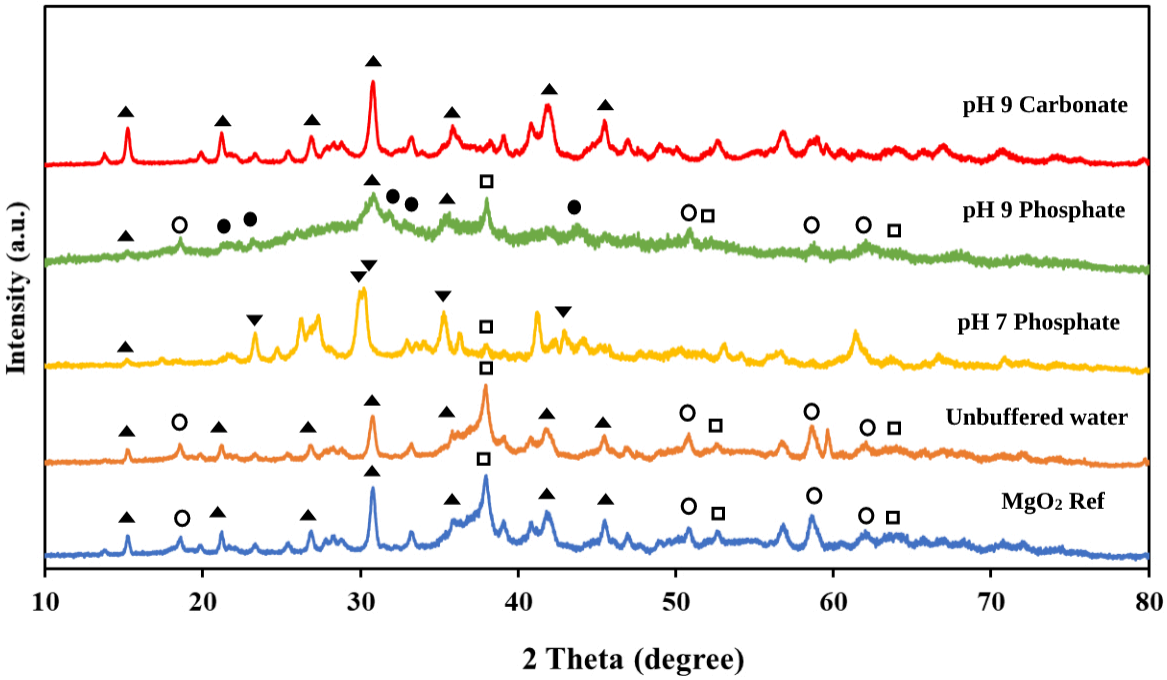

Fig. A2. The X-ray diffraction patterns of magnesium peroxide after 7 days exposure to different buffers (□) MgO_2, (○) $Mg(OH)_2$, (▲) $Mg_4(OH)_2(CO_3)_3.3H_2O$, (●) Na_2HPO_4, (▼) $Mg_2O_7P_2$.

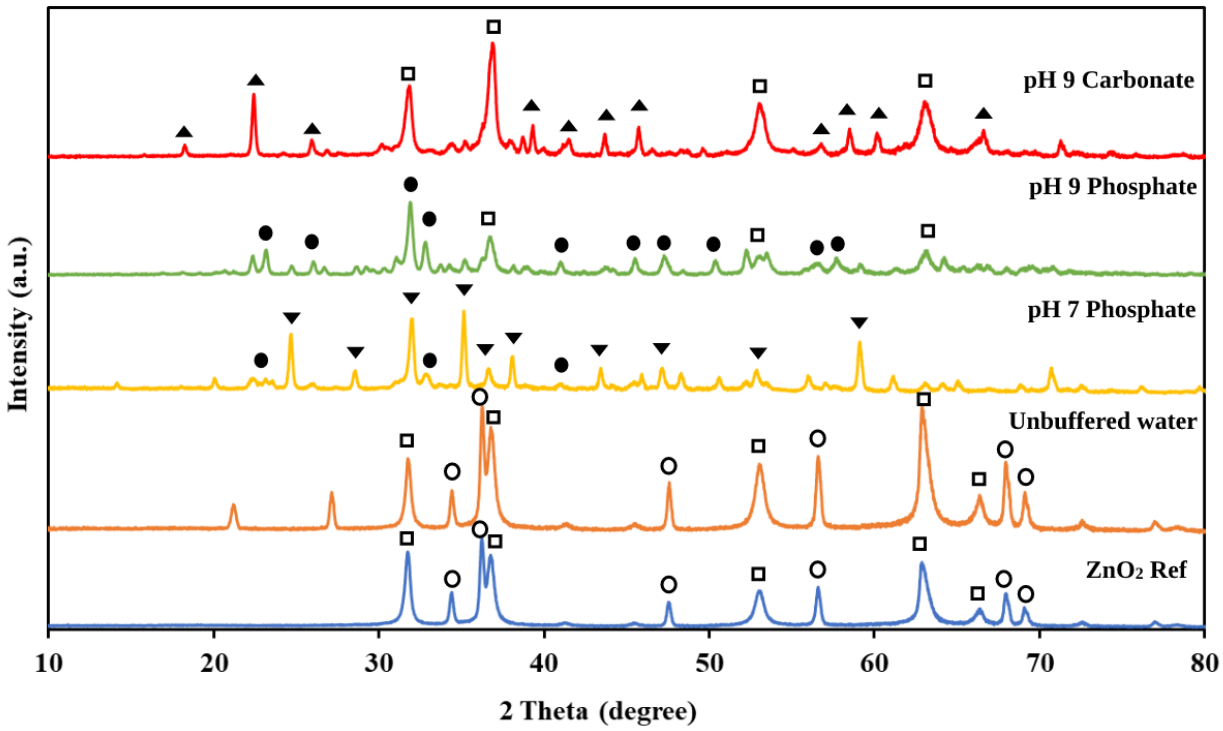

Fig. A3. The X-ray diffraction patterns of zinc peroxide after 7 days exposure to different buffers (□) ZnO_2, (○) ZnO, (▲) $Na_2Zn_3(CO_3)_4.3H_2O$, (●) Na_2HPO_4, (▼) $Na_6Zn_6(PO_4)_6.8H_2O$.

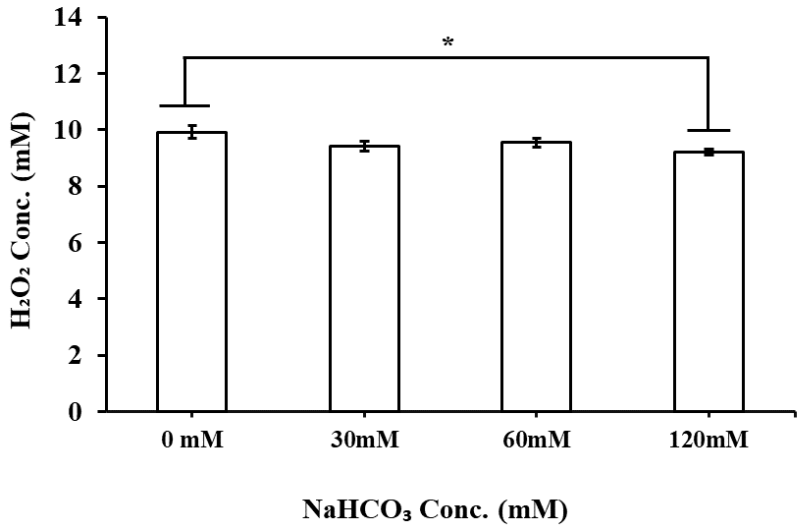

Fig. A4. Effect of added $NaHCO_3$ to PBS on stability of H_2O_2 after 5 hours. The pH value was maintained at 8.5 ± 0.1 by adding NaOH or HCl for the duration of experiment, * indicates $p<0.01$, N=3.

Appendix B. Supplemental figures of chapter 4

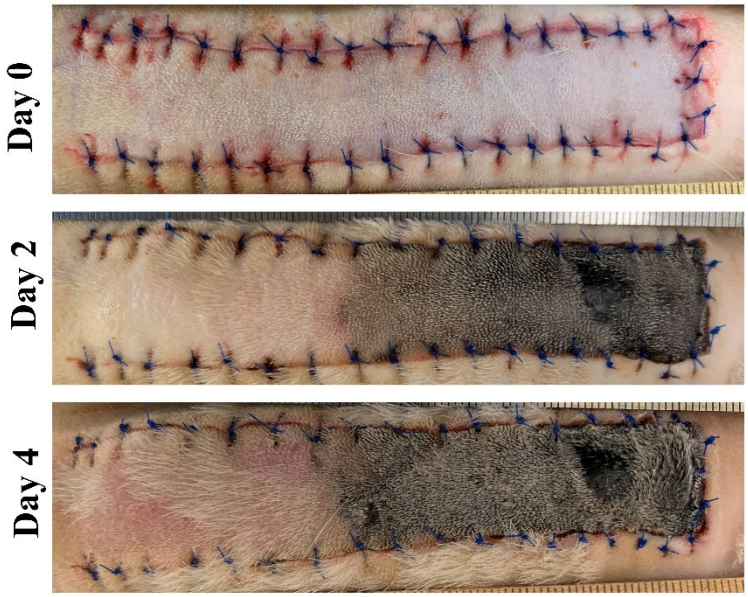

Fig. B1. Representative photographs of the skin flap on days 0, 2 and 4 for nitroglycerine. Two Trinipatch 0.2 mg/hr, 7cm^2 were applied after the operation and days 1, 2 and 4 over the flap.

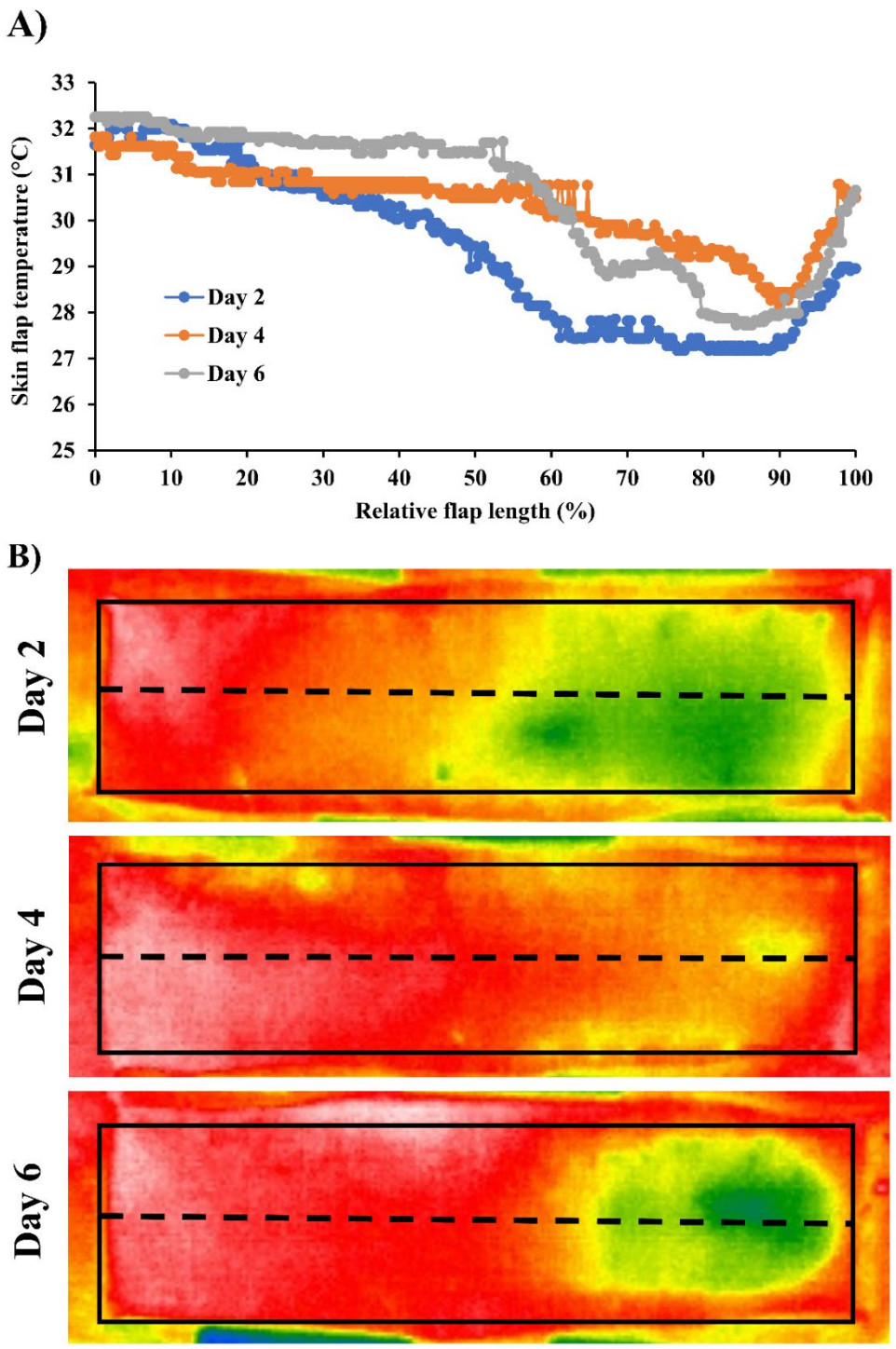

Fig. B2. (A) The temperature profile of control skin flap in the position of centre dashed line from its proximal (0%) to distal (100%) on days 2, 4 and 6, measured from IR images by MATLAB **(B)** IR images of the control flap on days 2, 4 and 6 (right side is the distal and left side is proximal). Dashed line indicated the position of temperature profile.

Appendix C. The proof of first manuscript submission

Acta Biomaterialia

Aqueous decomposition behavior of solid peroxides: effect of pH and buffer composition on oxygen and hydrogen peroxide formation.

--Manuscript Draft--

Manuscript Number:	AB-21-2893
Article Type:	Full length article
Keywords:	Oxygen; Hydrogen peroxide; Carbonate buffers; Solid peroxides
Corresponding Author:	Jake Barralet McGill University Department of Surgery montreal, PQ CANADA
First Author:	Arghavan Rastinfard
Order of Authors:	Arghavan Rastinfard
	Benjamin Dalisson
	Jake Barralet
Abstract:	The ability of solid peroxides to provide sustained release of both oxygen and hydrogen peroxide makes them potentially suitable for oxygen release or antibacterial applications. Most recent reports using solid peroxides to augment oxygen levels do so by compounding solid peroxide powders in polymers to retard the aqueous decomposition. Compounds with peroxidase activity may be added to reduce hydrogen peroxide toxicity. Peroxides are rarely pure and are mixed with oxide and themselves decompose to form hydroxides in water. Therefore, even if buffering strategies are used, locally the pH at the surface of aqueously immersed peroxide particles is inevitably alkaline. Since pH affects the decomposition of peroxides and hydrogen peroxide stability, this study compared for the first-time the aqueous decomposition products of hydrogen and inorganic peroxides that are in use or have been used for medical applications of have been evaluated preclinically; calcium peroxide (CaO 2), magnesium peroxide (MgO 2), zinc peroxide (ZnO 2), sodium percarbonate (Na 2 CO 3 .1.5H 2 O 2) and hydrogen peroxide (H 2 O 2). Since plasma can be approximated to be carbonate buffered phosphate solution, we maintained pH using carbonate and phosphate buffers and compared results with citrate buffers. For a given peroxide compound, we identified not only a strong effect of pH but also of buffer composition on the extent to which oxygen and hydrogen peroxide formation occurred. The influence of buffer composition was not previously appreciated, thereby establishing in vitro parameters for better design of intentional release of specific decomposition species.